DESIGN AND INTERPRETATIVE STUDIES OF SMALL-SIZE AND LOW-PROFILE ANTENNAS FOR HORIZONTALLY AND CIRCULARLY POLARIZED RADIATIONS

KITTIMA LERTSAKWIMARN

A THESIS SUBMITTED IN PARTIAL FULFILLMENT
OF THE REQUIREMENT FOR THE DEGREE OF
DOCTOR OF ENGINEERING IN ELECTRICAL ENGINEERING
FACULTY OF ENGINEERING
KING MONGKUT'S INSTITUTE OF TECHNOLOGY LADKRABANG
2014

KMITL-2014-EN-D-018-219

DESIGN AND INTERPRETATIVE STUDIES OF SMALL-SIZE AND LOW-PROFILE ANTENNAS FOR HORIZONTALLY AND CIRCULARLY POLARIZED RADIATIONS

KITTIMA LERTSAKWIMARN

A THESIS SUBMITTED IN PARTIAL FULFILLMENT
OF THE REQUIREMENT FOR THE DEGREE OF
DOCTOR OF ENGINEERING IN ELECTRICAL ENGINEERING
FACULTY OF ENGINEERING
KING MONGKUT'S INSTITUTE OF TECHNOLOGY LADKRABANG
2014

KMITL-2014-EN-D-018-219

หัวข้อวิทยานิพนธ์	การศึกษาวิเคราะห์และออกแบบสายอากาศขนาดเล็กและสัณฐานต่ำสำหรับแพร่กระจายคลื่นโพลาไรซ์แนวนอนและวงกลม
นักศึกษา	นางสาวกิตติมา เลิศศักดิ์วิมาน
รหัสนักศึกษา	54610152
ปริญญา	วิศวกรรมศาสตรดุษฎีบัณฑิต
สาขาวิชา	วิศวกรรมไฟฟ้า
พ.ศ.	2557
อาจารย์ที่ปรึกษาวิทยานิพนธ์	รศ.ดร. ชูวงค์ พงศ์เจริญพาณิชย์

บทคัดย่อ

วิทยานิพนธ์นี้นำเสนอสายอากาศขนาดเล็กและสัณฐานต่ำสำหรับแพร่กระจายคลื่นโพลาไรซ์แนวนอนและวงกลม การติดตั้งสายอากาศขนาดเล็กเป็นความต้องการหลักอันหนึ่งของอุปกรณ์ไร้สาย เช่น อุปกรณ์โทรคมนาคมเคลื่อนที่ต่างๆ ระบบอาร์เอฟไอดี และระบบโครงข่ายเซ็นเซอร์ไร้สาย (WSNs) ในวิทยานิพนธ์นี้นำเสนอสายอากาศที่ประกอบด้วยโครงสร้างสามส่วนซึ่งแพร่กระจายโพลาไรซ์เชิงเส้นและวงกลมในทิศทางขนานกับระนาบกราวนด์หรือองค์ประกอบของสายอากาศ สายอากาศเหล่านี้มีโครงสร้างวงแหวนแยก (SRA) เป็นพื้นฐานหลัก

บทที่ 2 นำเสนอสายอากาศวงแหวนแยกซึ่งมีโพลาไรซ์แนวนอนด้วยโครงสร้างสัณฐานต่ำ คุณลักษณะของสายอากาศวงแหวนแยกนั้นไม่มีผลกระทบจากระนาบกราวนด์ที่มีขนาดเล็ก ซึ่งแสดงให้เห็นว่าสายอากาศวงแหวนแยกสามารถนำไปติดตั้งกับโทรศัพท์มือถือขนาดกะทัดรัดได้โดยมีคุณลักษณะไม่แตกต่างจากสายอากาศที่ปราศจากระนาบกราวนด์

บทที่ 3 กล่าวถึงโครงสร้างวงแหวนแยกที่ได้ถูกปรับปรุงสำหรับแพร่กระจายคลื่นโพลาไรซ์วงกลมสำหรับนำมาประยุกต์ใช้กับเครื่องอ่านอาร์เอฟไอดี โครงสร้างซึ่งประกอบด้วยตัวแพร่กระจายคลื่นรูปตัวยูคู่ที่ดัดแปลงซึ่งคล้ายกับการออกแบบสายอากาศวงแหวนแยกที่ถูกผ่าซีกและระนาบกราวนด์ แขนด้านหนึ่งของรูปตัวยูถูกงอ 90 องศา เพื่อให้ทิศทางของลำคลื่นหลักและโพลาไรซ์วงกลมมีทิศทางขนานกับระนาบกราวนด์ได้ในโครงสร้างสัณฐานต่ำ

นอกจากนี้บทที่ 4 นำเสนอสายอากาศขนาดเล็กซึ่งสามารถแพร่กระจายคลื่นได้รอบทิศทาง โดยสายอากาศนี้สามารถประยุกต์ใช้งานเป็นสายอากาศลูกข่ายในระบบโครงข่ายเซ็นเซอร์ไร้สาย สายอากาศประกอบด้วยองค์ประกอบบ่วงแนวนอนที่ถูกล้อมรอบด้วยองค์ประกอบรูปตัวยูสององค์ประกอบและองค์ประกอบในแนวตั้ง ขนาดทางไฟฟ้าของสายอากาศคิดเป็น ka =0.467 ซึ่งน้อยกว่า 0.5 โดยที่ k คือ ค่าคงที่ที่ความถี่เรโซแนนซ์ และ a คือ รัศมีของของทรงกลมที่ล้อมรอบสายอากาศ ซึ่งสอดคล้องกับนิยามของสายอากาศขนาดเล็ก องค์ประกอบรูปตัวยูกับองค์ประกอบแนวนอนนั้นสามารถทำให้เกิดโพลาไรซ์วงกลมรอบทิศทาง

ทั้งนี้วิทยานิพนธ์นี้ได้ผลการทดสอบของสายอากาศต้นแบบสอดคล้องกับผลการจำลอง โดยมีค่าการสูญเสียย้อนกลับ < -10 dB และอัตราส่วนแกน ≤ 3 ตลอดย่านความถี่ใช้งานและกลไกของสายอากาศที่นำเสนอทั้งหมดมาจากการวิเคราะห์โดยการพิจารณาสนามแม่เหล็กไฟฟ้าและการกระจายกระแสไฟฟ้า

Thesis	Design and interpretative studies of small-size and low-profile antennas for horizontally and circularly polarized radiations
Student	Miss Kittima Lertsakwimarn
Student ID.	54610152
Degree	Doctor of Engineering
Program	Electrical Engineering
Year	2014
Thesis Advisor	Assoc. Prof. Dr. Chuwong Phongcharoenpanich

ABSTRACT

This thesis presents low-profile and small antennas for horizontal and circular polarization (CP) radiations. Installing small-size antenna is one of main requirements in wireless devices for various mobile telecommunications, RFID systems and wireless sensor network systems (WSNs). In this thesis, the proposed antennas consist of three structures which radiate linear or CP in parallel to the ground plane or their elements. These antennas are based on a split ring antenna (SRA). The SRA which has horizontal polarization with low-profile structure has been presented in Chapter 2. The characteristics of the SRA are not sensitive to the small ground plane. This denotes that the SRA can be installed on compact handsets keeping the same characteristics as that without ground plane. In Chapter 3, the split ring structure is modified for radiating CP to be applied for RFID reader application. The structure consists of modified double U-shaped radiators, which is similar to half-cut design of SRA and a ground plane. A part of the U-shaped arms is bent by 90˚ to direct a main beam and generate CP in the parallel direction to the ground plane even though the structure is low-profile. In addition, an electrically small antenna (ESA) which can generate omnidirectional CP has been presented in Chapter 4. It is available for an antenna sensor application in WSNs. The antenna consists of a horizontal loop element enclosed by two U-shaped elements and a vertical element. The electrical size of the antenna is ka = 0.467 (i.e. < 0.5, where k is the wave number at the resonant frequency and a is the radius of a sphere surrounding the antenna), which satisfies the definition of ESA. The U-shaped elements also contribute to the generation of omnidirectional CP with the vertical element.

Throughout this thesis, measured results of prototypes of antennas show good agreements with simulated results that of -10 dB $|S_{11}|$ and 3 dB axial ratio covering the operating frequency. Each mechanism of all the proposed antennas has been analyzed by observing electromagnetic field and current distribution.

ACKNOWLEDGEMENT

This thesis could not be completed without the invaluable helps from many people to whom I would like to express my appreciation.

First, I would like to give my deep sense of gratitude to my advisor, Associate Professor Dr. Chuwong Phongcharoenpanich, for his helpful suggestions, advice and encouragement throughout my study. I express my sincere thanks to Associate Professor Dr. Takeshi Fukusako of Kumamoto University, Japan for his intelligent advice, helpful suggestions and comments to my research.

I would like to thank all of my colleagues in Wireless Communication Laboratory for their friendship and help. Moreover, I would like to thank members of Fukusako's Laboratory for friendship and assistance throughout the duration of one year research student in their Laboratory.

I would like to acknowledge the Thailand Research Fund (TRF) which provided financial support to undertaken project through the Royal Golden Jubilee Ph.D. Program (Grant No. PHD/0324/2552).

I would like to express my appreciation to my parents for their patience, support and invaluable encouragement throughout the long period of my study.

At the end of my thesis, it is a pleasant task to express my thanks to all those who contributed in many ways to the success of this study and made it an unforgettable experience for me.

Kittima Lertsakwimarn

TABLE OF CONTENTS

TABLE OF CONTENTS (continued)

TABLE OF CONTENTS (continued)

LIST OF TABLES

LIST OF FIGURES

LIST OF FIGURES (continued)

LIST OF FIGURES (continued)

LIST OF FIGURES (continued)

CHAPTER 1

INTRODUCTION

This thesis is devoted to developments of several fundamental and novel antenna technologies for satisfying the requirements in many wireless applications, such as RFID (Radio Frequency Identification) technologies and antenna sensor applications. This chapter introduces the background and purposes of the studies on circularly polarized and/or electrically small antennas which are related to the RFID technology, sensor applications of antennas.

1.1 Background and Motivation

RFID system was first invented by Germans during World War II to detect and confirm that the aircraft is not foreign one when it returned to base. Such military technique has been converted to several industrial applications. Nowadays, RFID is a technology used widely for identification purpose in many applications such as in warehousing, retail, transportation and manufacturing [1]. The RFID system can be used in the different frequency bands. One frequency band becoming a standard for supply chain management is the ultra-high-frequency (UHF) band. The UHF band has been allocated for RFID application depending on countries such as 865-868 MHz in Europe, 902-928 MHz in North and South Americas, 950-956 MHz in Japan and some Asian countries whereas 920-925 MHz band is used in Thailand.

Many linearly polarized antennas for portable devices have been designed with small size and sufficient bandwidth. For RFID applications, e-field generated from linearly polarized antennas should be parallel to e-field in antennas at both reader/writers and RFID tags in order to get a consistent read. However, a problem of missing tag detection may take place due to a polarization mismatch. For avoiding this problem, the use of antennas radiating circular polarization (CP) can be a good option [2, 3]

Portable RFID readers in addition to fixed type of readers have been actively used in recent years. Considering this situation, antennas for handheld RFID readers have been required to have a low-profile and a small size structure with light weight [4-9]. Low-

profile and small circularly polarized antennas (CP antennas) still receive a lot of research attention, although other types of UHF RFID reader antennas with meandered, microstrip, and helical element have been published in the literature [4-8]. In [4], an antenna with four meandered monopole elements fed by a series feeding network has been reported, and another antenna with array of two bent elements is presented in [5]. In [6], double-sided, crossed-dipole antenna for CP radiation loaded with two metal strips for phase delay is published. A compact circularly polarized microstrip antenna has been presented in [7]. A monofilar backfire helix with ground plane is proposed as high gain CP antenna [8].

On the other hand, since 5-6 years ago, wearable RFID readers on a hand have appeared on the fields of health care and inspection services, so that they can use their both hands at their working places freely without holding their reader. For achieving such situation, a low-profile CP reader antenna is also required for wearable devices with a compact design. Requirements for the wearable readers using a CP antenna are that the main beam direction should be parallel to the ground plane to make the maximum use of the advantages of the low-profile design [9]. Furthermore, some microstrip antennas for typical commercial handheld readers have linear or circular polarization. However, such antennas based on microstrip structure limit the size and the bandwidth, and the main beam of those structures is directed to the normal direction to the ground [8]. In fact, it is probably difficult to apply such CP antennas [4]-[8] mentioned above for this purpose.

Several small-sized compact antennas which may be available for wearable devices have been published. Some study groups have reported horizontally polarized printed loop antennas in [10-11], and some groups have studied on open-loop antennas generating CP [12, 13]. Moreover, an inverted-L CP antenna and a slender CP antenna have been reported in [14, 15], respectively. However, the main beam direction is not parallel to the ground, and the bandwidth is not sufficient. A study group has recently reported a low-profile antenna with high radiation efficiency in [16, 17], but the polarization is linear. For now, circularly polarized and low-profile antennas radiating parallel to the ground plane has not been found.

On the other hand, wireless sensor networks (WSNs) have given rise to many applications. WSNs can be classified as distributed computing and communication

systems that are an integral part of the physical space they inhabit. They are commonly used in the distributed sensing systems as well as the monitoring and control applications, such as in monitoring structural health, wildlife tracking, and factory monitoring.

The use of WSN generally consists of a collection of sensors used to monitor specific variables over a region of interest. Monopole antennas have been utilized in most sensor nodes because they achieve an omnidirectional radiation pattern desired for communication links between the sensor nodes. However, typical monopole antenna elements perpendicular to ground are not mechanically stable, and thus require additional packaging to avoid node failure from the unexpected outdoor environments [18]. A low-profile and horizontally polarized antennas with omnidirectional pattern is a good choice to reduce the size of the package which still has the similar radiation pattern to the monopole antenna on the planar surface parallel to ground. Moreover, antennas with horizontally polarized omnidirectional radiation pattern in the azimuth plane can be applied for many applications such as base stations and wireless communications. Such antennas are useful for, especially, polarization diversity combined with vertically polarized omnidirectional antennas, such as the disk-loaded monopole antennas. This results in compact polarization diversity antenna systems.

A low-profile antenna has a metallic strip with a small fraction of a wavelength ($<< \lambda_0$, usually $0.003\lambda_0 \leq$ height $\leq 0.005\lambda_0$) above a ground plane [19]. Low-profile antennas installed on a back conductor can effectively reduce the electrical effect from backing material such as IC-chip, electrical circuits and coupling with other antennas [16]. Many low-profile antennas, such as disk loaded monopoles, tend to be vertically polarized radiator [16, 20-24]. In [20], a loop structure can be miniaturized by using inductors. A loop-shaped inverted-F wire antenna (LIFA) has been presented in [21]. In [22], a vertically polarized cavity-backed composite slot loop antenna (CBCSLA) with omnidirectional radiation in the horizontal plane having extremely small height is presented. An inductively coupled capacitively loaded monopole antenna (ICCLMA) consisting of two metal layers, a feeding pin and a shorting pin has been presented for achieving a high gain, low-profile and miniaturized antenna with omnidirectional vertically polarized radiation [23]. In [24], a folded monopole antenna with capacitively coupled parasitic elements in the same plane is studied.

The Alford loop antenna in the wire type was firstly reported to achieve an omnidirectional horizontal polarization [25]. Several modifications of the Alford loop antenna have been presented in [26]-[27]. Other techniques for achieving omnidirectional and horizontal polarization have also been studied. For example, four flag-shaped radiators are connected to four tapered strip lines terminated with a small circular patch at the center on both sides of a substrate [28]. A series-fed array of loop antenna, which consists of four μ-negative transmission lines (MNG-TL), was presented in [29]. Even though these antennas can radiate an omnidirectional radiation pattern with horizontal polarization, but they are not low-profile antennas. However, as far as the author know, no research has studied on the compact low-profile antenna having horizontally polarized omnidirectional radiation pattern.

On the other hand, CP antennas with an omnidirectional radiation pattern are found in multiple applications, e.g. in mobile communications systems, wireless local area network (WLAN) systems, and wireless sensor networks (WSNs). For example in the WSNs, the polarization mismatch between the receiving and transmitting antennas could be effectively reduced by an omnidirectional CP antenna that covers the entire azimuth directions. Previous research works [30–38] proposed various antenna designs with omnidirectional CP. In [30], the omnidirectional CP was achieved using normal-mode helical antennas with very small diameters relative to the wavelength. According to [31], the helical antenna is a combination of short poles and small loops to generate vertical and horizontal polarizations with 90-degree phase difference and equal amplitude when $\pi D = \sqrt{2S\lambda}$ where D is the diameter of the helix and S is the spacing between turns. To achieve a 50 Ω impedance matching, the required element length of the helical antenna is too long to be electrically small. A previous research in [32] adopted the concept of the normal-mode helical antenna to generate CP, but additional elements for CP generation were arrayed with an equal interval in the azimuth plane. In [33], four pairs of an L-shaped monopole and a horizontal copper line were fed with a crossed power distribution network. The structure in [34] utilized the zeroth-order resonance and four curved branches and pins, while that in [35] used the zeroth- and first-order modes of an epsilon negative (ENG) transmission line and three curved branches and pins. In [36, 37], the researchers employed the Alford loop structure with a top-loaded cylindrical monopole. In [38], the antenna structure, which resembles a bird nest and acts

as a polarizer, generated omnidirectional CP using a monopole and multiple dielectric slabs. In addition, modern electronic devices require smaller and more light weight antennas, so electrically small antennas (ESAs) are an interesting research topic for modern wireless communication systems such as RFID and WSNs.

Since ESAs are small compared to the wavelength at the resonant frequency, the small size also hinders achieving sufficient impedance bandwidth and radiation efficiency. The definition of an electrically small antenna is to satisfy the following condition;

$$ka < 0.5, \tag{1.1}$$

where k $(= 2\pi/\lambda)$ is the free space wave number, and a is the radius of a sphere circumscribing the maximum dimension of the antenna. According to [39], the minimum quality factor (Q), has been defined as;

$$Q_{\min} = \frac{1}{ka} + \frac{1}{k^3 a^3} \tag{1.2}$$

Basically, typical ESAs such as short dipoles or small loops have usually small resistance and large reactance components in impedance. Therefore, it is difficult for such antennas to be matched to the required impedance such as 50 Ω [40]. Several techniques were proposed for miniaturization of antennas, e.g. a meandered element with a capacitive feed structure [16, 41], complementary split ring resonators (CSRRs) [42] and split ring resonators (SRR) [43, 44], and combining antennas with high impedance surfaces or artificial magnetic conductors (AMC) [45].

Other research experimented with circularly polarized ESAs, e.g. parasitic array antenna in [5], an electrically small slender helical antenna in [15], and modified multi-arm spherical helix antenna with air-core in [46]. Although they are CP antennas, the radiation pattern is not omnidirectional. As a result, the author's review of existing literatures has found no research on the omnidirectional CP generation from an ESA for potential applications in WSNs and mobile handset.

1.1.1 Novelties and significant findings

The novelties in the researches are mentioned here. The proposed antennas throughout this thesis are developed from a split ring antenna (SRA). This structure has a compact size with respect to wavelength (at operating frequencies) due to a capacitive coupling, linearly polarized and bidirectional main beams in parallel to the element.

1. Low-profile split ring antenna: A ground plane is installed in the vicinity of the SRA. The low-profile antenna can have horizontally polarized radiation to the ground plane. This is because the e-field in the vertical direction to the ground has a symmetrical distribution with opposite direction about the y-z plane at the center of the ground. This results in canceling the radiation of vertical electric field in between the element and the ground plane. Therefore, the impedance is not sensitive to the difference between the two structures with and without the ground plane.

2. Low-profile CP antenna: Half-cut SRA structure and a capacitive feeding line radiates CP parallel to the ground plane even though the structure is low profile. The bent part of the half-cut SRA forms a U-shaped slot with the two elements of SRA and a combination of SRA element and the ground plane, which contributes to achieve 90˚-phase difference of orthogonal electric field components. The capacitive feeding structure includes an L-and an F-shaped stub with a capacitive gap for matching.

3. Electrically small CP antenna: This antenna introduces a novel concept to generate CP. The antenna generates mainly the vertical electrical field at the aperture, but the electric field is rotated in the far region. The rotation is achieved using two U-shaped elements surrounding a smaller loop coupled electrically with a feeding line. The U-shaped elements minimize the structure size to fit the definition of ESA and generate the omnidirectional CP radiation.

1.1.2 Simulation and experiment

The antennas are modelled using the simulation software CST microwave studio which includes modules based on numerous different methods including transmission-line matrix (TLM) method, finite element method (FEM), method of moments (MoM), multilevel fast multipole method (MLFMM) and shooting boundary ray (SBR), each offering distinct advantages in their own domains. In this thesis, two domains solver were

used: the time domain solver of TLM for studying the field propagating through a component and the frequency domain solver of FEM for studying the electrically small structures or devices with a high *Q*-value. The optimal structural parameters are doing to get the target of the design.

The mechanism in this thesis is mainly discussed by observing the electric field distribution around the element using the CST software. When the current exists on an element, the electric field is finally generated with the same direction as the current making the vector potential in the same direction. The electric field at every point in space is generated from a current element which consists of a pair of positive and negative charges. Typically the electric field is directed from positive to negative charges.

After fabricating the antenna, the measurements are carried out in anechoic chamber. Agilent S-parameter network analyzer 8722ES, which covers the frequency range from 50 MHz to 40 GHz, is used for S_{11}, axial ratio and radiation pattern measurements.

1.2 Thesis Outline

As referred above, this chapter has mentioned about the background and novelties of this thesis. The remaining portion of this thesis consists of remaining four chapters.

Chapter 2 presents the low-profile antenna with horizontally polarized omnidirectional radiation by split ring structure. The antenna has been studied in case with and without ground plane. The radiation mechanism of horizontally polarized omnidirectional radiation is discussed by considering the distributions of electric field. The simulated antenna is fabricated, and the results show good agreements. The effects of the ground plane are studied with size variation and distance to the substrate.

Chapter 3 discusses the design of circularly polarized antenna radiating parallel to the ground plane. The antenna structure consists of double U-shaped strip structures and a capacitive feeding line. This structure is a half-cut structure of the split ring antenna to generate circular polarization. Effects of structural parameters are studied such as bending angle on the element and feeding structure. The antenna is also fabricated and measured. Finally, the simulated and measured results are consistent each other.

Chapter 4 deals with the electrically small antenna design that has omnidirectional radiation pattern in horizontal plane. The antenna generates CP with the structure of a horizontal loop element enclosed by two U-shaped elements and a vertical element from a feeding point on the ground plane. The structure of coupled U-shaped elements with an inner fed loop through a magnetic coupling minimizes the structure size to fit the definition of electrically small antenna. The effect of U-shaped element and length of feeding line are discussed. This research also introduces a mechanism that generates omnidirectional CP from the electrically small antennas. A prototype antenna shows good agreements between simulated and measured results.

Chapter 5 summarizes the results, advantages and applications of the research. Future scopes are also addressed.

CHAPTER 2

A LOW-PROFILE AND COMPACT SPLIT-RING ANTENNA WITH HORIZONTALLY POLARIZED OMNIDIRECTIONAL RADIATION

2.1 Introduction

This chapter presents a compact, planar and low-profile SRA having a ground plane for radiating horizontal polarization in omnidirection. The SRA consists of a fed inner ring and coupled outer split ring for impedance matching, although only a single small loop has usually small resistance and large reactance. The capacitive coupling element can match the impedance to 50-*j*0 Ω and miniaturized the antenna size. The performances of SRA with and without ground plane are demonstrated, and the mechanisms for the performances are also explained by observing the electric field (e-field) distribution.

2.2 Compact Split-Ring Antenna

2.2.1 Antenna Design

Figure 2.1 shows the proposed antenna structure consisting of a fed inner ring and a coupled outer split ring printed on a dielectric substrate of Arlon Diclad522 (ε_r = 2.6, tan δ = 2.0 × 10^{-4}) with 0.8 mm thickness. The dimensions are of 45.5 mm (0.14λ_0) in length (L) and 50 mm (0.153λ_0) in width (W). The length and width of the inner and outer rings are optimized so as to resonate at the UHF RFID band around 920 MHz. The dimensions of the proposed antenna are shown in Table 2.1. The SRA structure can reduce the overall size of the antenna because the capacitive coupling between the two rings makes the resonance at a low frequency [16], [47].

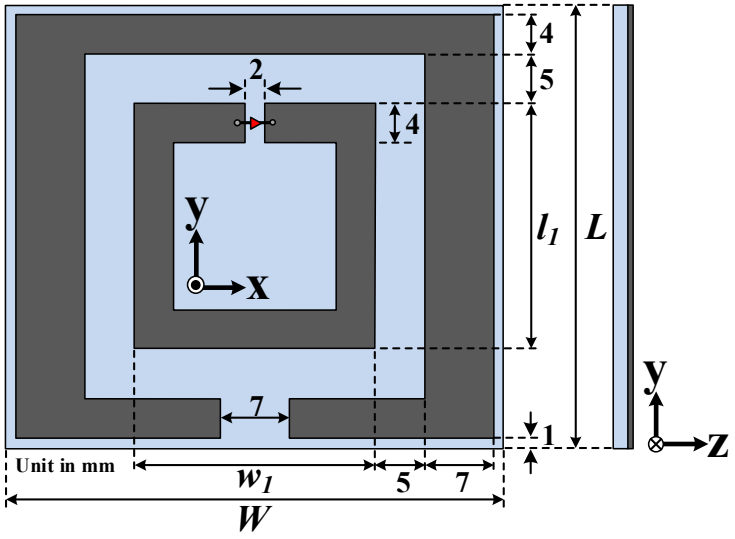

Figure 2.1 Geometry of the proposed antenna.

Table 2.1 The structural parameters of the compact split-ring antenna.

Parameter	Dimension (mm)
W	50.0
L	45.5
w_1	24.0
l_1	25.5

2.2.2 Experimental Results

Photographs of the fabricated antennas are shown in Fig. 2.2. The antenna is fed through the bazooka balun because the feeding point should be balanced as shown in Fig. 2.2(b). Figure 2.3 shows the simulated and measured results of $|S_{11}|$. The simulated and measured -10-dB $|S_{11}|$ bands can cover the UHF RFID band (920-925 MHz) with 1.5% and 1.3% bandwidth, respectively.

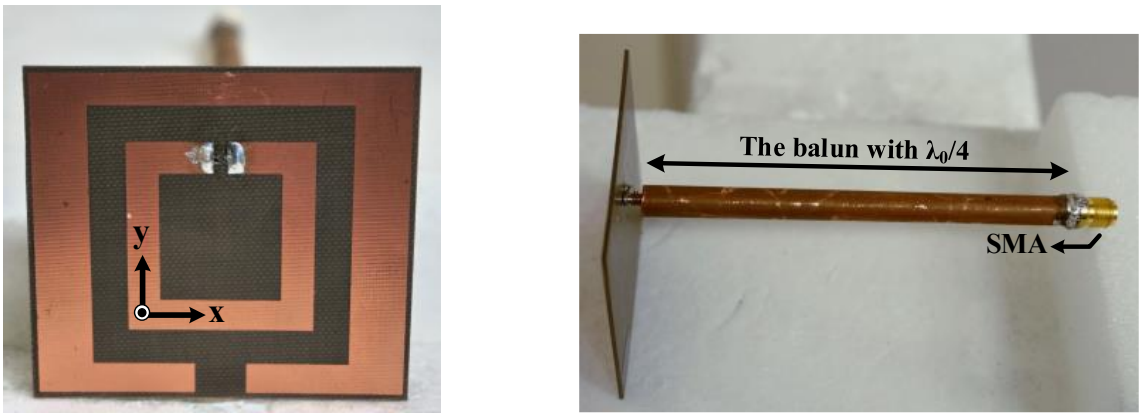

(a) (b)

Figure 2.2 Photograph of fabricated prototype (a) front view and (b) side view.

Figure 2.4 shows the simulated and measured radiation patterns of E_ϕ and E_θ in the x-y, y-z and x-z planes at 920 MHz. The simulated and measured cross-polarizations of E_θ are lower by 20 dB than the co-polarizations of E_ϕ in omnidirection of the x-y and y-z planes and the antenna has maximum gain of 1.7 dBi along the +y-direction at 920 MHz. The antenna provides nearly omnidirectional patterns in these two planes.

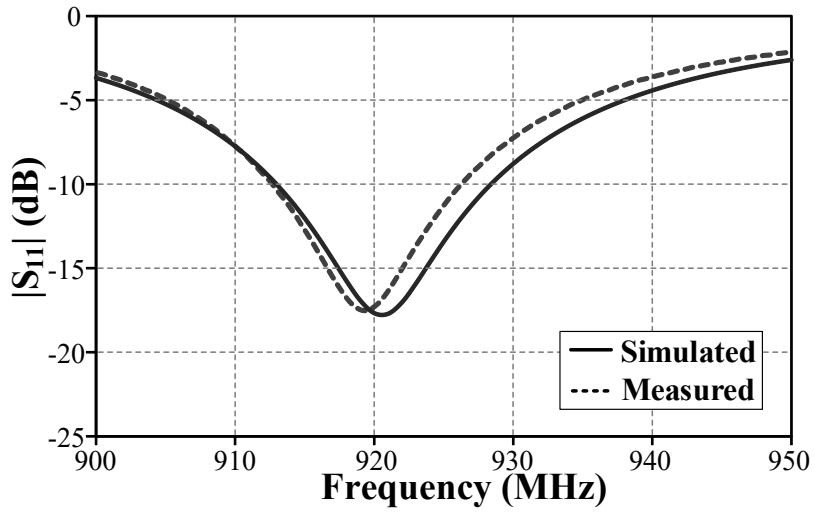

Figure 2.3 Simulated and measured $|S_{11}|$.

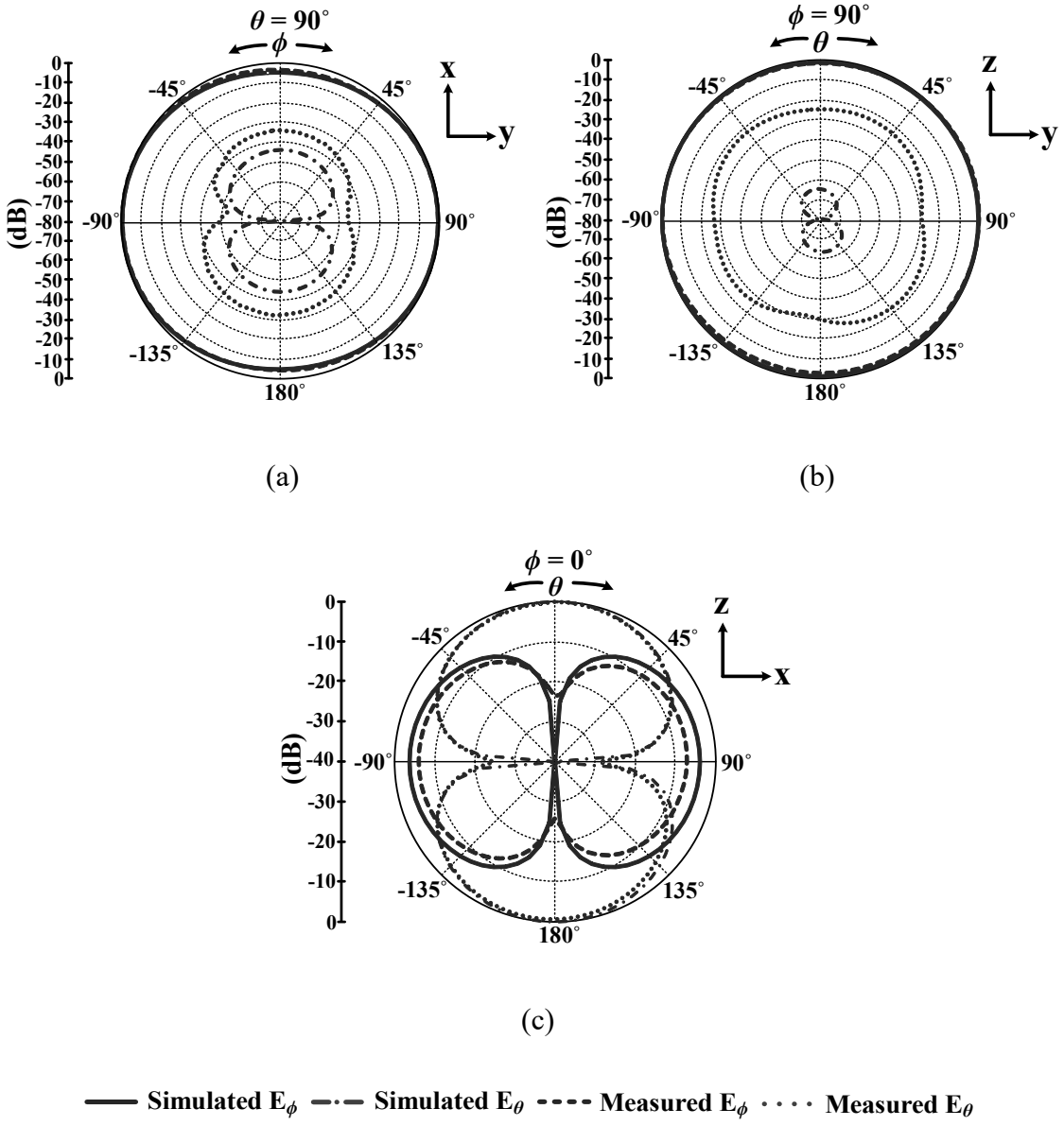

Figure 2.4 Radiation patterns at 920 MHz in (a) x-y plane, (b) y-z plane and (c) x-z plane.

2.2.2 Effect of Capacitive Coupling

The effect of capacitive coupling between the outer and inner rings is studied with respect to the input impedance characteristics of the SRA. For this study, the inner ring is removed, and a feeding point is installed at the middle of the outer split ring with balance feeding resulting in being like a folded dipole antenna, however, both the ends of the folded element forms a capacitive gap. The outer split ring has the same size as the parameters shown in Table 2.1. Figures 2.5(a) and (b) illustrate input resistance and reactance of the SRA and the folded dipole antenna, respectively. As shown in the figures, the capacitive coupling between inner and outer rings significantly makes additional resonance frequency at a low frequency of around 920 MHz. On the other hand, the folded dipole antenna shows a bigger kink (with dotted line) at the low frequency of the Smith chart as shown in Fig. 2.5(c). When the inner ring is installed, the kink, shown with the solid line, passes through the circle of VSWR = 2. The total length of folded dipole antenna (outer ring) is approximately half-wavelength at resonance frequency (920 MHz), however the folded dipole has inductive impedance because of the effect of the capacitive gap at the element ends. Therefore, we can take it that the combination of the inductive impedance of the folded dipole and the capacitive coupling with the inner ring makes the additional resonance at 920 MHz. As a result, the use of the capacitive coupling yields the impedance matching to the SRA at this frequency.

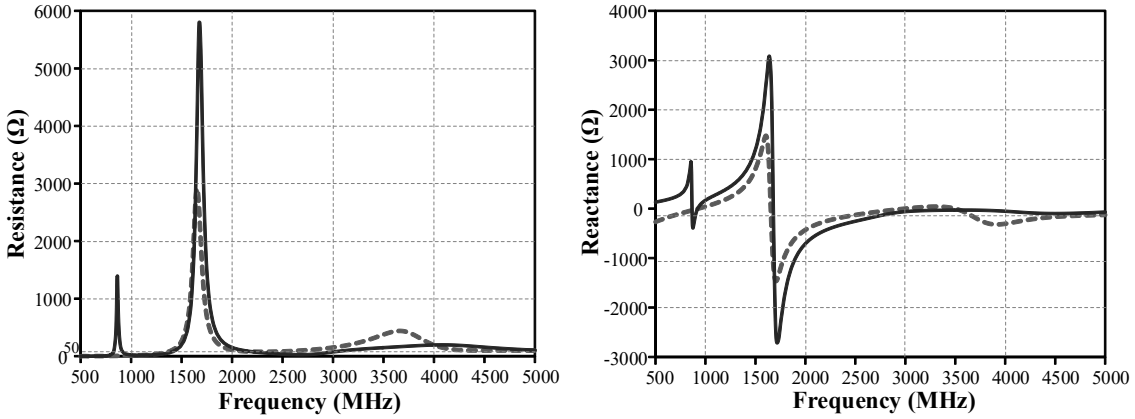

(a) (b)

Figure 2.5 Simulated input impedance of folded dipole and split ring antennas: (a) Input resistance, (b) Input reactance and (c) Smith chart characteristics.

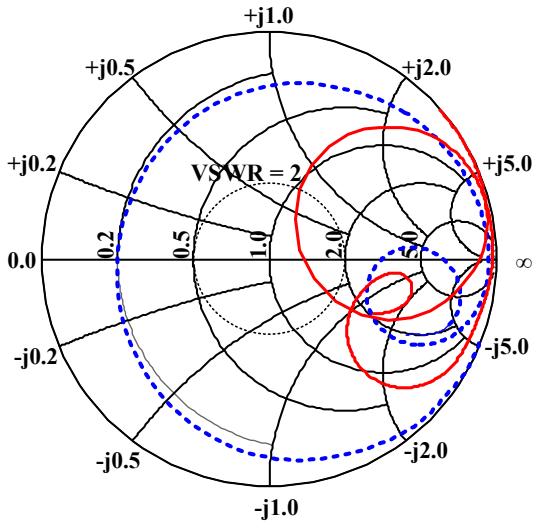

(c)

---- Folded Dipole Antenna —— Spilt Ring Antenna

Figure 2.5 (Continued)

2.3 Compact Split-Ring Antenna with Ground Plane

In Fig. 2.6, a ground plane has been installed with the same size as the substrate. The dimensions are of 45 mm ($0.138\lambda_0$) in length (L) and 50.5 mm ($0.155\lambda_0$) in width (W). The air interval s between the substrate and ground plane is chosen as 10 mm ($0.036\lambda_0$) as shown in Fig. 2.6(b) considering the impedance matching. When s = 10 mm having the ground plane with the same dimension as the upper element substrate, the impedance bandwidth is narrower than 15 MHz, which is sufficient value for some applications such as RFID and mobile telecommunications. The effects of variation in the size of ground plane and the air interval will be discussed in Sections 2.3.2 and 2.3.3, respectively. In addition, we can sufficiently regard the antenna with s = 10 mm as low profile. Furthermore, we can make sure that the vertical component is suppressed in such a situation that the vertical component may be easily radiated. The dimensions of the proposed antenna with ground plane are shown in Table 2.2.

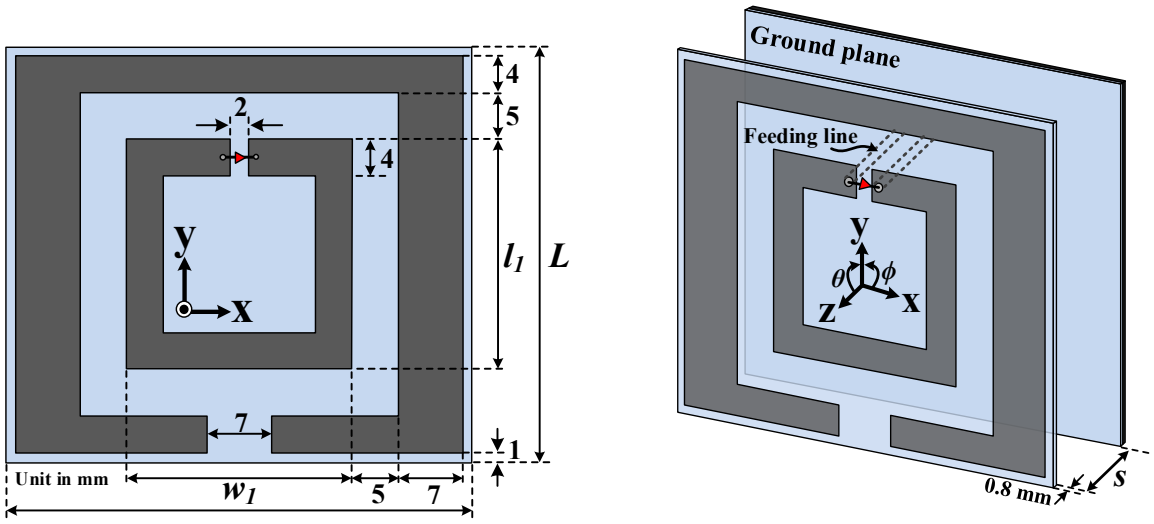

(a) (b)

Figure 2.6 Geometry of the proposed antenna with ground plane: (a) Front view and (b) Perspective view.

Table 2.2 The structural parameters of split-ring antenna with ground plane.

Parameter	Dimension (mm)
W	50.5
L	45.0
w_1	25.0
l_1	24.5

2.3.1 The Radiation Mechanism of Horizontally Polarized Omnidirectional Radiation by Discussing the Distributions of Electric Field

The radiation mechanism of horizontal polarization from the low-profile antenna is discussed in this section. From the results, the proposed antennas with and without ground plane can radiate horizontal polarization to the ground or substrate. The mechanisms for the behavior are explained by discussing the distributions of e-field. The e-field distributions of the SRA without the ground plane in the x-y plane are shown in Fig. 2.7 at ωt = 0˚ and 90˚, where the voltage at the feeding point is assumed to be

$V = V_0 \sin \omega t$. For $\omega t = 0^\circ$, the e-field distribution on the SRA structure show weak strength as shown in Fig. 2.7(a). At $\omega t = 90^\circ$, the strongest e-field distribution can be found around in the two rings of the antenna. Many of the e-field vectors are parallel to x-direction as shown in Fig. 2.7(b).

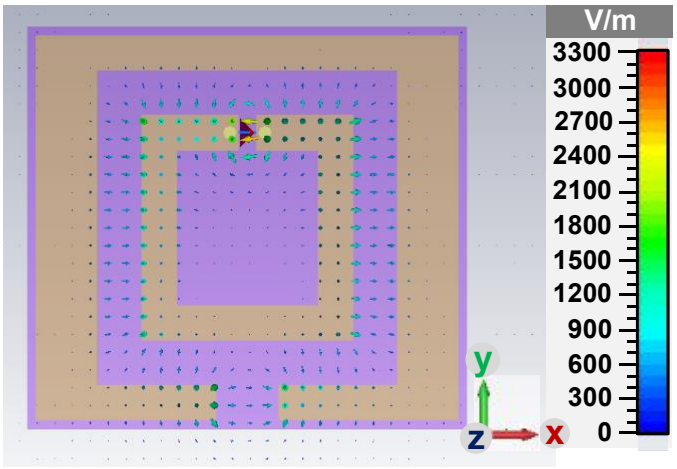

(a)

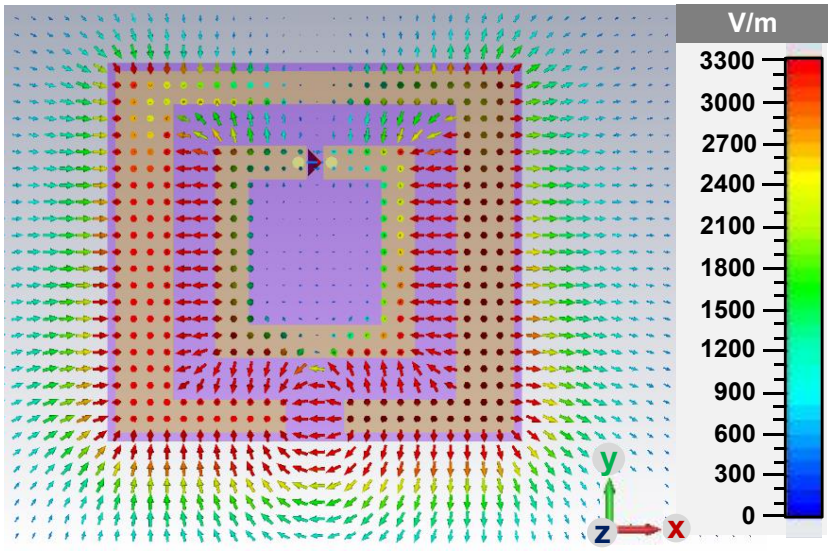

(b)

Figure 2.7 Electric field distributions of the antenna without ground plane in the x-y plane on the element surface at 920 MHz with (a) $\omega t = 0^\circ$, and (b) $\omega t = 90^\circ$.

Next, the SRA structure with the ground plane is discussed. Figure 2.8 shows the e-field distribution in the x-y plane at ωt = 0˚ and 90˚. At ωt = 0˚, the e-field shows asymmetric distribution to the y-z plane but the strength is weak as shown in Fig. 2.8(a). At ωt = 90˚, the similar e-field distribution as that in Fig. 2.7(b) can be observed as shown in Fig. 2.8(b).

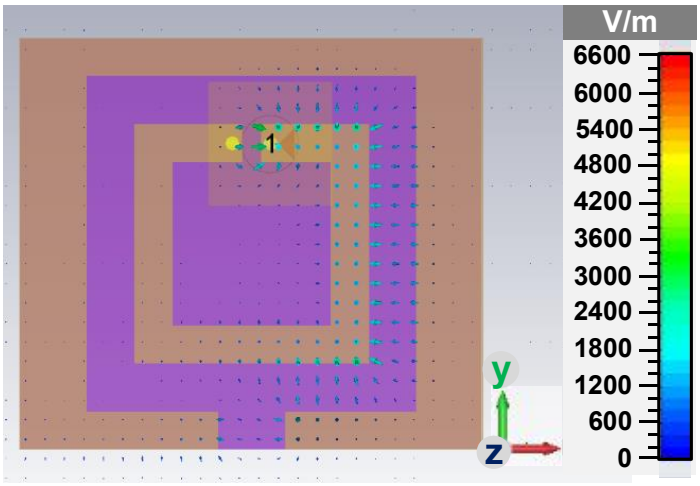

(a)

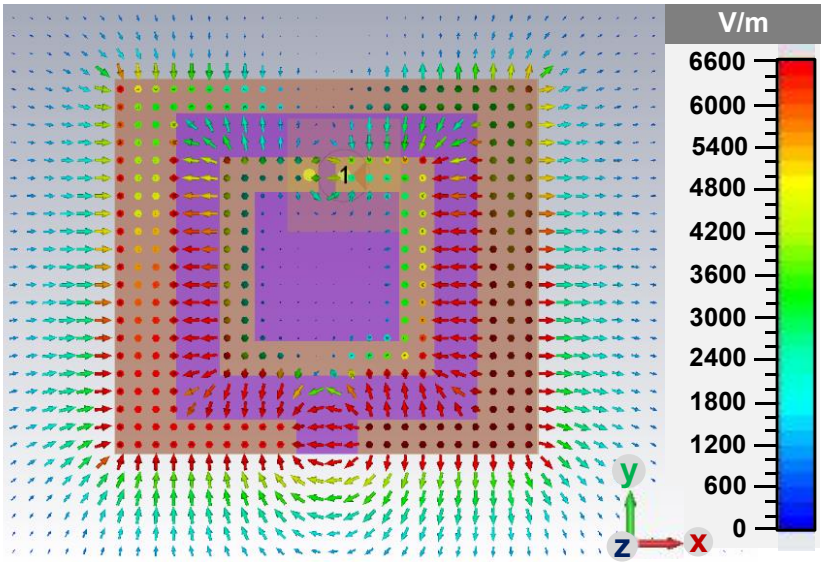

(b)

Figure 2.8 Electric field distributions of the antenna with ground plane in the x-y plane on the element surface at 920 MHz with (a) ωt = 0˚, and (b) ωt = 90˚.

From the results, the antenna can radiate horizontal polarization either with or without the ground plane. Figure 2.9 shows the e-field distributions in the x-z plane at distances of 20 mm from the center of substrate along the y-axis at ωt = 0˚ and 90˚. At ωt = 0˚, the e-field distribution is very weak as shown in Fig. 2.9(a). At ωt = 90˚, the e-field strength is symmetrical about the y-z plane at the center of the ground, and the vertical z-components to the ground plane is mainly observed. Each e-field distribution in the left- or right-half part in Fig. 2.9(b) has the opposite direction to the e-field in the other part. This results in cancelling the radiation of vertical z-component in the far field. Therefore, the low-profile antenna can radiate horizontal polarization to the ground plane, even if the ground plane is installed.

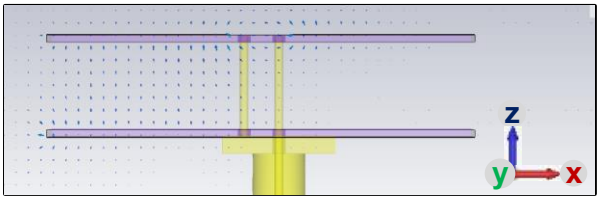

(a)

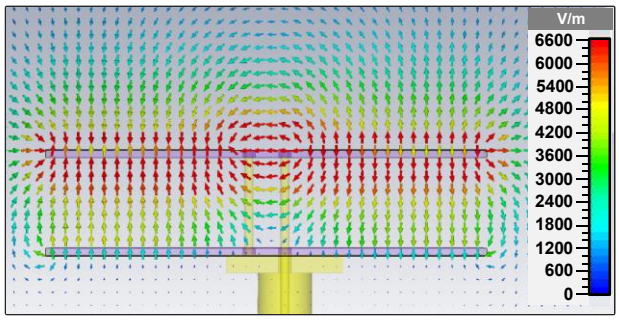

(b)

Figure 2.9 Electric field distribution in the x-z plane at a distance of 20 mm from the center of substrate along the y-axis (a) at ωt = 0˚ and (b) at ωt = 90˚.

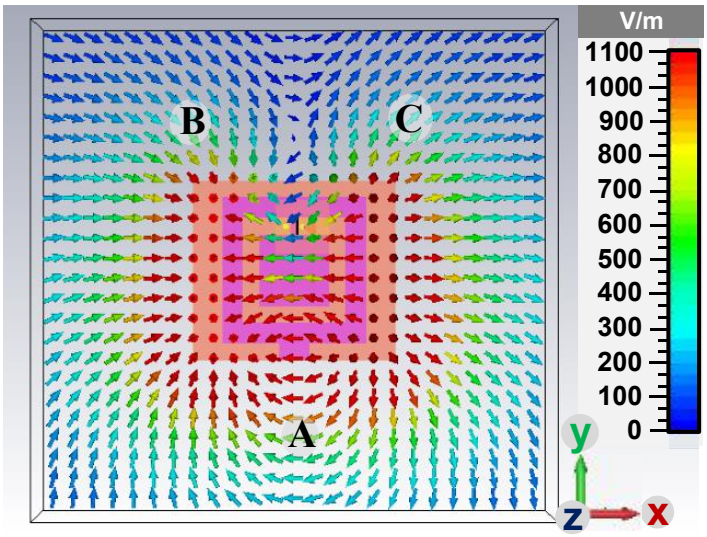

Figure 2.10 Electric field distribution in the x-y plane at a distance of 7 mm above the surface of the upper substrate at $\omega t = 90^{\circ}$.

The omnidirectional radiation pattern can be explained by the e-field distribution in the x-y plane at $\omega t = 90^{\circ}$ as shown in Fig. 2.10. The e-field behavior is explained here using the points *A*, *B*, and *C* in the figure. At the point *A*, strong e-field distribution directed parallel to x-direction is observed. The e-field at point *B* goes into the antenna element, and the e-field at *C* goes out of the element. The e-fields at points *B* and *C* are continuously connected in the far region. Given the fact that e-field is always continuous at a boundary, we can understand that the e-field distribution in Fig. 2.10 has a continuous distribution in the far region surrounding the antenna. Considering the behavior of e-field at the points *A*, *B* and *C*, the e-field finally forms a vortex-like e-field distribution which is parallel to the x-y plane at $\omega t = 90^{\circ}$, however showing such distribution in farther region is difficult because the simulating computer has an insufficient memory size. As a result, we can understand that the proposed antenna can have the horizontally polarized omnidirectional radiation pattern.

Similarly, we can observe the other omnidirectional radiation pattern in the y-z plane. As seen in the Figs. 2.8 and 2.10, we can find that the e-field is parallel to x direction around the antenna. On the other hand, as discussed as Fig 2.9, the radiation of e-field directed to ±z-directions is cancelled in the far field. These behaviors contribute to radiate the omnidirectional pattern in the y-z plane.

2.3.2 Effect of the Ground Plane Size

The effect of the ground plane size is discussed. The ground plane is extended in all directions in the x-y plane by parameter *g* as shown in Fig. 2.11.

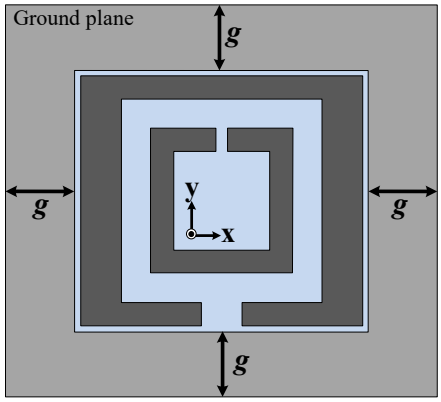

Figure 2.11 Direction of extension parameter *g*.

The simulated input impedance characteristics and $|S_{11}|$ as a function of *g* are shown in Fig. 2.12. From the results in Fig. 2.12(a), the kink size gets gradually magnified when expanding *g*. As a result, we can see that the ground plane size is affecting on the impedance of the proposed antenna.

The simulated radiation patterns in the y-z plane at the respective resonance frequencies with several *g* values are shown in Fig. 2.13. With an increase in *g* from 0 mm to 40 mm, the radiation pattern becomes bi-directional pattern when *g* = 40 mm as shown in Fig. 2.13(a). At the same time, the cross-polarization in ±z-direction (ϕ = 90˚, θ = 0˚, 180˚) becomes the strongest when *g* = 40 mm but is still lower by 20 dB than the co-polarization as shown in Fig. 2.13(b). Similarly, the cross-polarization in ±y-direction is not changed significantly.

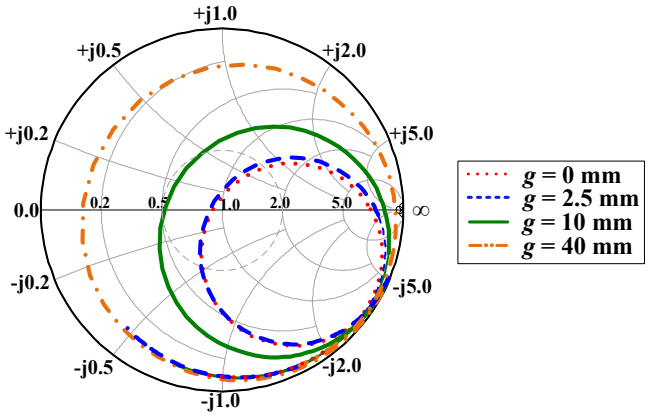

(a)

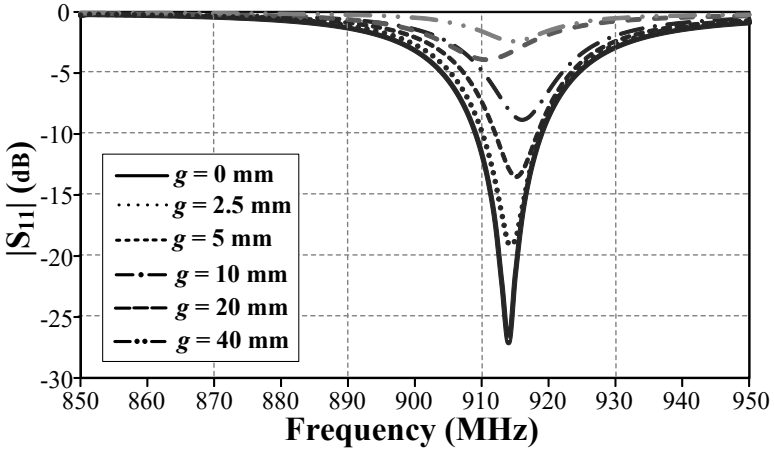

(b)

Figure 2.12 Simulated (a) input impedance characteristics and (b) $|S_{11}|$ characteristic as a function of g.

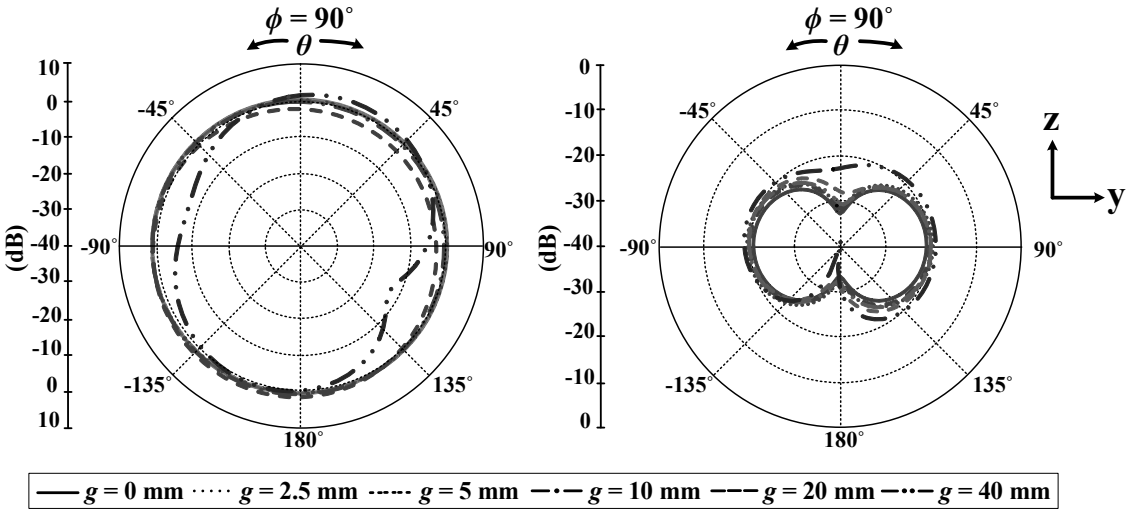

(a) (b)

Figure 2.13 Simulated radiation patterns in the y-z plane at respective resonance frequencies as a function of g (a) Co-polarization (E_ϕ), (b) Cross-polarization (E_θ).

The e-field distribution in the x-z plane with a larger ground size of g = 40 mm is shown in Fig. 2.14. Compared to Fig. 2.9(b), the e-field is spread from the element edges with the extension of g. This effect of edge yields the e-field directed to diagonal directions in x-z plane, therefore, the diagonal e-field arrows have components in z- and x-directions. The z-component of e-field around either the left or right edge is directed to the opposite direction in the z-direction to the z-component around the other edge. This results in cancelling out each other in the far field. Therefore, the vertical z-component to the ground is not radiated. On the other hand, with an increase in g, the component of e-field around both edges have gradually gets stronger at close positions of < $\lambda/4$ to the ground plane. Therefore, the input impedance is reduced and gets difficult to be matched well to 50 Ω as shown in Fig. 2.12. For good impedance matching, the horizontal component should be reduced, or the ring elements should not exist at a close position to the ground plane.

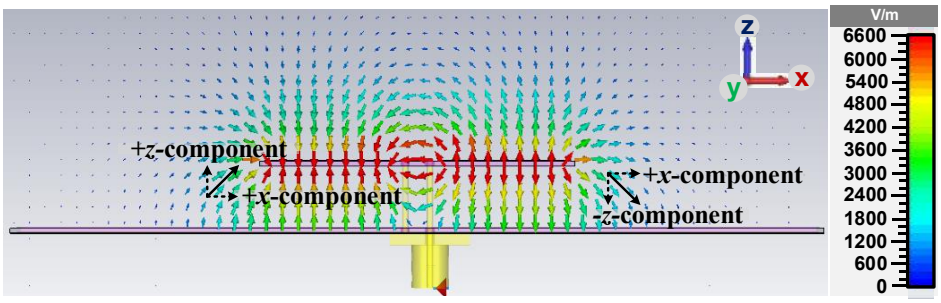

Figure 2.14 Electric field distribution in the x-z plane at distances of 20 mm from the center of substrate along the y-axis at $\omega t = 90^{\circ}$ for $g = 40$ mm.

2.3.3 Effect of Air Interval (*s*) between the Substrate and Ground Plane

In the case of the antenna with the ground plane, $|S_{11}|$ characteristics and radiation patterns are not changed significantly compared to the structure without ground plane. In Fig. 2.15, the impedance characteristics without ground plane are shown with a dotted line at the right side of the Smith chart circumference. When the ground plane is installed, the kink is shifted a little (solid line) along the circumference clockwisely as shown in Fig. 2.15. The shift is due to the two parallel feeding lines which have capacitive characteristics because, as shown with the dashed line in Fig. 2.15, the impedance is close to the impedance with no ground plane when the parallel feeding lines are removed.

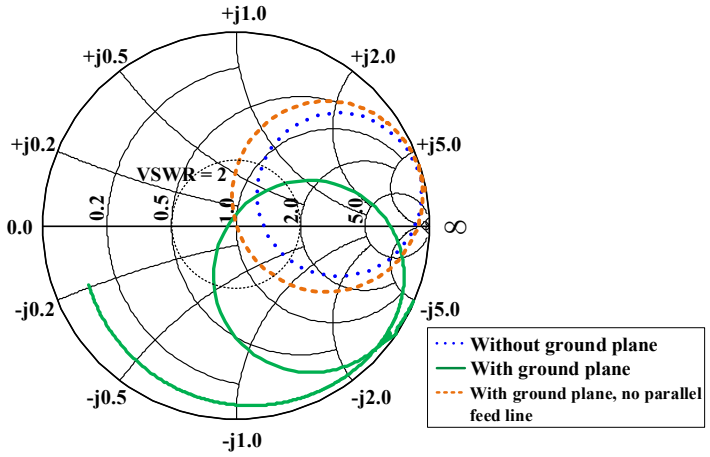

Figure 2.15 Effect of the ground and the parallel feeding line on the simulated input impedance characteristics.

The effect of the air interval s is discussed keeping g = 0 mm. The simulated input impedance characteristics are shown in Fig. 2.16 as a function of s. When s = 0 mm, the input impedance is too small resulting in a small kink around the circumference of the Smith chart (dotted line). When the s is increased from 3 mm to 13 mm, the kink becomes larger to achieve VSWR < 2 around the resonance frequency after being shifted clockwisely along the circumference of the Smith chart. Figure 2.17 shows the simulated radiation patterns in the y-z plane at the respective resonance frequencies of 1489, 887, 913, 924, and 898 MHz with an increase in s from 0 to 13 mm, however the pattern is not changed significantly in the range from s = 3 to 10 mm. The co- and cross-polarizations are not significantly changed except when s = 0 mm. As a result, the impedance is not sensitive to s in the range of around 3 to 10 mm, and the low-profile structure is available in this range. This is because, as discussed in Section 2.3.1, the contribution to radiation of the e-field from the interval is finally canceled out. Considering the e-field behavior in the interval, this behavior is also the reason why the impedance is not sensitive to the difference between the two structures with and without the ground plane as shown in Fig. 2.15. However, when s < 3 mm, the horizontal components of e-field get weaker because they are parallel to the ground plane, therefore, the impedance is affected by such small s value.

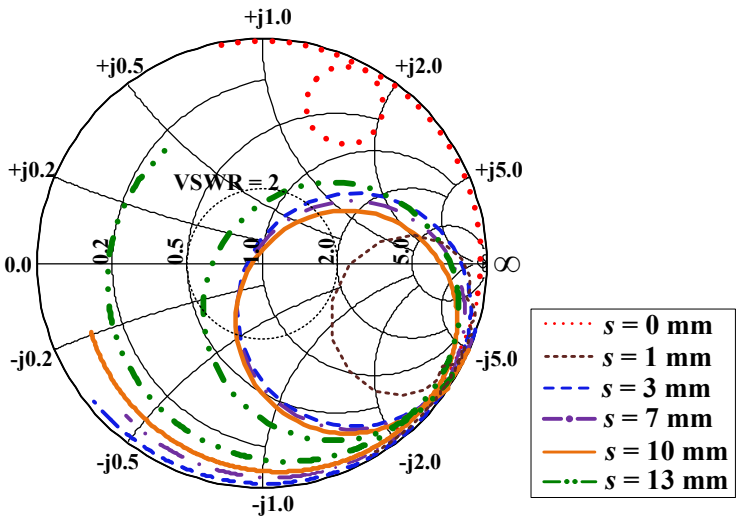

Figure 2.16 Simulated input impedance characteristics as a function of s.

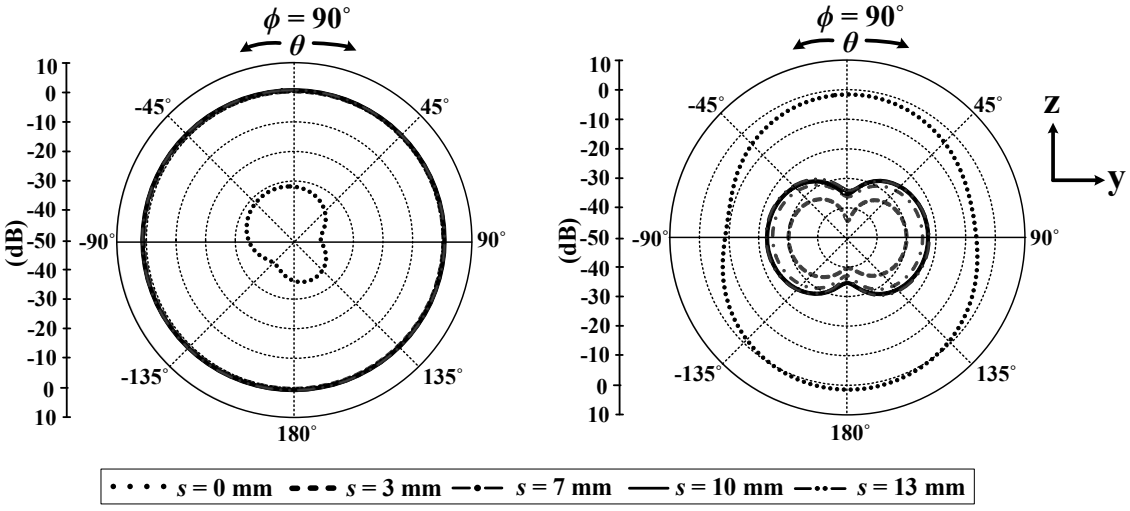

(a) (b)

Figure 2.17 Simulated radiation patterns in the y-z plane at respective resonance frequencies as a function of s (a) Co-polarization (E_ϕ) (b) Cross-polarization (E_θ).

Finally, the effect of the environment surrounding the antenna is discussed. As far as $s \geq 3$mm, the SRA with a small ground plane size of $g \leq 10$ mm has the similar performance as the antenna without ground plane. Hence, the characteristics of SRA are not sensitive to the small ground plane. This indicates that the SRA can be installed on compact handset applications keeping the same characteristics as that without ground plane. On the other hand, when $g > 10$ mm (large ground planes) and $s = 10$ mm, the antenna has small impedance around the resonance frequency with a large kink in Smith chart, as shown in Fig. 2.12(a). A decrease in s from 10 mm to 1 mm yields a smaller kink as shown in Fig. 2.16. As shown in the Fig. 2.18 for $g = 40$ mm and $s = 1$ mm, as an extreme example, the input impedance can be matched well to 50 Ω with $|S_{11}| < -10$ dB. The use of a larger ground plane has also advantages such as reducing the effects of the backing material on the antenna characteristics, however we have to note that the bandwidth is narrower in this case.

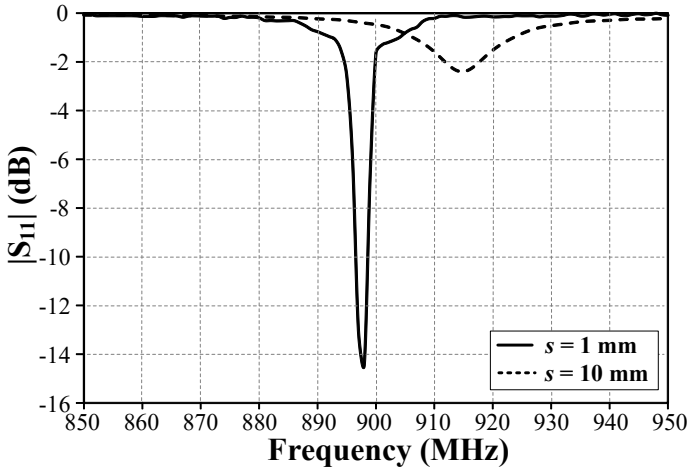

Figure 2.18 Simulated $|S_{11}|$ characteristics for a large ground plane with g = 40 mm.

2.3.4 Experimental Results

Figure 2.19 shows the photograph of prototype of the antenna with ground plane. The ground plane with the same size as the upper substrate is installed. Since the ground plane of the antenna is small, a bazooka balun has been equipped to suppress the leakage current on the coaxial cable. The simulated and measured results of $|S_{11}|$ are shown in Fig. 2.20. Comparing Fig. 2.20 with Fig. 2.4, the simulated and measured bandwidth is decreased by 0.5% each after installing the ground plane. The simulated and measured gains along +y-direction at 920 MHz are 1.45 dBi and 1.1 dBi, respectively, and the radiation efficiency is 99%. However, as shown in Fig. 2.21, the polarization and the radiation patterns are unchanged essentially from the pattern in Fig. 2.5 as far as using this size of ground plane. Polarization is still parallel to the substrate and ground, and the radiation pattern is still omnidirectional. Moreover, the ground plane has only a small effect on the antenna gain.

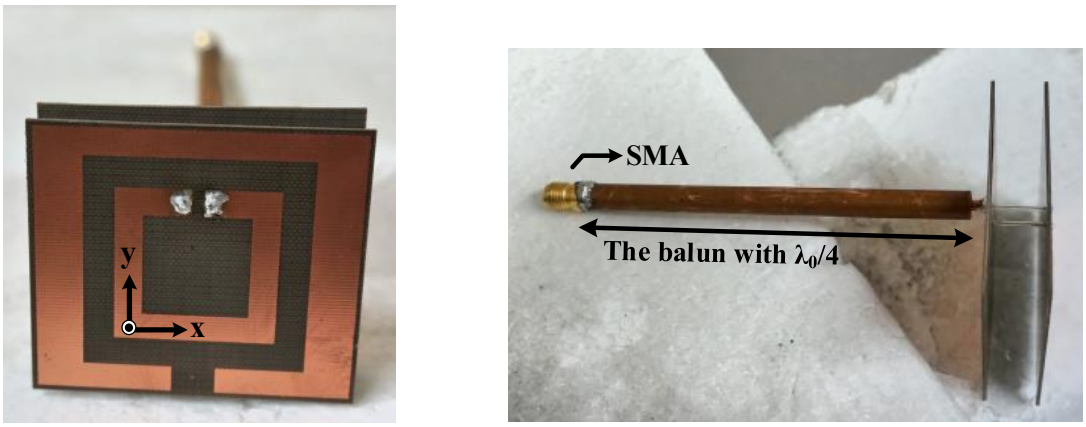

(a) (b)

Figure 2.19 The photograph of prototype antenna with ground plane.

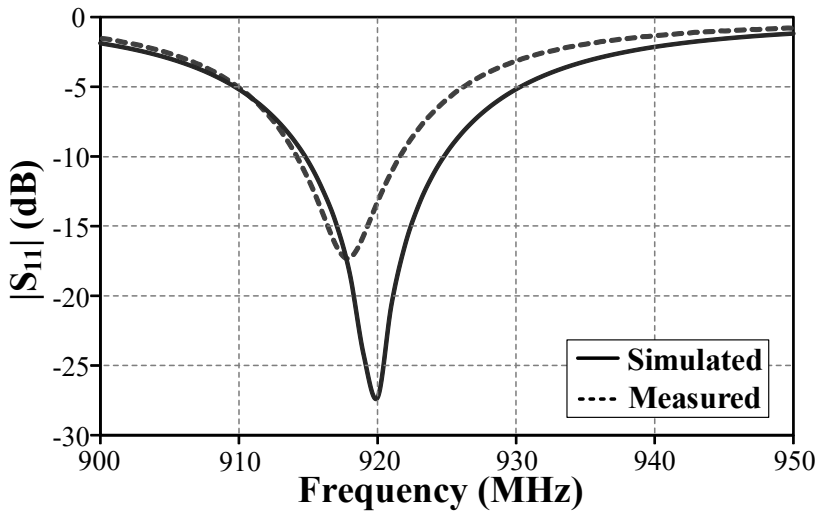

Figure 2.20 Simulated and measured $|S_{11}|$ characteristics.

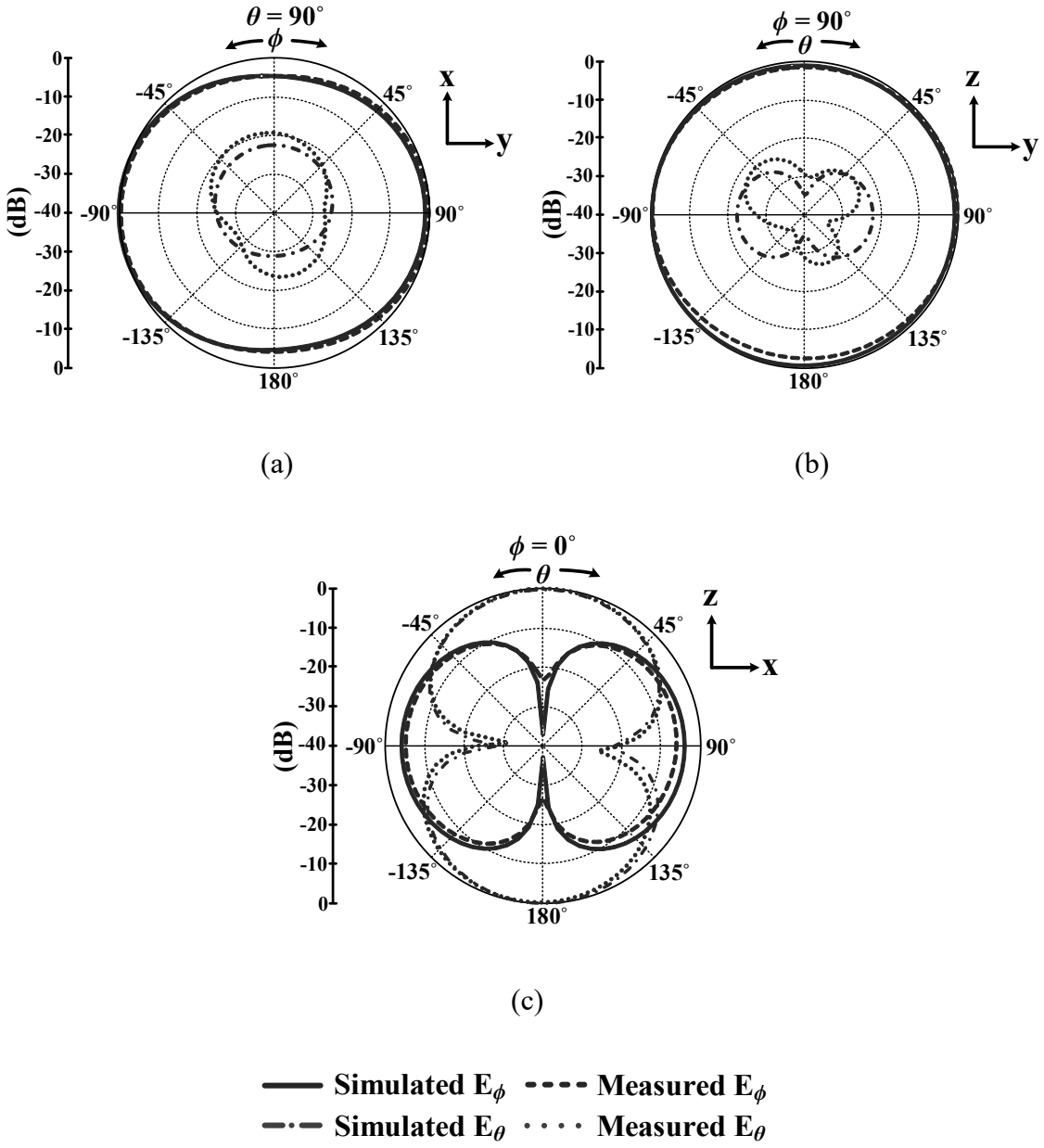

Figure 2.21 Radiation patterns at 920 MHz in (a) x-y plane, (b) y-z plane and (c) x-z plane.

2.4 Conclusion

This chapter has presented a compact and low-profile SRA with horizontally polarized omnidirectional radiation pattern. The simulated and measured results show that the antenna can radiate horizontal polarization and has approximately omnidirectional radiation pattern. The mechanism for achieving the low-profile structure and obtaining horizontally polarized omnidirectional radiation pattern can be explained by observing the electric field distributions.

With the advantages of low-profile structure, a low-profile polarization diversity antenna can be achieved by combining the SRA with a low-profile vertically polarized monopole antenna for base station and RFID reader applications [48]. Furthermore, the proposed SRA is a fundamental structure to be developed to CP antennas in the following chapters.

CHAPTER 3

LOW-PROFILE ANTENNA WITH DOUBLE U-SHAPED ARMS RADIATING CIRCULAR POLARIZATION PARALLEL TO GROUND PLANE

3.1 Introduction

For designing an RFID reader antenna, a CP antenna is suitable for a system which has unpredictable polarization alignment of the RFID tag. For advantages of a wearable reader, the reader should be low-profile. Therefore, a CP antenna should have a low-profile structure and a main beam parallel to the ground plane.

In the results in Chapter 2, the low-profile SRA can radiate horizontal polarization parallel to the ground plane in omnidirection. However, the polarization is linear. To generate CP, e-field must have two orthogonal (perpendicular) components with equal magnitude and 90-degree phase difference. The SRA in chapter 2 has been modified. In this chapter, the author proposes a combination of a half-cut structure of SRA (double U-shaped) and capacitive feeding structure for mainly matching impedance. A part of the antenna has bent by 90˚ in the x-y plane to make the main beam directed in the y-direction. The principle to generate CP in this antenna is also discussed in the chapter by observing the electric field (e-field) distribution.

3.2 Antenna Design

Figure 3.1 shows the proposed antenna structure consisting of double U-shaped strips and a capacitive feeding structure of both sides of Arlon Diclad 522 ($\varepsilon_r = 2.6$) with a thickness of $h = 0.8$ mm. The dimension is $L = 87$ mm ($0.27\lambda_0$) × $W = 37$ mm ($0.11\lambda_0$) in length and width. The air gap between radiating element and ground plane is chosen as 11.8 mm ($0.036\lambda_0$) as shown in Fig. 3.1(b). The length and width of double U-shape are optimized because these dimensions affect on the resonance frequency at which the length of U-shape is $\lambda_0/4$ as shown in Fig. 3.1(c). One of the arms of the U-shape (bent element) is bent by 90˚ in the x-y plane from the radiating element. This forms

a U-shaped slot with the ground plane on the bent element in the z-x plane. Figure 3.1(d) shows the capacitive feeding structure which is installed underneath the radiator (double U-shaped elements) and includes an L-shaped stub and an F-shaped stub with a capacitive gap for matching. The ground plane size is chosen so as to minimize the axial ratio (AR) in the y-direction and not to allow the leakage current on the coaxial cable. The ground plane size is extended in the +x and –y-directions with the same size by g = 20 mm, respectively from the substrate dimension. This effect will be discussed in Section 3.2.4.

The double U-shaped radiator determines the resonance frequency. Considering the principle to generate CP discussed later, the structure should have a half-cut structure of the split-ring resonator antenna [47] with the same resonance frequency as shown in Fig. 3.2. For making a low-profile structure on the ground plane, the feeding structure shown in Figure 3.1(d) should be used so as to keep sufficient impedance characteristics as discussed later. Furthermore, a part of the arms should be bent by 90˚ in the x-y plane so that the main beam can be directed in the y-direction. Table 3.1 shows the optimized structural parameters of the proposed antenna.

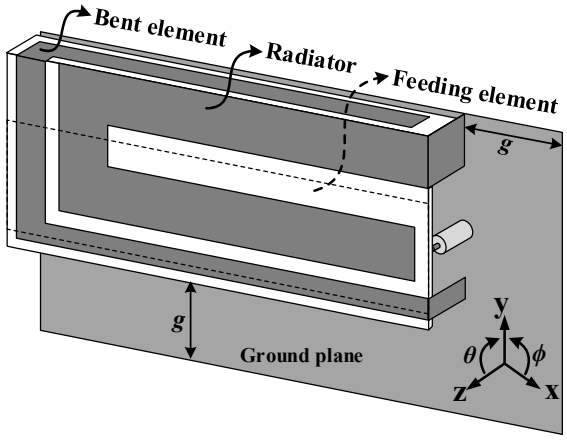

(a)

Figure 3.1 Geometry of the proposed antenna (a) Perspective view (b) Side view (c) Radiating element (d) Feeding element.

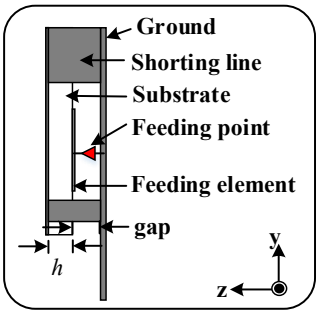

(b)

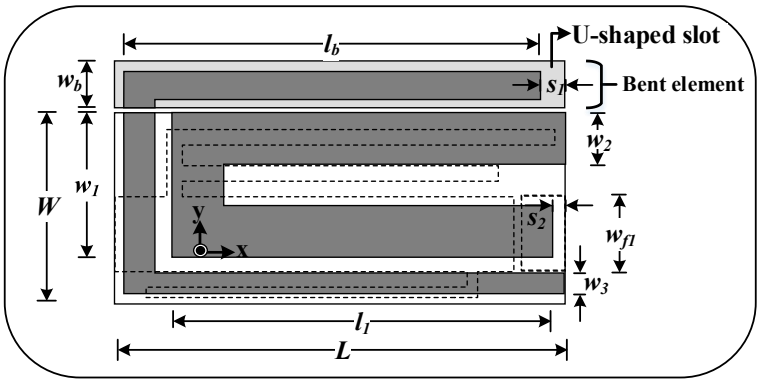

(c)

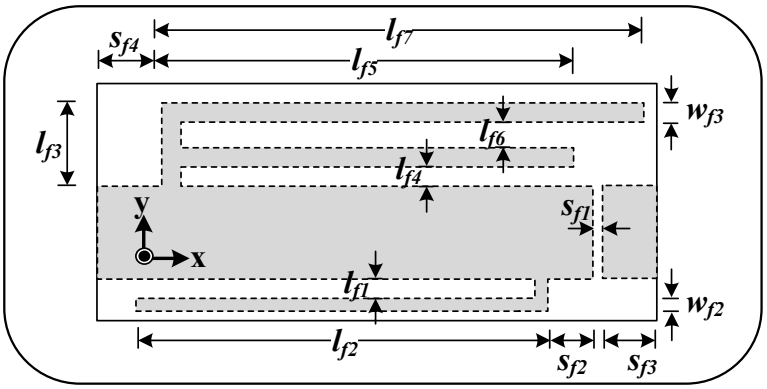

(d)

Figure 3.1 (Continued)

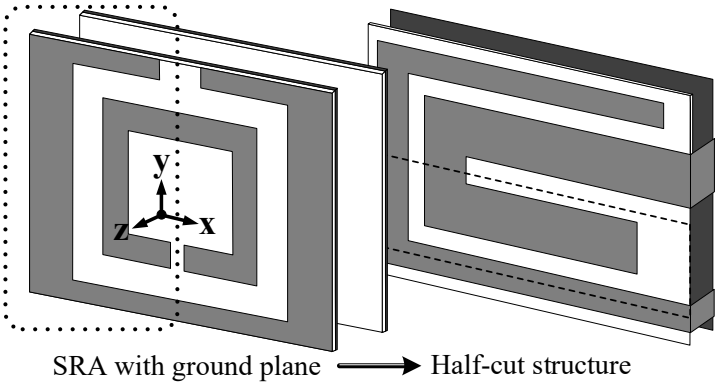

Figure 3.2 The antenna evolution.

Table 3.1 The optimized structural parameters of the antenna with double U-shaped arms.

Parameter	Size in mm	Parameter	Size in mm	Parameter	Size in mm	Parameter	Size in mm
L	87.0	w_b	9.0	s_{f1}	1.5	l_{f4}	3.0
W	37.0	l_b	80.5	s_{f2}	7.0	l_{f5}	61.0
h	0.8	s_1	10.0	s_{f3}	8.5	l_{f6}	4.0
w_1	28.0	s_2	5.0	s_{f4}	10.0	l_{f7}	75.0
w_2	10.0	w_{f1}	14.5	l_{f1}	3.0	g	20.0
w_3	4.0	w_{f2}	2.0	l_{f2}	64.0	gap	11.8
l_1	73.5	w_{f3}	3.0	l_{f3}	13.0		

3.3 Effects of Structural Parameters

The proposed antenna is low profile and can radiate CP in y-direction with respect to the ground plane. This chapter discussed the effects of structural parameters on AR and antenna gain.

3.3.1 Effects of Bent Element

One of interests in this antenna is a fact that CP is radiated in y-direction with $\theta = 90^{\circ}$ even though the structure is low-profile. Bending a part of U-shaped elements with a bent angle α (from 0° to 90°), as shown in Fig. 3.3, contributes to increase the θ angle of main beam direction in y-z plane ($\phi = 90^{\circ}$).

The input impedance characteristics can be kept the same, as shown in Fig. 3.4(a), in this range of α. When $\alpha = 0^{\circ}$, the peak gain can be observed in z-direction at 0° as shown in Fig. 3.4(b). With an increase in α from $30^{\circ}$to 90°, the main beam direction θ is shifted from 0° to 70° in y-z plane. For $\alpha = 90^{\circ}$, the 3-dB AR can be observed at $\theta = 90^{\circ}$ in y-z plane as shown in Fig. 3.4(c).

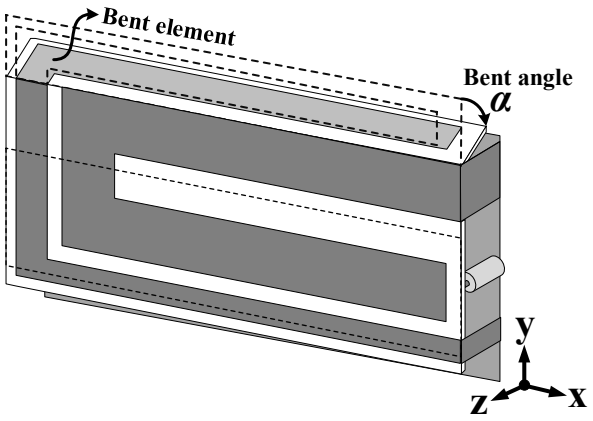

Figure 3.3 Direction of bending angle α on the element.

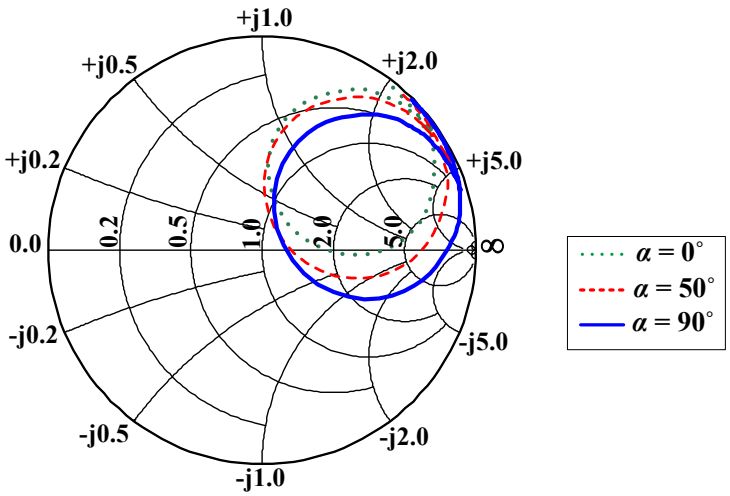

(a)

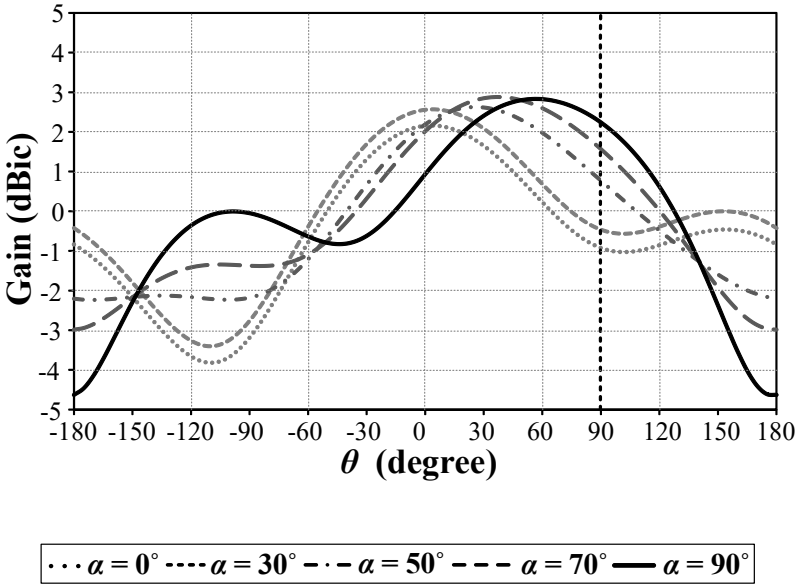

(b)

Figure 3.4 Simulated results of (a) input impedance characteristics with α (b) antenna gain pattern and (c) AR pattern of the proposed antenna in y-z plane at 925 MHz as a function of bending angle α ($\phi = 90^{\circ}$).

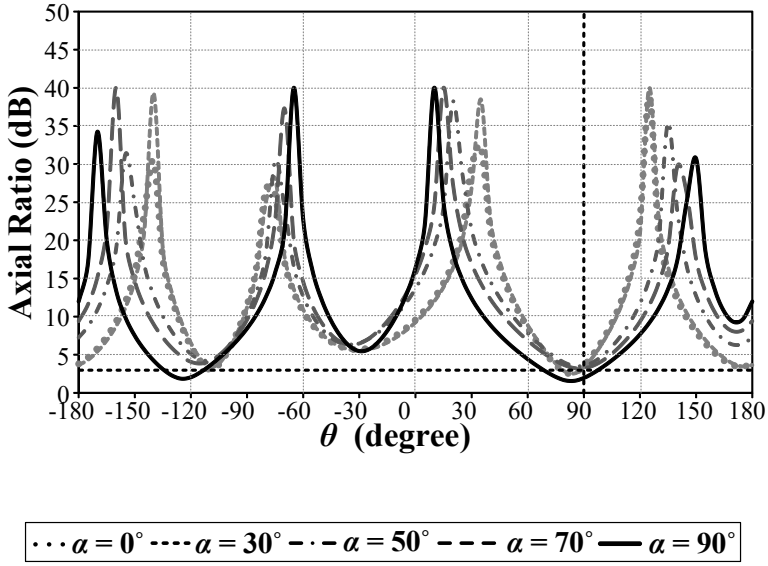

(c)

Figure 3.4 (Continued)

3.3.2 Effects of L-shaped and Capacitive Gap Feeding Structure

Effects of the stubs in feeding structure are discussed. The use of a coupled feeding line with the radiator element is one of techniques for designing low-profile antennas [16] to cancel the inductivity at a frequency range with around 50-Ω impedance. Figure 3.5 shows the evolution of feeding structure that starts from a simple rectangular strip to the proposed structure with adding capacitive gap, L-shaped stub on a lower edge of line, short stub, long stub and F-shaped stub on an upper edge.

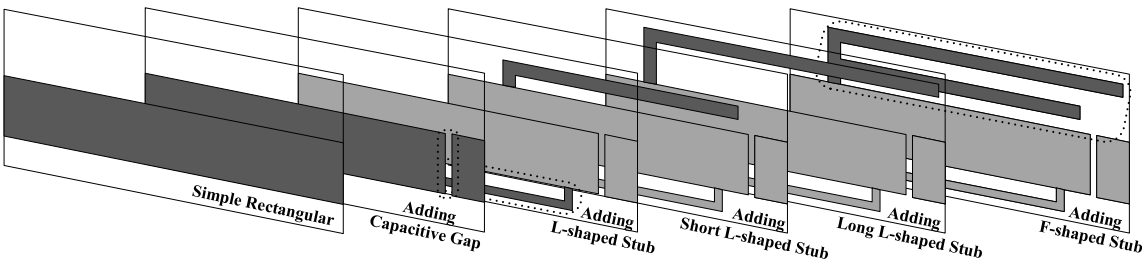

Figure 3.5 Feeding structure evolution.

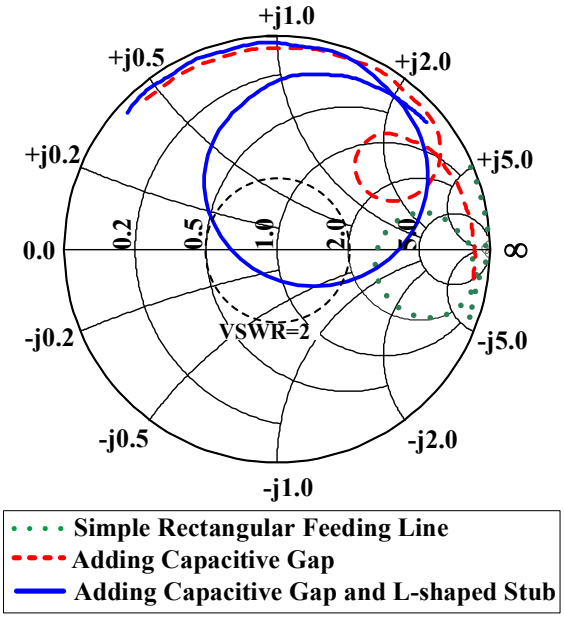

Figure 3.6 Simulated input impedance characteristics when gap and L-shaped stub are installed.

For matching to 50-Ω with a sufficient bandwidth, the capacitive gap and the L-shaped stub are installed resulting in the shift of the characteristics as shown in Fig. 3.6. With the simple rectangular feeding structure, the input impedance characteristic shows a small kink (with a dotted line) at the right side of the Smith chart centering the horizontal axis. When only the capacitive gap is installed, the kink is shifted to a different place (the kink shown with a dashed line) along the circle of a real axis counterclockwisely. After this, when the L-shaped stub having a parallel capacitance is installed, the kink, shown with a solid line, is magnified passing the center showing a narrow bandwidth since the kink size is still bigger than the circle of VSWR = 2.

3.3.3 Effects of F-Shaped Stub Feeding Structure

As the final step, the F-shaped stub is installed for enhancing bandwidth. The F-shaped stub is a combination of short and long L-shaped stubs. Figure 3.7(a) shows the effect of installing the short and long L-shaped stubs on input impedance characteristics. When the short stub is installed, the impedance can be matched well to 50 Ω with a sufficient bandwidth, however, as shown in Fig. 3.7(b), the main beam direction is around 60˚. On the other hand, when the long stub is installed, the main beam direction is shifted

closer to $\theta = 90^{\circ}$ as shown in Fig. 3.7(b), however, the impedance bandwidth is narrow as shown in Fig. 3.7(a) with a larger kink.

The F-shaped stub has the both functions of the short and long stubs, that is, the short stub is required for matching, and the long stub is for radiating CP in the direction at $\theta = 90^{\circ}$. Similarly, the F-shaped stub makes a small kink inside the circle of VSWR = 2 in Smith chart and also makes the main beam direction closer to $\theta = 90^{\circ}$ resulting in 3-dB AR in +y direction as shown in Figs. 3.7(b) and (c). With the metallic arm along +y direction of the long or F-shaped stub, the e-field inside radiator can be perpendicular to the ground plane and the stub element nearby U-shaped slot. This behavior leads to direct the main beam closer to $\theta = 90^{\circ}$. As a result, in the final structure, the simulated and measured impedance can be matched to 50-Ω as shown in Fig. 3.7(a) with the simulated bandwidth of 18 MHz, and the main beam direction is at $\theta = 70^{\circ}$ as the results will be shown in Section 3.5. In the direction at $\theta = 90^{\circ}$, AR can be kept less than 3 dB with a sufficient simulated gain of 1.8 dBic.

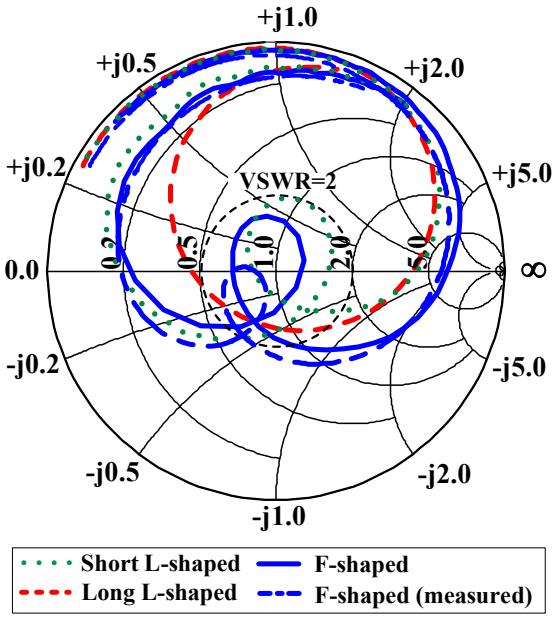

(a)

Figure 3.7 Simulated results of (a) input impedance characteristics (b) normalized magnitude and (c) AR pattern with θ ($\phi = 90^{\circ}$) in y-z plane at 925 MHz when the short, long, and F-shaped stubs are installed.

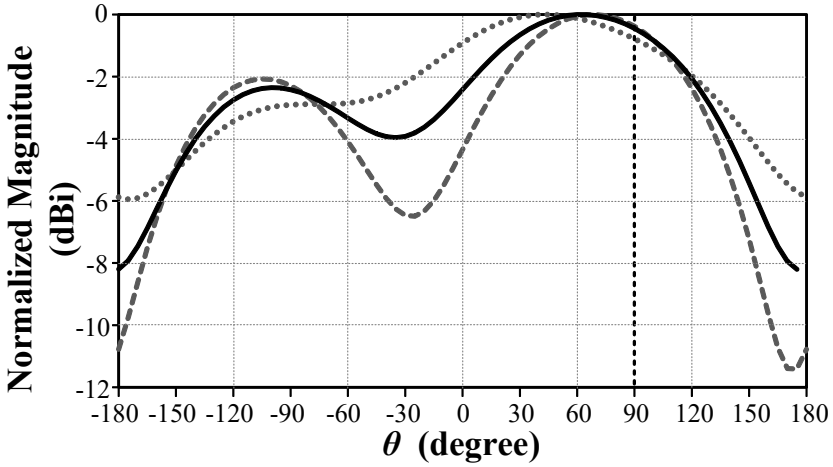

(b)

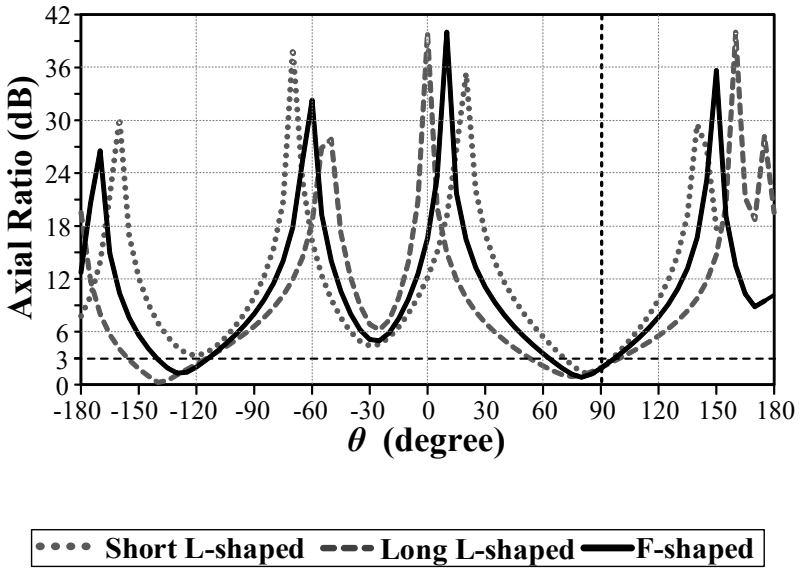

(c)

Figure 3.7 (Continued)

3.3.4 Effects of Ground Plane Size

Figure 3.8(a) shows the variation in AR pattern with the ground plane size. Comparing the size (default) which is the same as the radiator in x-y plane, the ground plane is extended by g = 20 mm in +x- and –x, +x and –y, –x and –y, and ±x and y-directions at the same time. When the ground is extended in +x and –y-directions, the AR is minimized at around $\theta = 90^{\circ}$. This extension in the +x-direction contributes to have the

e-field, near the open end of radiator, directed in x or z direction in wider area of x-z plane at $\omega t = 0^{\circ}$ or 90°, respectively. In this case, the half-power beamwidth (HPBW) is about 105° covering the $\theta = 90^{\circ}$ direction as shown in Fig. 3.8(b).

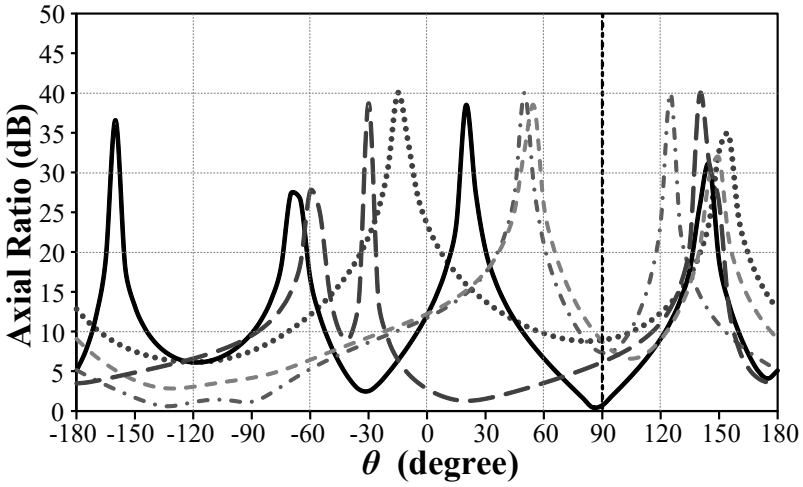

(a)

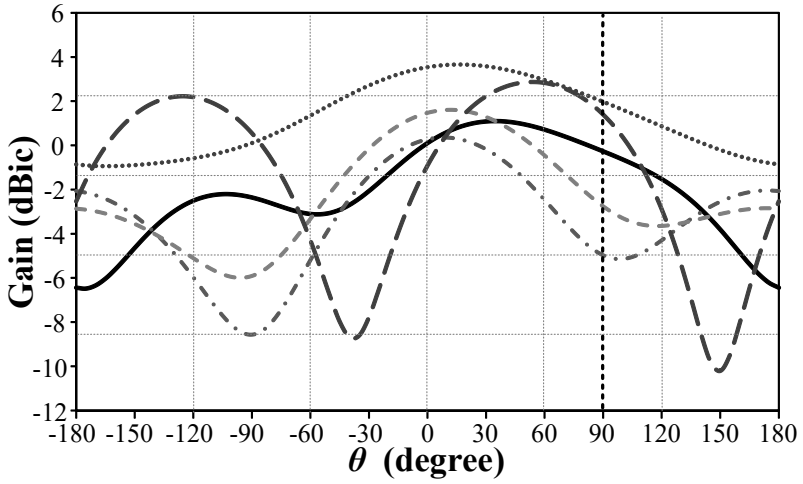

(b)

Figure 3.8 Simulated results of (a) AR pattern and (b) antenna gain in y-z plane at 925 MHz as a function of the ground plane size by $g = 20$ mm ($\phi = 90^{\circ}$).

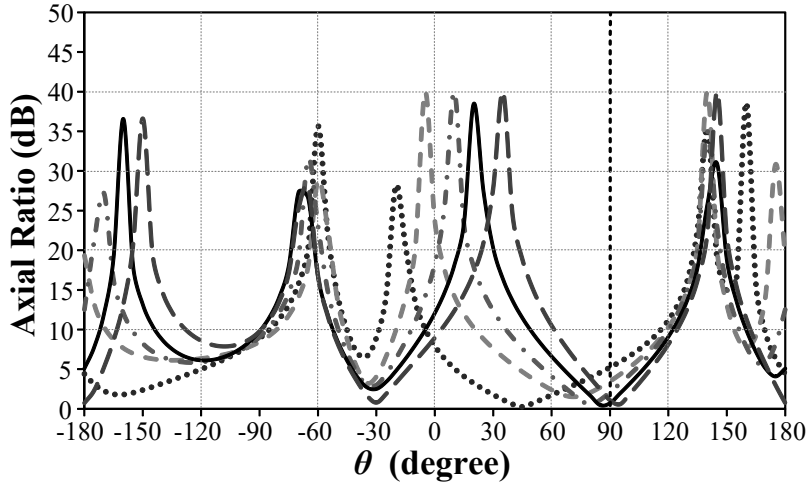

(a)

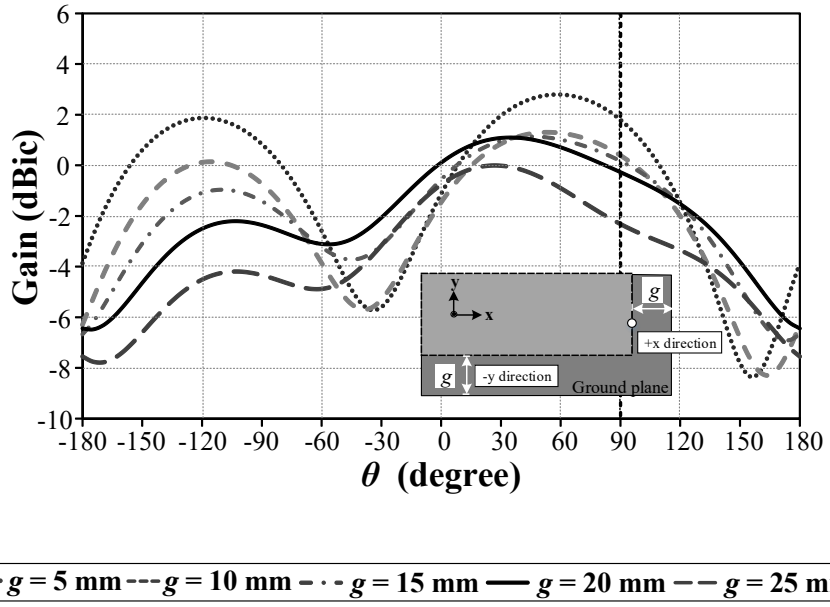

(b)

Figure 3.9 Simulated results of (a) AR pattern and (b) antenna gain in y-z plane at 925 MHz as a function of the extension in +x and –y-directions g ($\phi = 90^{\circ}$).

For the extension in the +x and –y-directions, the main beam direction in which the minimum AR can be obtained gets closer to $\theta = 90^{\circ}$ with an increase in g from 5 to 25 mm as shown in Fig. 3.9(a). For g = 25 mm, the angle for the minimum AR is the closest to $\theta = 90^{\circ}$, however, the antenna gain at $\theta = 90^{\circ}$ is smaller than that for g = 20 mm as shown in Fig. 3.9(b). Therefore, the parameter g should be chosen as 20 mm for this design.

Choosing g = 20 mm with the extension in the +x and –y-directions, we have confirmed that the ground plane size has a sufficient area enough to suppress the leakage current on the coaxial cable.

3.4 The Generation Mechanism of Circular Polarization by Discussing the Distribution of Electric Field

The antenna elements have two metallic layers sandwiching the dielectric substrate to equip the radiator and the feeding structure with L-shaped and F-shaped stubs. The radiator and the feeding structure have been overlapped as shown in Fig. 3.1(c). The e-field (electric field) distributions at ωt = 0˚ and 90˚, where the voltage at feeding point is assumed to be $V = V_0 \sin \omega t$ are shown in Fig. 3.10. At ωt = 0˚, the strongest field of Z-component is found mainly around the U-shaped slot on the bent element as shown in Fig. 3.10(a). As shown in Fig. 3.11(a), e-field directed to +z with high density can be found, however, the e-field to –z shows low density. This asymmetrical distribution is due to the difference in the presence of the radiator and ground plane. At ωt = 90˚, strong field directed in x and ±z-directions can be found on the U-shaped slot as shown in Fig. 3.10(b), however, the components in ±z-directions are finally canceled out by each other in the far field. Since the length between feeding point (around x = 0 mm) on feeding line and the bent part of the U-shaped slot is about half wavelength, the voltage at feeding line gets lower at 90˚ phase than that at the bent point in the U-shaped slot. Therefore e-field is pulled into the feeding line as shown in Fig. 3.11(b) resulting in having a symmetrical distribution between ±z-directions. As a result, at ωt = 90˚, only the x-component at the bent part of the U-shaped slot contributes to radiate. With the same analogy, the e-field generates CP with 90˚-phase difference of orthogonal e-field components at ωt = 180˚ and 270˚, respectively.

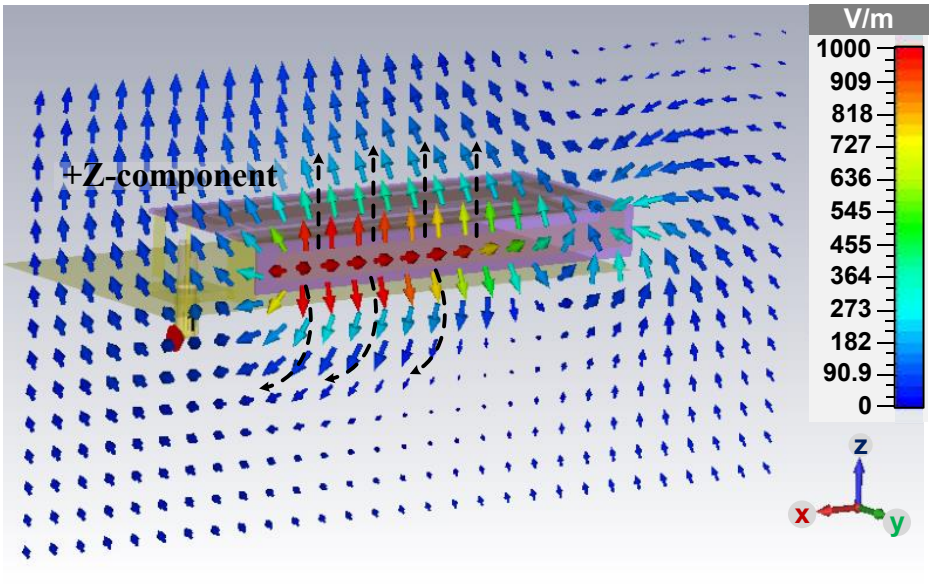

(a)

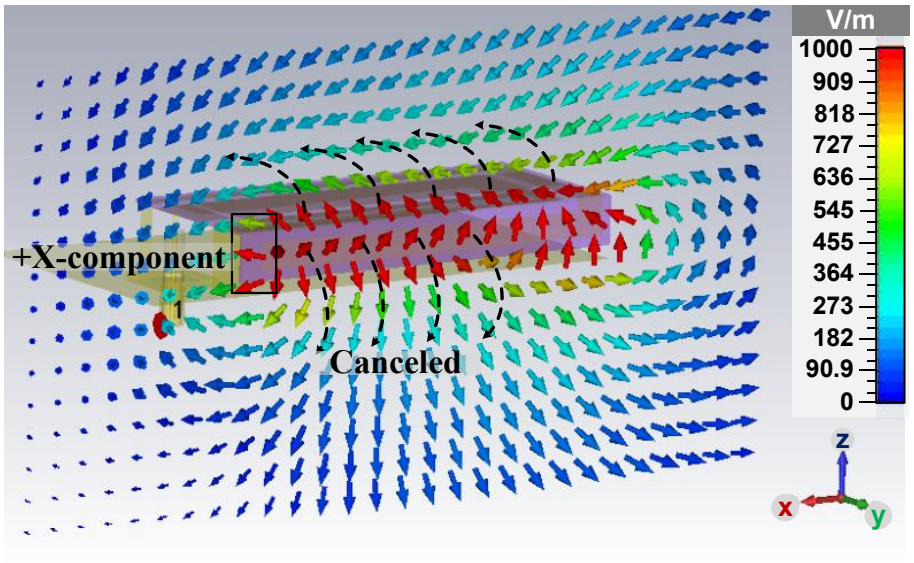

(b)

Figure 3.10 Electric field distributions at 920 MHz in x-z plane at 26.5 mm away from feeding point along y axis (a) for $\omega t = 0^{\circ}$, (b) for $\omega t = 90^{\circ}$.

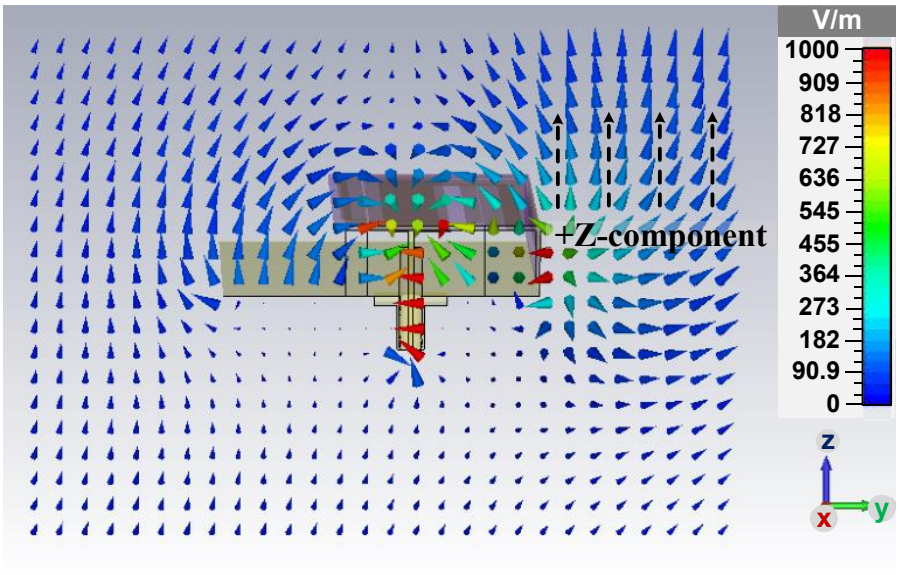

(a)

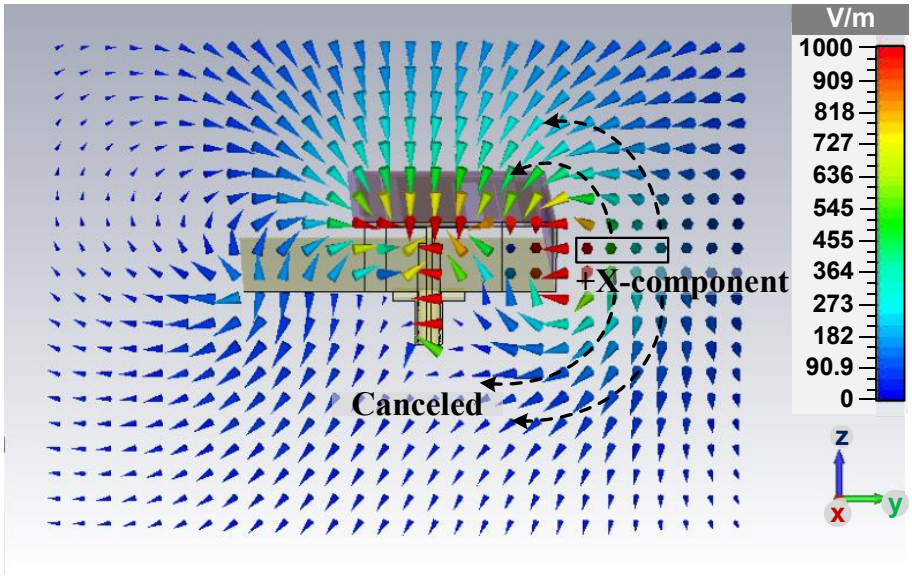

(b)

Figure 3.11 Electric field distributions at 920 MHz in y-z plane at 0 mm away from feeding point along x axis (a) for $\omega t = 0^{\circ}$, (b) for $\omega t = 90^{\circ}$.

On the other hand, this antenna radiates the same sense of CP which the 3-dB AR can be obtained at $\theta = -120^{\circ}$. This radiation is explained by the e-field behavior around feeding point outside of radiating element. At $\omega t = 0^{\circ}$, the normal e-field can be observed by the same principle of U-shaped slot mentioned above. At $\omega t = 90^{\circ}$, the e-field is pulled

into the feeding point following the same principle of above explanation. Therefore, the e-field rotates in clockwise direction with respect to –y-direction.

3.5 Experimental Results

Figure 3.12 shows the photograph of fabricated antenna.

(a)

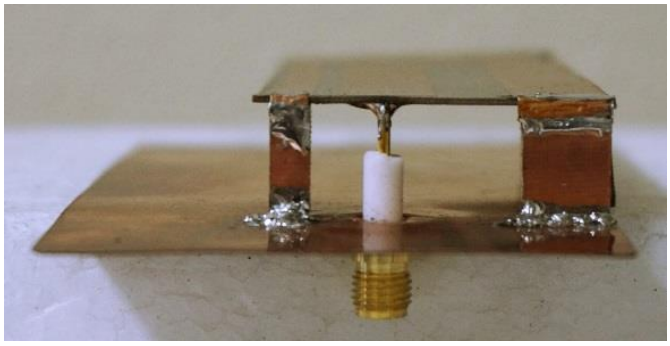

(b)

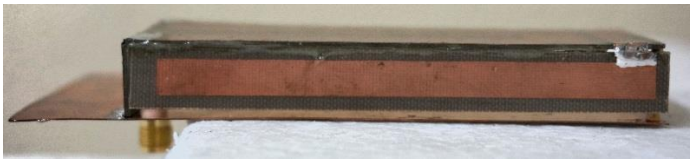

(c)

Figure 3.12 Photograph of the fabricated antenna: (a) front view, (b) side view, and (c) bottom view.

Figure 3.13 shows the simulated and measured $|S_{11}|$ characteristics. The simulated and measured $|S_{11}|$ bandwidth at -10 dB are found from 916 MHz to 934 MHz (1.8%) and 916 MHz to 930 MHz (1.4%), respectively, covering a typical UHF RFID band (920 to 925 MHz: Thailand).

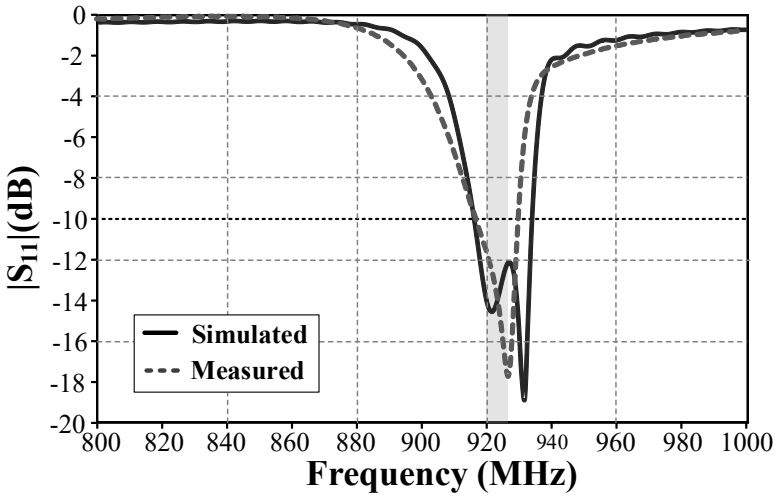

Figure 3.13 Simulated and measured $|S_{11}|$.

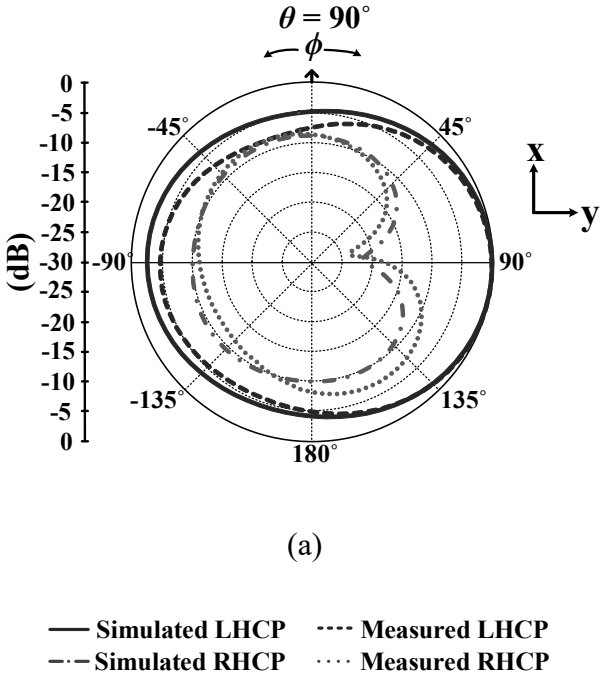

(a)

Figure 3.14 Radiation patterns at 925 MHz (a) x-y plane (b) y-z plane.

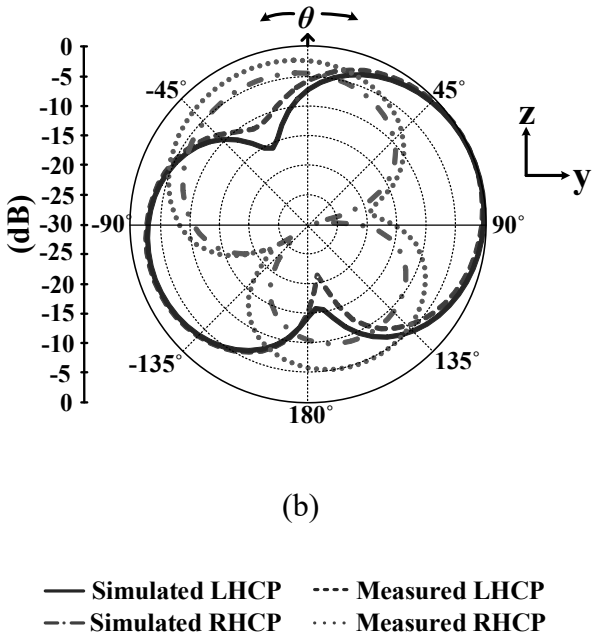

(b)

Figure 3.14 (Continued)

The simulated and measured radiation patterns of left-hand CP (LHCP) and right-hand CP (RHCP) at 925 MHz are shown in Fig. 3.14 in x-y plane and y-z plane. The simulated and measured HPBW of RHCP are 105˚ and 110˚, respectively, in y-z plane where the main beam (RHCP) direction is declined only by 20˚ from y-direction (parallel to ground plane). However, the obtained gain in y direction is slightly lower by only 0.6 dB than that in the main beam direction. The simulated and measured gains are 1.8 dBic and 2.8 dBic, respectively in y-direction. The radiation patterns of RHCP and LHCP have been normalized by the simulated and measured peak gain of RHCP (Co-polarization), respectively. Therefore, we can understand that, in y-direction, the cross-polarization of LHCP is more than 15 dB lower than RHCP. This indicates that the AR in y-direction is less than 3 dB. Furthermore, considering the discussion below, it can be said that the measured results of radiation patterns show reasonable agreements with simulated results.

As shown in Fig. 3.15(a), the AR in y-z plane are less than 3 dB in the θ angle range from 70˚ to 95˚ and from 70˚ to 90˚ for simulated and measured results, respectively. In the boresight direction at $\theta = 90^{\circ}$, the measured AR is higher by approximately 1 dB than the simulated AR, although the measured AR is at around 3 dB. Considering the results of radiation performances discussed above with Figs. 3.14 and 3.15, we can find small differences between the simulated and measured results, although they show reasonable

agreements. The small differences are mainly due to fabrication errors, especially those are related to our hand-made fabrications of U-shaped slot. As shown in Fig. 3.15(b), the 3-dB AR in y-direction can also be observed in UHF band. As a result, we can understand that the proposed antenna can radiate CP in y-direction covering the UHF RFID band.

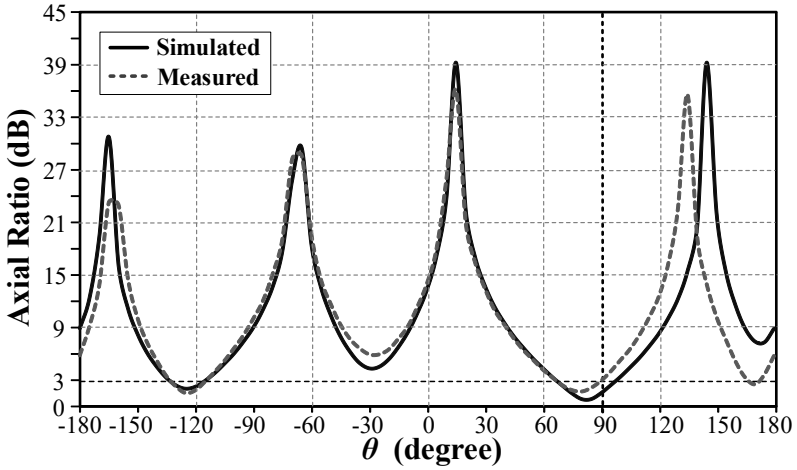

(a)

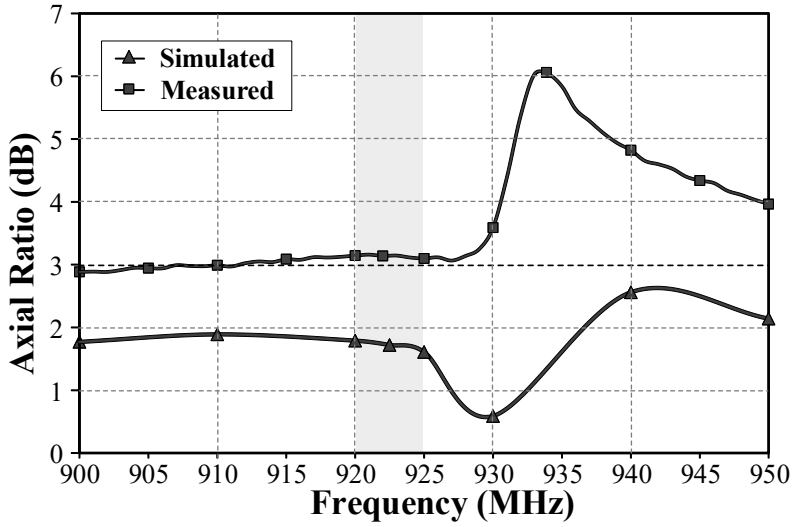

(b)

Figure 3.15 Simulated and measured AR pattern of the proposed antenna in y-z plane ($\phi = 90^{\circ}$) at 925 MHz (a) as a function of θ and (b) as a function of frequency at $\theta = 90^{\circ}$.

3.6 Conclusion

This chapter has proposed a low-profile and circularly polarized antenna with double U-shaped arms considering an application for handheld RFID readers from 920 MHz to 925 MHz band. The structure consists of a modified double U-shaped radiator and ground plane. A part of arms of the radiator has been bent by 90˚ in x-y plane for directing CP radiation parallel to the ground plane (θ = 90˚). For keeping sufficient impedance bandwidth for RFID band, some matching stubs and a capacitive gap have been installed on the feeding structure, and the design process has been discussed. In addition to them, the effects of ground plane size on the CP direction have been discussed, and a sufficient antenna gain has been also confirmed in this direction. The measured results show good agreements with the simulated results. Furthermore, the principle for generating CP has been analyzed taking notice of e-field distributions. Based on this principle, the U-shaped slot can contribute to achieve a low-profile antenna for radiating CP parallel to the ground plane.

CHAPTER 4

ELECTRICALLY SMALL ANTENNA RADIATING CIRCULAR POLARIZATION WITH OMNIDIRECTIONAL RADIATION PATTERN IN HORIZONTAL PLANE

4.1 Introduction

Applications of wireless sensor networks are of interest to the most diverse fields. Omnidirectional CP antennas are widely implemented in WSNs because they can effectively reduce polarization mismatch among the nodes. In last few years, trend of the communication devices has dramatically decreased weight and size. The challenge in designing a small antenna is to keep sufficient performance properties such as impedance, radiation efficiency and pattern, especially in electrically small antennas (ESAs) which have very small size compared to wavelength. In literature reviews, many researches proposed various antenna designs with omnidirectional CP. However, author's review of existing literatures has found no research on ESAs generating CP in omnidirection.

This chapter proposes an ESA with omnidirectional CP radiation pattern with potential applications in WSNs and mobile handsets. A novel concept to generate CP is also discussed by observing electric field (e-field) distribution.

4.2 Antenna Design

Figure 4.1(a) is the perspective view of the antenna structure with Arlon Diclad522 (ε_r = 2.6, tanδ = 2.0×10^{-4}) having upper and lower substrates with 0.8-mm thickness (h) each. Both substrates are of identical dimensions, i.e. 48 mm (0.14λ_0) in length (L) and 20 mm (0.06λ_0) in width (W). Underneath the upper substrate, a rectangular feeding element with a length of l_1+l_2 is electromagnetically coupled with two U-shaped elements that enclose the loop element, as shown in Fig. 4.1(b). A vertical element is connected to rectangular feeding element and is perpendicular to lower substrate.

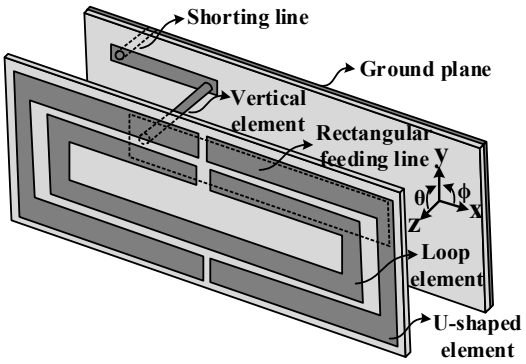

(a)

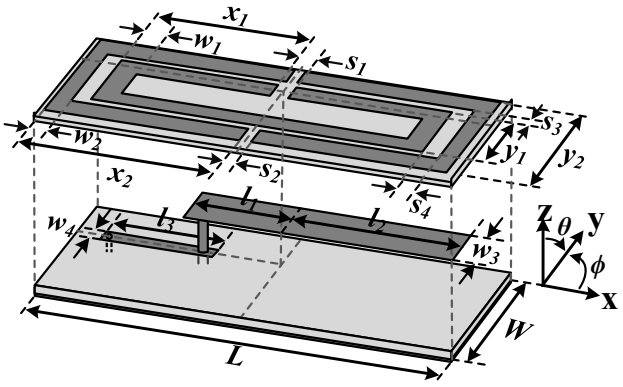

(b)

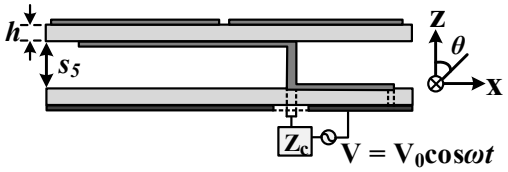

(c)

Figure 4.1 Geometry of the proposed antenna (a) Perspective view (b) Slanted view and (c) Side view.

The electrical size of the antenna is ka = 0.476 (i.e. < 0.5), which satisfies the definition of ESA [49]. As shown in Fig. 4.1(c), the interval between both substrates (s_5) is 12.2 mm ($0.036\lambda_0$), and Z_c is the impedance of feeding circuit. Underneath the lower substrate is the ground plane. On top of substrate, it is a parallel inductive stub which is connected to vertical element for impedance matching.

Table 4.1 presents the optimal structural parameters. The target is to generate omnidirectional CP in x-y plane with 3-dB axial ratio using the ESA with $ka < 0.5$. Due to equipment limitations of fabrication and simulation environment, the final frequency is 893 MHz even though the target operation frequency was in 900 MHz band. Therefore, 893 MHz was used as the test frequency.

Table 4.1 The optimized structural parameters of ESA.

Parameter	Size in mm	Parameter	Size in mm
W	20	s_4	2
L	48	s_5	12.5
x_1	19	w_1	2.5
x_2	23	w_2	2
y_1	10	w_3	6
y_2	18	w_4	2
s_1	2	l_1	10
s_2	1	l_2	23
s_3	1	l_3	10

4.3 The Generation Mechanism of Circular Polarization by Discussing the Distribution of Electric Field

This section describes the mechanism of CP generation, assuming that this antenna is fed with $V = V_0 \cos \omega t$, where V is the voltage at feed point. Figures 4.2 and 4.3 illustrate the e-field distributions at different distances from the nearest substrate edge in y-z plane.

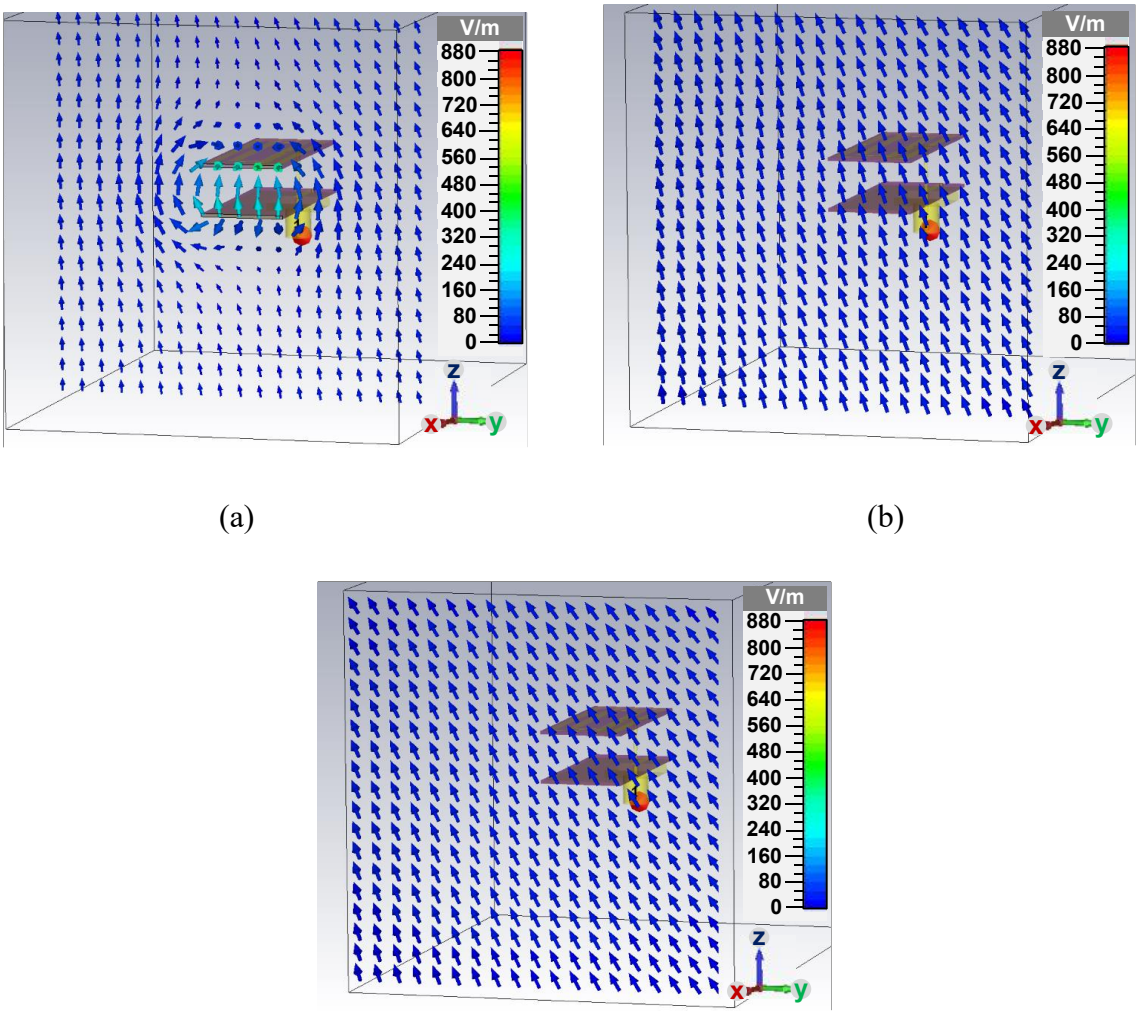

(a) (b)

(c)

Figure 4.2 The electric field distributions in the y-z plane at (a) 0 mm, (b) 20 mm and (c) 37 mm away from the substrate edge along the x axis at $\omega t = 0^{\circ}$.

In Fig. 4.2(a), at $\omega t = 0^{\circ}$ and 0 mm distance from the substrate edge (defined as "the very near region") along x-axis, the e-field between elements on the upper substrate and the ground plane is directed toward +z-direction. Figures 4.2(b) and (c) indicate that, at distances of 20 mm and 37 mm ("the far region") from the substrate edge along x-axis, almost all the e-fields are directed toward +z-direction, and the strongest current flows along vertical element in +z direction when $\omega t = 0^{\circ}$.

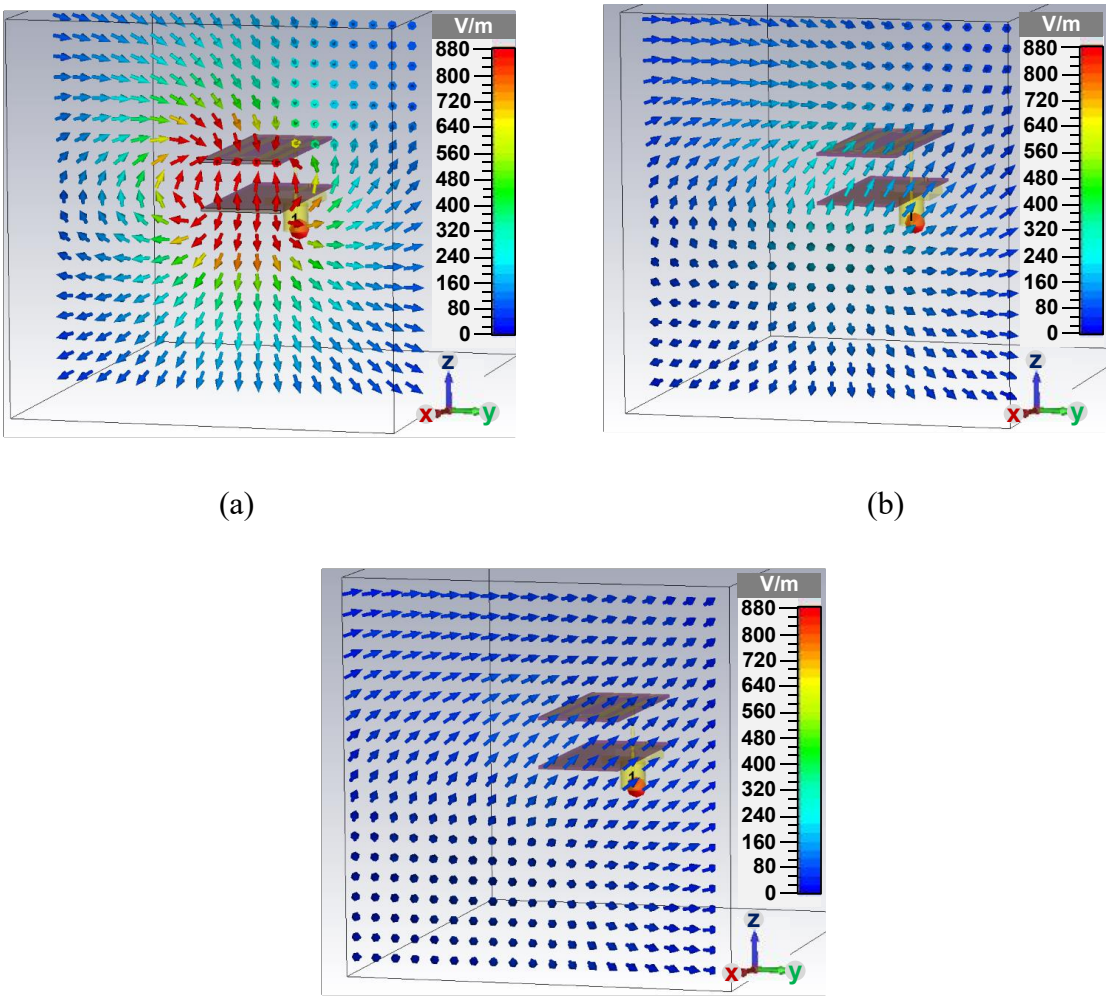

(a) (b)

(c)

Figure 4.3 The electric field distributions in the y-z plane at (a) 0 mm, (b) 20 mm and (c) 37 mm away from the substrate edge along the x axis at $\omega t = 90^{\circ}$.

In Fig. 4.3(a), at $\omega t = 90^{\circ}$, the e-field at a 0 mm distance from the substrate edge is directed toward the +z-direction, similar to the distribution at $\omega t = 0^{\circ}$. However, in Figs. 4.3(b) and (c), most of the e-fields at the 20 mm and 37 mm distances are turned and directed to +y-direction farther away from the initial edge.

With each advance in phase at the feeding signal, the e-field is rotated by 90˚ compared to the e-field at the previous phase in the far region, as shown in, for example, Figs. 4.2(c) and 4.3(c) in which $\omega t = 0^{\circ}$ and $\omega t = 90^{\circ}$, respectively. The arrowheads of the e-fields at $\omega t = 180^{\circ}$ and 270° are in reverse of those at $\omega t = 0^{\circ}$ and 90°, respectively. Thus the proposed antenna generates CP, as a result. In Figs. 4.3(b) and (c), the e-fields at the

distances of 20 mm and 37 mm are not a complete 90˚ turn due to an insufficient computer memory to simulate the farther regions. A comparison of both figures nevertheless indicates a gradual 90˚ turn of the e-field farther from the x-axis.

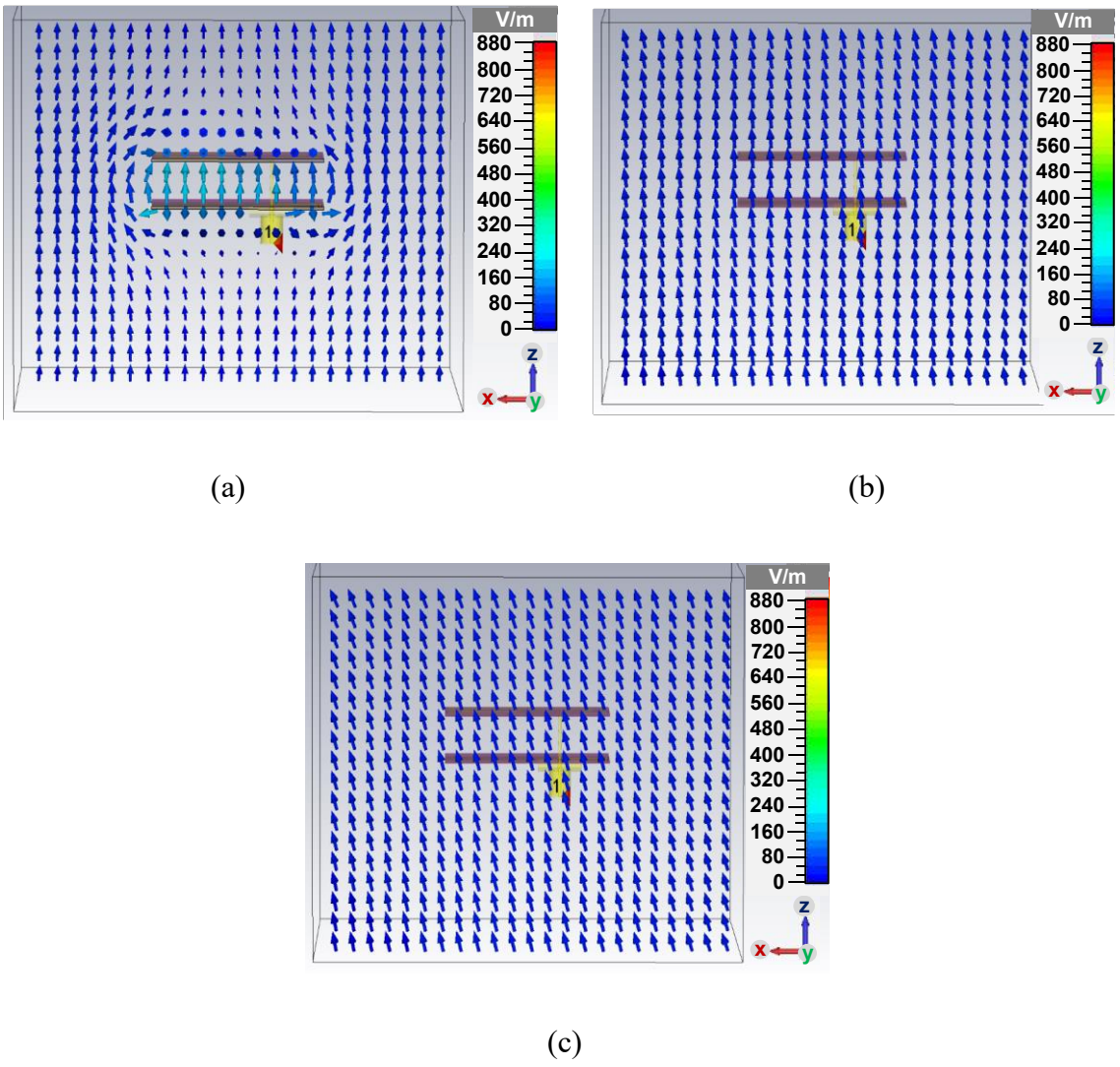

Figure 4.4 The electric field distributions in the x-z plane at (a) 0 mm, (b) 20 mm and (c) 28 mm away from the substrate edge along the y axis at $\omega t = 0^{\circ}$.

In the x-z plane, similar e-field behaviors were also observed. In Figs. 4.4(a), (b) and (c), at $\omega t = 0^{\circ}$ and distances of 0 mm, 20 mm and 28 mm ("the far region") from the nearest substrate edge along the y-axis, the e-fields are directed toward the +z-direction. In Fig. 4.5(a), at $\omega t = 90^{\circ}$ and 0 mm distance, the e-field is still directed toward the +z-direction, while in Figures 4.5(b) and (c) at 20 mm and 28 mm distances, almost all the e-fields are directed to the -x-direction. Thus, the e-field does not rotate in the very near

region but rotates in the far region, a feature distinct from the conventional CP antennas. The e-field rotations in Figs. 4.2(c) and 4.3(c) and in 4.4(c) and 4.5(c) indicate the generation of CP in both y-z and x-z planes.

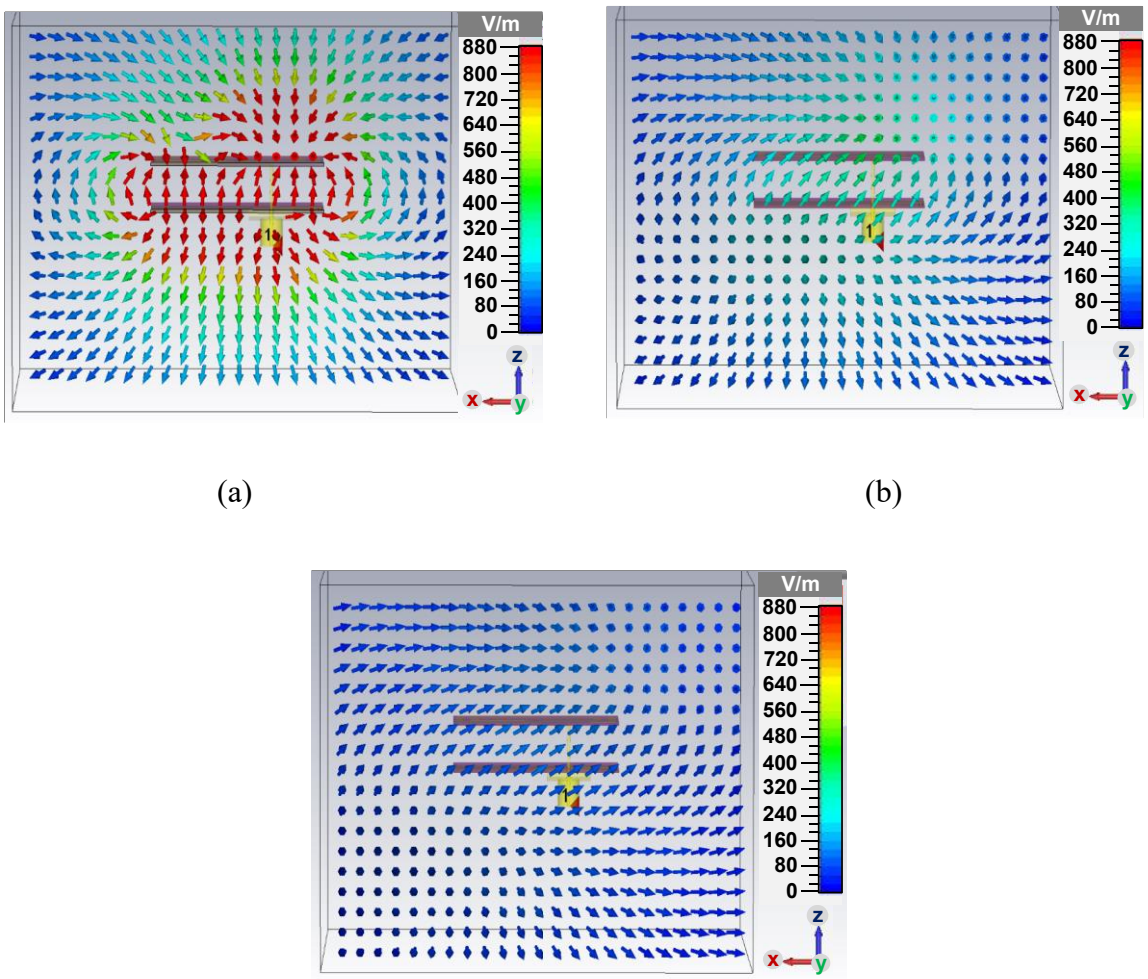

Figure 4.5 The electric field distributions in the x-z plane at (a) 0 mm, (b) 20 mm and (c) 28 mm away from the substrate edge along the y axis at $\omega t = 90^{\circ}$.

In the proposed structure, the U-shaped elements contribute to the CP generation, which can be explained with an e-field in the x-y plane. Figure 4.6(a) shows the e-field distribution at $\omega t = 0^{\circ}$ in the x-y plane at 2 mm above the surface of the upper substrate. At $\omega t = 0^{\circ}$, the strongest current travels in the +z direction on the vertical element which emits the most e-fields. The e-field distributions at the 0 mm, 20 mm and 37 mm distances on the y-z plane are shown in Figs. 4.2(a), (b) and (c), while those at the 0 mm, 20 mm and 28

mm distances on the x-z plane are illustrated in Figs. 4.4(a), (b) and (c). Thus, it is possible to conclude that the e-field at $\omega t = 0^\circ$ is mainly originated from the conductive current on the vertical element and have the same direction as the conductive current since no e-field is detected in the gaps between the U-shaped elements and around the edge, as shown in Figs. 4.4(a)-(c) and 4.6(a). At this phase, the current existing on the vertical element has the strongest amplitude. The direction of the e-field distribution in the far region is almost parallel to the z-axis.

On the other hand, with respect to the phase advancing from 0˚ to 90˚, positive and negative electric charges occur at the terminals between the U-shaped elements and are separated moving along the U-elements from the gaps. The charges induce e-fields resulting in the horizontal e-field distribution parallel to the x-y plane at $\omega t = 90^\circ$. The current on the vertical element and the e-field in the far region at $\omega t = 90^\circ$ become weaker, thus allowing for observation of the horizontal e-fields in the gaps, as shown in Fig. 4.6(b). As the horizontal e-fields becomes strongest at $\omega t = 90^\circ$, they are turned by 90˚ in the x-z plane and are almost parallel to the x-y plane in the far region. The continuously spread e-fields from the two gaps are joined together to form a vortex-like e-field distribution parallel to the x-y plane at $\omega t = 90^\circ$, as shown in Fig. 4.6(b).

In the vortex distribution, each e-field arrow in the far region is not directed to the nearest part on the U-shaped elements, as seen in Fig. 4.6(b). Given the fact that an e-field, whose direction is the same as the electric line of force, is typically directed from positive charges to negative charges, it is possible to speculate from Fig. 4.6(b) that *b* and *b´* have positive charges, and *a* and *a´* have negative charges. Thus, the e-field is possibly not directed to the vicinity of *b* and *b´* but to that of *a* and *a´* by making a detour to avoid the vicinity of positive charges. This phenomenon results in the e-field being parallel to the y-z and x-z planes in the far region, satisfying the boundary condition in both planes in which the e-field is continuous.

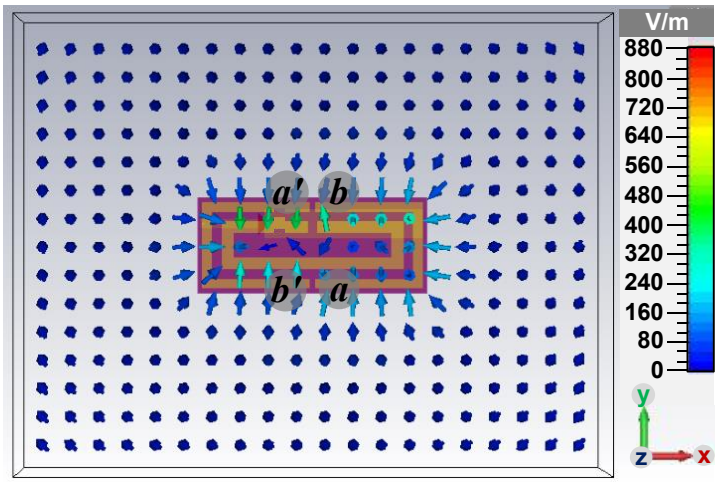

(a)

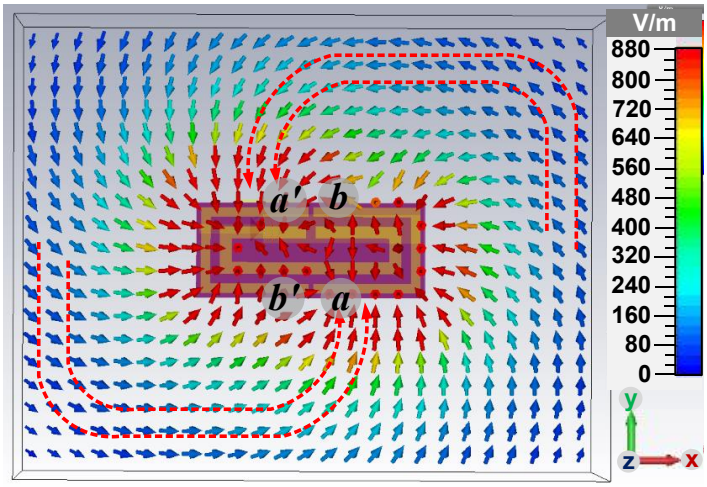

(b)

Figure 4.6 The electric field distributions in the x-y plane at 2 mm distance above the surface of the upper surface of the upper substrate (a) for ωt = 0˚ and (b) for ωt = 90˚.

The e-field in the far region is typically parallel to the current on the most adjacent part of either of the U-shaped elements. However, the ±x-direction e-fields in the far region are influenced by the closest y-parallel part of either of the U-shaped elements. The ±y-direction e-fields are also influenced by the closest x-parallel part of either of U-elements. Given that the currents on both U-shaped elements are continuous, this fact contributes to the vortex-like distribution of the entire e-field in the x-y plane at ωt = 90˚.

Furthermore, at ωt = 90˚, the vertical e-field is observed between the U-shaped elements and the ground plane. However, this vertical e-field is concentrated in the very near region and thus has little effect on the e-field rotation in the far region.

From Figs. 4.2, 4.3, 4.4 and 4.5, a small difference exists in the amplitude of the e-fields in the far region at ωt = 0˚ and 90˚, although the AR could be maintained at approximately 3 dB or less (as show the results in next section). At ωt = 0˚, the e-field in the +z-direction is originated mainly from the current on the vertical element. The antenna radiates LHCP as co-polarization. If the feeding line and the vertical element are symmetrically turned in the x-y plane by 180˚ with respect to the y-axis, the CP sense will be switched from LHCP to RHCP. This is because at ωt = 90˚ the relationship between the positive and negative charges at the gap terminal is reversed.

4.4 Effects of Structural Parameters

This section is concerned with the antenna structure and the effects of structural parameters on the antenna. The evolution of the antenna structure is first presented, followed by the studied results of the structural parameters.

4.4.1 Effects of Antenna Evolution

Figure 4.7 illustrates the evolution of the proposed antenna. It starts with a loop element with balanced feeding structure, as shown in Fig. 4.7(a). The loop antenna radiates linear polarization and its circumference (L_C) is approximately one wavelength. By following the loop antenna dimensions as prescribed in Table 4.1, the resulting resonance frequency is approximately 3 GHz.

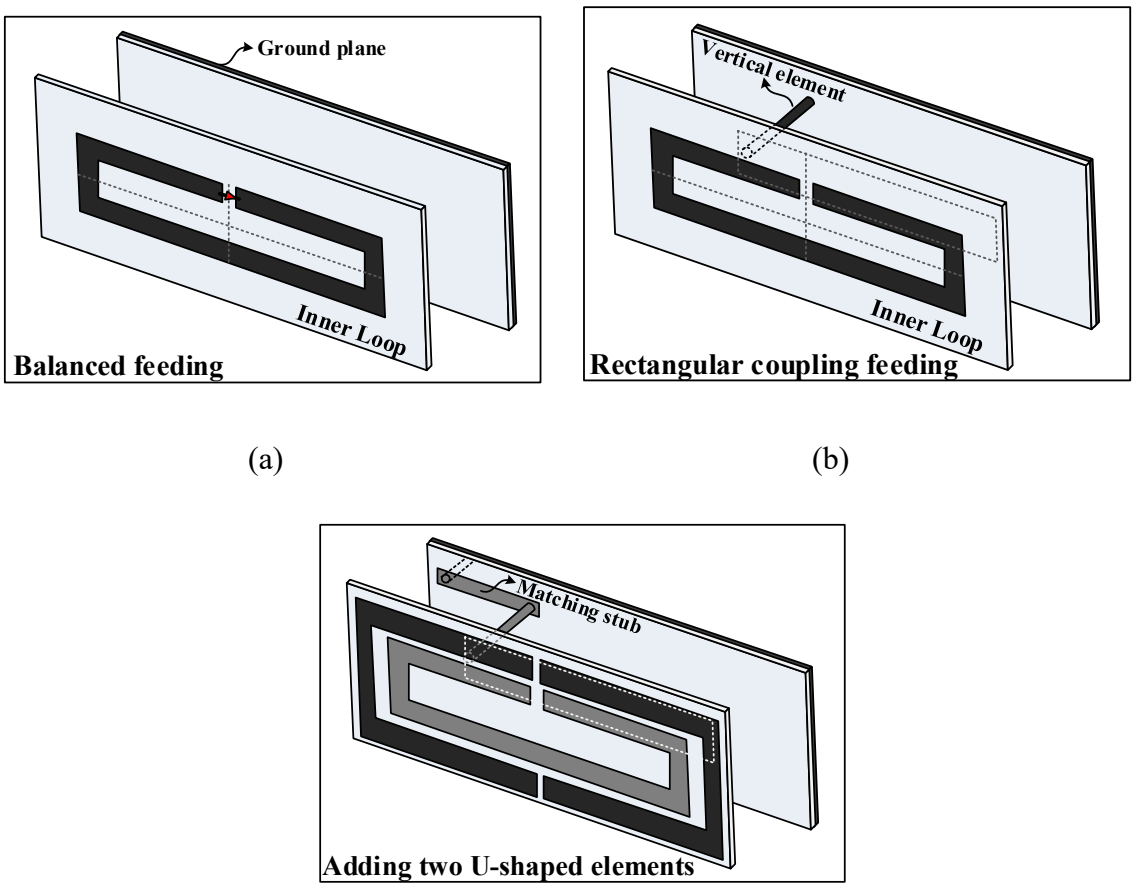

Figure 4.7 The antenna evolution: (a) the loop structure with a gap feeding, (b) the loop element fed by the coupled rectangular feed line and a vertical element, and (c) the structure with the U-shaped elements and the matching stub.

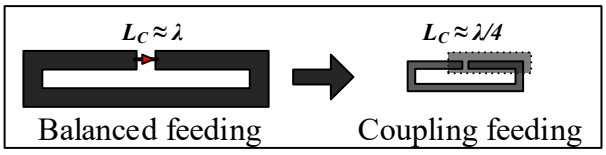

Figure 4.8 Size comparison of loop antenna with balanced feeding and that of coupling feeding.

When a rectangular feeding element and the loop element are coupled together, the resonant frequency is reduced to less than 1 GHz, as shown in Fig. 4.7(b). This feeding structure makes possible an antenna of electrically small size with the loop's $L_C \approx \lambda/4$, as shown in Fig. 4.8 [16].

The U-shaped elements are then placed enclosing the loop element, as shown in Fig. 4.7(c). The U-shaped elements contribute to the generation of omnidirectional CP. In Fig. 4.9, variations in the simulated AR in azimuth angles are reduced using the U-shaped elements. Thus, the 3-dB AR can be maintained omnidirectionally.

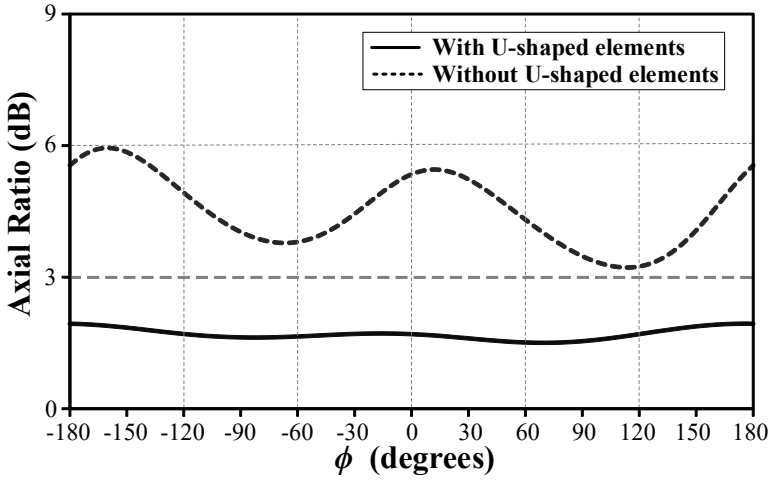

Figure 4.9 The simulated effect of the U-shaped elements on AR pattern at the resonant frequency with ϕ ($\theta = 90^{\circ}$) in the x-y plane.

Although the structure without the U-shaped elements is similar to that with a horizontal loop and a vertical element, it is difficult to obtain the omnidirectional 3-dB AR pattern, as shown in Fig. 4.9. *ka* was 0.421 without the U-shaped elements; however, with the U-shaped elements, *ka* increased to 0.475 but is still less than 0.5.

A parallel inductive stub is connected to the vertical element to achieve a 50 Ω impedance matching, as shown in Fig. 4.7(c). A reduction in the antenna size and the omnidirectional CP are attributable to the coupling feeding structure and the U-shaped elements, respectively.

4.4.2 Effects of Length of Rectangular Feeding Structure (l_1+l_2)

For generating omnidirectional CP, the current distribution should be uniform on throughout the two U-shaped elements, and the current should be generated by 90° phase lag compared to the current on the vertical element. This section details the effects of l_1

and l_2 with respect to AR. As previously shown in Fig. 4.1(c), $l_1 + l_2$ is the total length of the feeding line installed underneath the U-shaped elements and the loop.

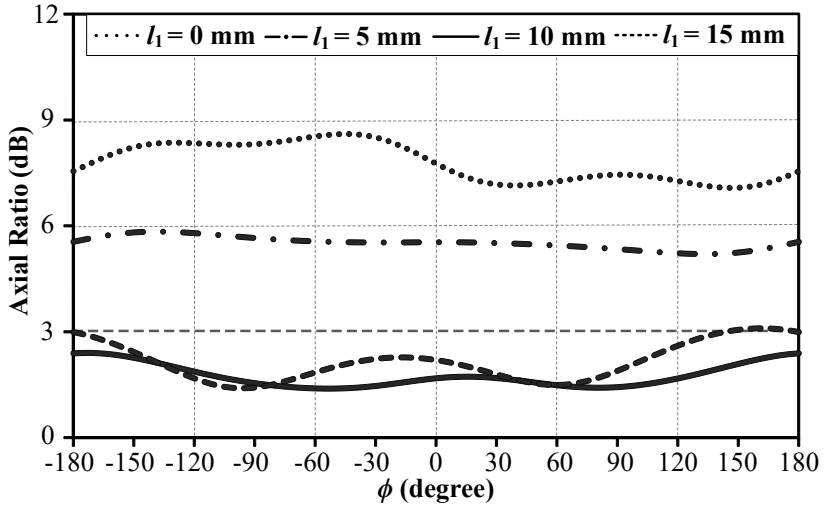

Figure 4.10 The simulated AR at the resonant frequency with ϕ ($\theta = 90^\circ$) in the x-y plane as a function of l_1 for l_2 = 23 mm.

Figure 4.10 shows the effect of the l_1 on the AR pattern in the x-y plane when l_2 = 23 mm. An increase in l_1 from 0 to 15 mm leads to a gradual decrease in AR to < 3 dB omnidirectionally. The current distribution on the U-shaped and loop elements at ωt = 0˚ and 90˚ are shown in Figs. 4.11, 4.12, and 4.13. It can see that the current distribution on the U-shaped and loop element at ωt = 0˚ and 90˚ is uniform, as shown in Figs. 4.11(a) and (b). This is because, as shown in Fig. 4.6(b), the equivalent voltage $V_{a'b}$ between points $a'$and b is identical to $V_{ab'}$ between points a and b', even though the length of either U-shaped element is quarter-wavelength. It was observed that if l_1 is too short (i.e. l_1 < 10 mm), $V_{a'b}$ becomes stronger than $V_{ab'}$, resulting in the non-uniform current distribution on the U-shaped elements, as shown in Figs. 4.12(a) and (b), even though the current distribution on the loop element is relatively uniform. This contributes to small variation in AR with ϕ. As a result, the $V_{a'b}$ and $V_{ab'}$ depend on the l_1 because the current on the feeding line varies with respect to position on the line. Therefore, the l_1 affects the distribution of horizontal e-field and AR.

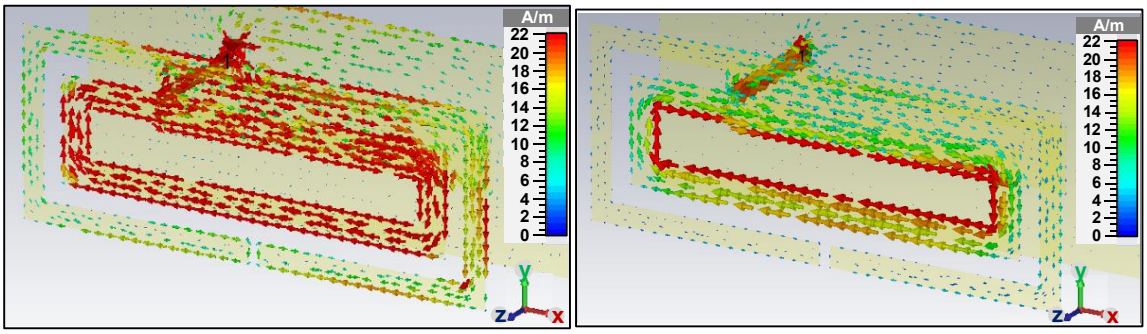

(a) (b)

Figure 4.11 The current distribution when l_1 = 10 mm and l_2 = 23 mm in (a) ωt = 0˚ and (b) ωt = 90˚.

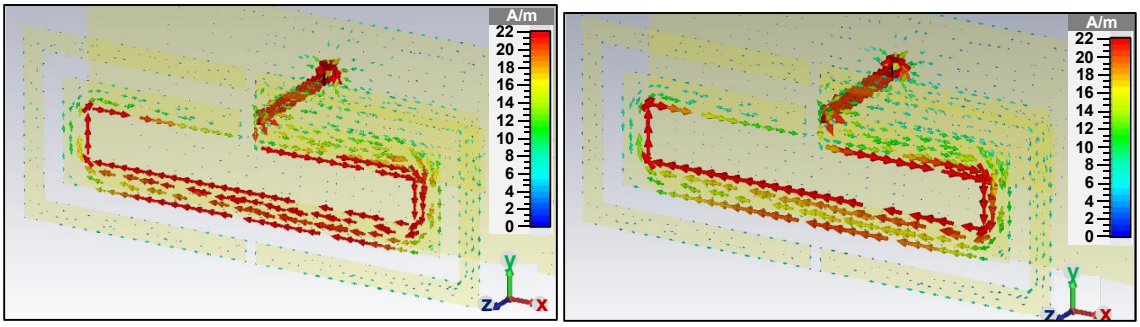

(a) (b)

Figure 4.12 The current distribution when l_1 = 0 mm and l_2 = 23 mm in (a) ωt = 0˚ and (b) ωt = 90˚.

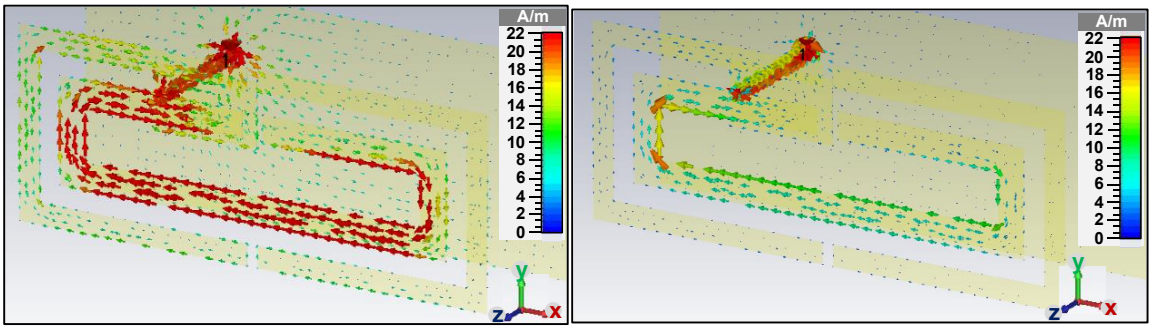

(a) (b)

Figure 4.13 The current distribution when l_1 = 10 mm and l_2 = 0 mm in (a) ωt = 0˚ and (b) ωt = 90˚.

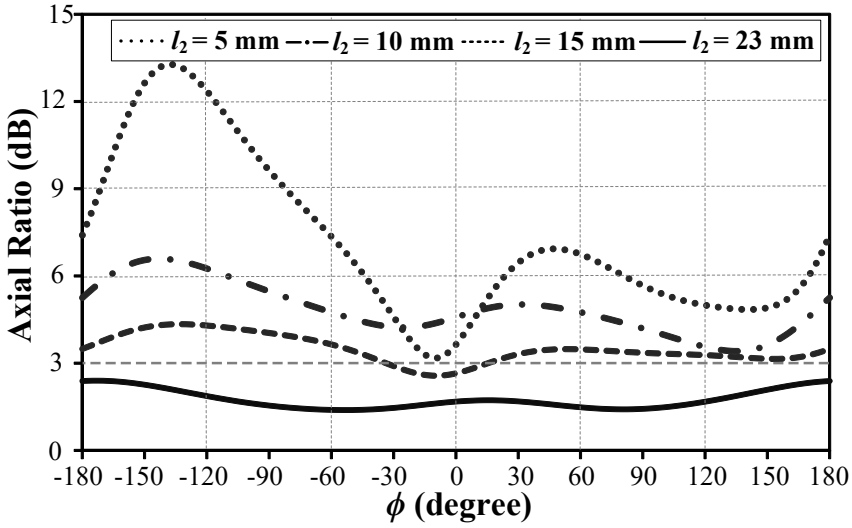

Figure 4.14 The simulated AR at the resonant frequency with ϕ ($\theta = 90^{\circ}$) in x-y plane as a function of l_2 for l_1 = 10 mm.

Figure 4.14 illustrates the effect of l_2 on the AR pattern in the x-y plane when l_1 = 10 mm. As l_2 increases from 5 to 23 mm, AR gradually decreases and becomes < 3 dB omnidirectionally. In Figs. 4.13(a) and (b), for l_2 = 0 mm, at $\omega t = 90^{\circ}$ the current on the loop element becomes weaker with an advance of phase. This is probably due to an impedance mismatch attributable to the large capacitance from the series stub coupled with the gaps between the U-shaped and loop elements. Moreover, the current is non-uniform on the U-shaped elements. Strong current was observed on only one of the U-shaped elements, which is more adjacent to the vertical element. No omnidirectional CP pattern is found in this scenario.

4.5 Experimental Results

Figures 4.15 (a) and (b) are photograph images of the prototype antenna. Since the ground plane is small, a quarter-wavelength bazooka balun is attached to suppress the leakage current on the coaxial cable [16], as shown in Fig. 4.15(b).

(a)

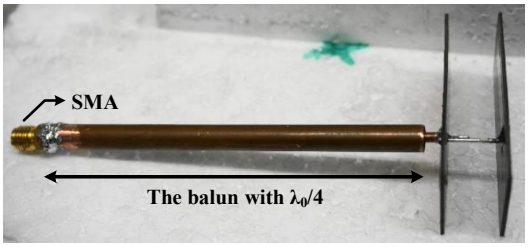

(b)

Figure 4.15 Photograph of the proposed antenna: (a) Top view (b) Side view with a feeding cable and a balun.

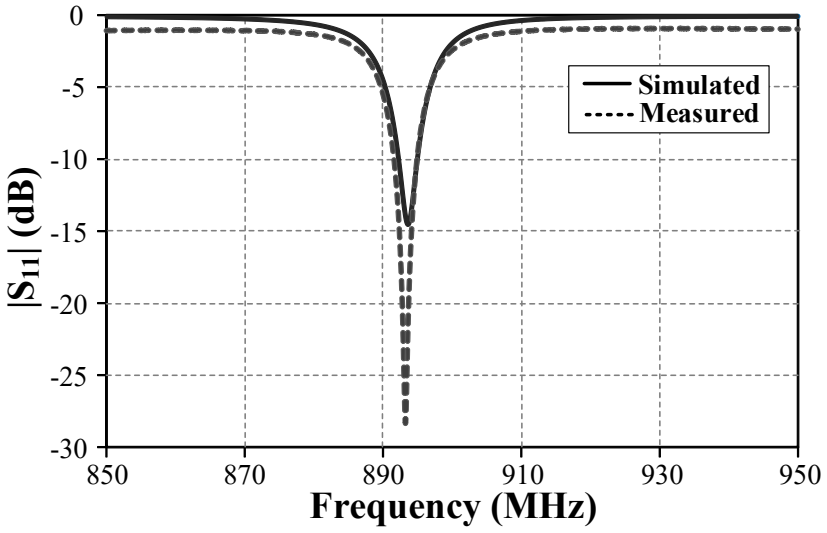

Figure 4.16 The simulated and measured $|S_{11}|$ characteristics.

The performance of ESA is assessed based on the radiation quality factor (Q_r), and $Q_r = Q_t/\eta$, where Q_t is total Q value, and η is the radiation efficiency. ESAs normally have a narrow impedance bandwidth due to a high Q value [50]. Figure 4.16 illustrates the

simulated and measured $|S_{11}|$, which are at their minimums when the resonant frequency is 893 MHz. This research focuses on $|S_{11}|$ of ≤ -6 dB, which is the criterion of small mobile terminals. In Fig. 4.13, the bandwidths of the simulated and measured $|S_{11}|$ at -6 dB are about 5 MHz. With respect to the efficiency of miniaturization, the antenna is evaluated by $C = (Q/Q_{\min})/\eta$, where $Q_{\min}$ is the minimum Q defined by (1.2), and the ideal C is 1. Table 4.2 presents the quantitative evaluation of the proposed antenna and [16]. The simulated C of the proposed antenna is 14.73, which is close to that of the quarter-wavelength capacitively-fed meandered-line antenna (QCFMA) of 11.23 for a high radiation efficiency planar, electrically small and linearly polarized antenna with a back conductor [16]. Previous studies by [51, 52] reported the miniaturized dipole antennas with a low C of 2-10. However, except [16] and an improved report using an additional element [41], no research on low-profile, planar and ESAs with a low C has ever been presented.

Table 4.2 Quantitative evaluation of the antenna.

Parameter	Antenna	QCFMA [16]
ka	0.475	0.452
Q	64.64	98.52
Q_{min}	11.40	13.04
η	0.38	0.67
C	14.73	11.23

The simulated and measured radiation patterns of left-hand CP (LHCP) and right-hand CP (RHCP) in the x-y and y-z planes are illustrated in Fig. 4.17. Figure 4.17(a) shows that the cross-polarization of RHCP is 15 dB lower than that of LHCP in the omni-direction of the x-y plane. In Fig. 4.17(b), the main beam (LHCP) direction in the y-z plane declines by 5˚ from the y-direction which is parallel to the ground plane. The measured radiation patterns show reasonable agreement with the simulated results. However, the measurement taken at phase -90˚ in the y-z plane differs from the simulation. The disparity is due to there being only one azimuth turntable in the anechoic chamber in which the measurement was carried out, thereby requiring turning the antenna by 90˚ for y-z measurement. Although the feeding cable was wrapped with absorbers, the impact of the antenna turning was not completely suppressed. Furthermore, a typical ESA is very sensitive to even a small change

in the environment. Therefore, there are small discrepancies between the simulated and measured results at θ = 90˚ and θ = -90˚ in Fig. 4.17(b). In addition, the simulated and measured gains along the +y-direction are -2 dBic and -3 dBic, respectively.

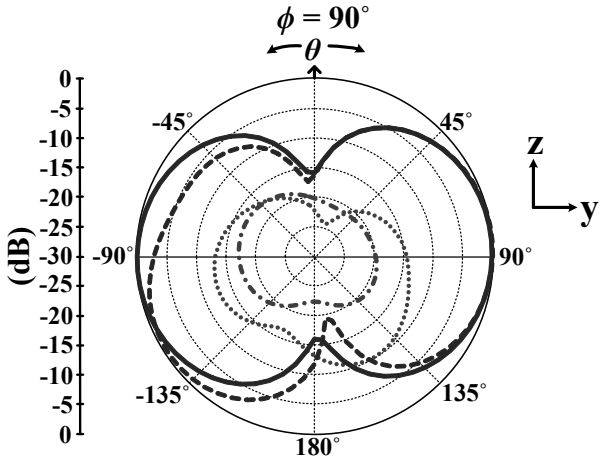

(a)

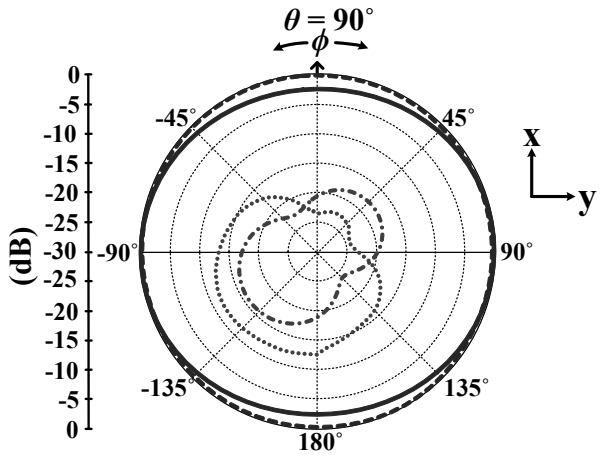

(b)

Figure 4.17 The simulated and measured radiation patterns: at 893 MHz (a) x-y plane and (b) y-z plane.

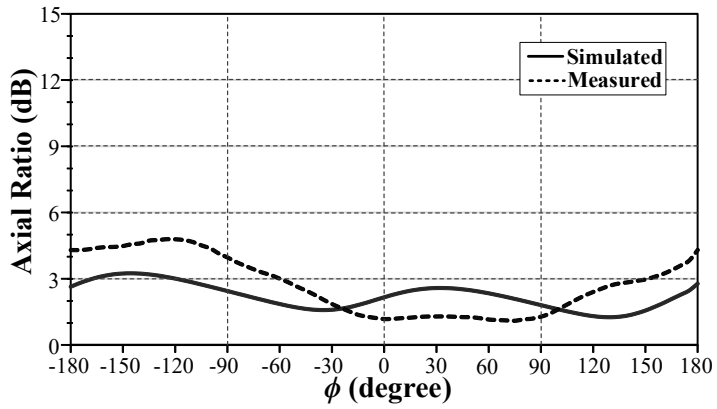

(a)

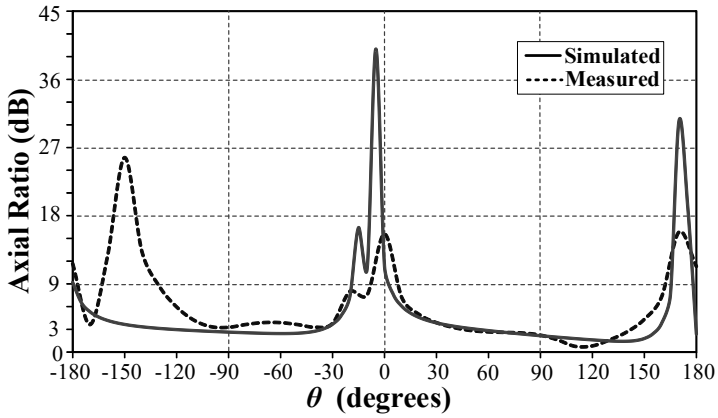

(b)

Figure 4.18 Simulated and measured AR of the antenna in (a) x-y plane and (b) x-z plane at 893 MHz as a function of ϕ.

As shown in Fig. 4.18, the simulated and measured axial ratio (AR) patterns of the proposed antenna are of omnidirectional CP pattern in the x-y plane and x-z plane for AR $\leq$ 3 dB. In Fig. 4.18(a), the experimental AR pattern in the x-y plane is very similar to that of the simulation. The measured AR is $\leq$ 3 dB for ϕ of -30˚ to 120˚and is greater than 3 dB but less than 5 dB for ϕ outside this range. In the same figure, it can be observed that the simulated AR for $\phi \approx$ -150˚ is approximately 3.1 dB, which could be further improved by more precise optimizations in micrometer orders. Furthermore the measured result in Figure 4.18 shows some errors which are possibly due to fabrication errors and measurement environment such as the feeding cable, supporting styrene foam and unexpected reflections even in the anechoic chamber. Small differences of the simulated

and measured AR are attributable to a high Q value accompanying an ESA, which could result in fabrication errors.

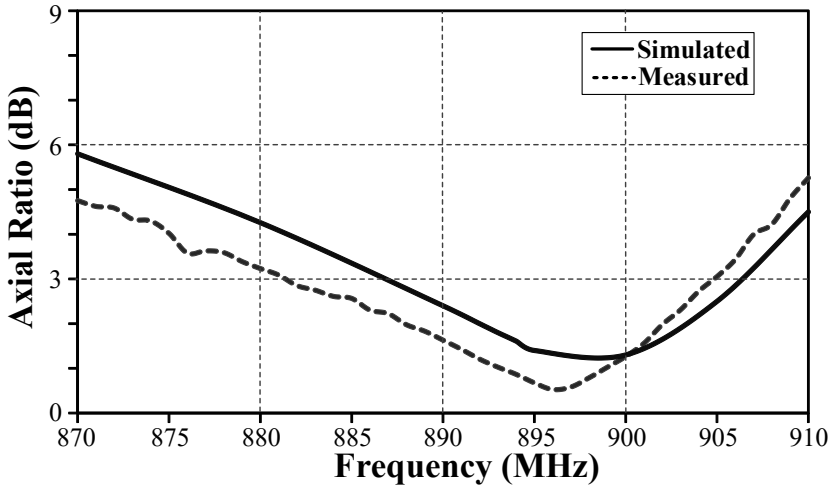

Figure 4.19 The simulated and measured AR in x-y plane (θ = 90˚) as a function of frequency at ϕ = 90˚.

Figure 4.19 shows the simulated and measured AR in the x-y plane (θ = 90˚) relative to frequency at ϕ = 90˚. The bandwidth of 3-dB AR is approximately 15 MHz, which is wider than the -6-dB $|S_{11}|$ bandwidth of 5 MHz.

4.6 Conclusion

The author has presented an electrically small antenna which can generate omnidirectional CP in far field with ka < 0.5. The e-field distributions are utilized to demonstrate the principle of CP generation. The simulated and measured results show reasonable agreement. Furthermore, this research investigates the miniaturization efficiency using the minimum Q value.

Despite its narrow bandwidth, the antenna is reasonably adequate for WSN applications for which an antenna sensor is required. One application example is the use of an antenna sensor with RFID chip utilizing the frequency shift to detect the dielectric variation property of material [53],[54]. The omnidirectional CP of antenna reduces multipath effect and thereby allows for measurement from any direction.

CHAPTER 5

CONCLUSIONS

5.1 Advantages and Applications

This thesis deals with low-profile, linearly and circularly polarized antennas radiating parallel to the ground plane. The designing started from an SRA which consists of an outer ring coupled with a fed inner ring radiating horizontal polarization to the element. The effects of an additional ground plane which is installed underneath the SRA are discussed in Chapter 2. The ground plane size and the air interval between SRA element and ground plane have only a small effect on impedance characteristics. However, the radiation pattern of antenna is still horizontally polarized to the ground plane. Therefore, it can achieve the radiation like a monopole antenna on a ground plane and have a very low-profile structure and potential applications in base stations and wireless communications.

The half-cut design of the original structure of SRA is proposed in Chapter 3. The structure consists of a modified double U-shaped radiator and a ground plane. The proposed antenna is designed for a wearable handheld reader which has usage to wear onto a hand. It can allow us to use both hands freely to work without holding the reader. The antenna can achieve circular polarization with the main beam direction parallel to the ground plane. A capacitive feeding structure including an L-shaped stub, an F- shaped stub and a capacitive gap are installed underneath the radiator (double U-shaped elements) for keeping the sufficient impedance bandwidth. As the results, the proposed antenna can radiate CP in the y-direction covering the UHF RFID band in Thailand (920 – 925 MHz).

One of the interests which have been presented in the thesis is ESA since recent communication devices tend to be reduced. The device may be used in the application such as WSNs. The advantage of omnidirectional circularly polarized antenna in WSNs is to reduce the multipath effect and to allow wireless connections in any direction. They also avoid the polarization mismatch between transmitter and receiver. In previous research works, the proposed ESAs radiate linear and circular polarizations but no research has discussed ESA with omnidirectional CP. Therefore, discussion of design of ESA, in particular, radiating omnidirectional CP should be important and a challenging project. A

novel design of ESA which has omnidirectional CP is presented in Chapter 4. The structure of a vertical element, a fed loop element, coupled feeding structure and the U-shaped elements can reduce its overall size to the electrically small size of $ka = 0.475$ which satisfies the definition of ESA of $ka < 0.5$. The U-shaped elements also contribute to the generation of omnidirectional CP with the vertical element. The proposed antenna has a different mechanism with conventional CP antennas, in which the e-field is rotated only in far field by horizontal elements.

Additionally, mechanisms of all the antennas in this thesis are explained by observing e-field distributions. As a result, such observations allow us to interpret the mechanism of respective antennas. This must be another unique approach in addition to new designs mentioned in this thesis.

5.2 Future Scope

Three new structures have been presented in this thesis. The SRA which has horizontal polarization with low-profile structure has been presented in Chapter 2. With advantages of the low-profile structure, a compact polarization diversity antenna should be fabricated in near future by combining the SRA with a low-profile vertically polarized monopole antenna for such as base stations and RFID reader applications [52].

In Chapter 3, the CP antenna radiating parallel to the ground plane is proposed for mainly wearable RFID readers. From the results, the main beam direction is shifted by only 20˚ from the parallel direction to the ground plane. A combination of the antenna and a meta-surface may be another technique to improve radiation property, especially an important reduction of back radiation will be achieved.

Chapter 4 has presented an ESA with omnidirectional CP. Although the bandwidth is narrow due to high Q value, it is sufficient for an antenna sensor application in WSNs to detect precious variation in electrical parameters of materials located near by the antenna. For other applications, matching circuit will be required to improve the bandwidth of the antenna.

5.3 Final Remarks

The important contributions of the thesis have been described. The overall research approach consists of followings:

1. The antennas are designed based on a SRA. The SRA consists of a fed inner ring and a coupled outer split ring. The capacitive coupling between the inner and outer split rings makes the antenna compact. The antenna radiates horizontal polarization even though it has a ground plane. Therefore, it is available to be applied for polarization diversity devices being combined with a low-profile vertically polarized antenna.

2. To modify the linearly polarized split ring structure to circularly polarized and low-profile antenna with the main beam direction parallel to ground plane yields better usage for wearable UHF-RFID reader. The combination between capacitive feeding line and U-shaped slot on the bent part contributes to radiate the orthogonal e-field components with 90˚-phase difference.

3. A novel concept to generate CP by an ESA has been proposed. The antenna can have a potential application for WSNs.

4. The mechanisms of the antenna performances has been explained by observing the e-field distributions.

5. The proposed antennas have been successfully fabricated. The measured results of respective prototype antennas show good agreements with simulated results.

6. The proposed antennas radiate linear or circular polarization in parallel to the ground plane or their elements.

Throughout the studies mentioned in this thesis, the author thinks that the proposed ideas and obtained results can open new vistas to develop wireless systems such as various mobile telecommunications, RFID systems and WSNs.

REFERENCES

[1] K. Finkenzeller, **RFID Handbook**, 2nd ed. Wiley, New York, 2003.

[2] X. Chen, G. Fu, S.-X. Gong, Y.-L. Yan, and W. Zhao, "Circularly Polarized Stacked Annular-Ring Microstrip Antenna with Integrated Feeding Network for UHF RFID Readers," **IEEE Antennas and Wireless Propagation Letters**, vol. 9, 2010, pp. 542–545.

[3] W.-G. Lim, W.-I. Son, K.-S. Oh, W.-K. Kim, and J.-W. Yu, "Compact Integrated Antenna with Circulator for UHF RFID System," **IEEE Antennas and Wireless Propagation Letters**, vol. 7, 2008, pp. 673–675.

[4] J.-H. Bang, C.B. Ochir, H.-S. Koh, E.-J. Cha, and B.-C. Ahn, "A Small and Lightweight Antenna for Handheld RFID Reader Applications," **IEEE Antennas and Wireless Propagation Letters**, vol. 11, 2012, pp. 1076–1079.

[5] J. J. Yu and S. Lim, "Design of an Electrically Small, Circularly Polarized, Parasitic Array Antenna for an Active 433.92 MHz RFID Handheld Reader," **IEEE Transactions on Antennas and Propagation**, vol. 60, no. 5, 2012, pp.2549–2554.

[6] Y.-F. Lin, Y.-K. Wang, H.-M. Chen, and Z.-Z. Yang, "Circularly Polarized Crossed Dipole Antenna with Phase Delay Lines for RFID Handheld Reader," **IEEE Transactions on Antennas and Propagation**, vol.60, no.3, 2012, pp.1221–1227.

[7] N. Nasimuddin, Z. N. Chen, and X. Qing, "Asymmetric-Circular Shaped Slotted Microstrip Antennas for Circular Polarization and Propagation and RFID Applications," **IEEE Transactions on Antennas and Propagation**, vol.58, no.12, 2010, pp.3821–3828.

[8] P.V. Nikitin and K.V.S. Rao, "Helical Antenna for Handheld UHF RFID Reader," **in Proceedings of the 4th Annual IEEE International Conference on RFID (RFID '10)**, Orlando, Fla, USA, April 2010, pp.166–173.

[9] S.-H. Chang and W.-J. Liao, "A Novel Dual Band Circularly Polarized GNSS Antenna for Handheld Devices," **IEEE Transactions on Antennas and Propagation**, vol.61, no.2, 2013, pp.555–562.

[10] K. Wei, Z. Zhang, and Z. Feng, "Design of a Wideband Horizontally Polarized Omnidirectional Printed Loop Antenna," **IEEE Antennas and Wireless Propagation Letters**, vol. 11, 2012, pp. 49– 52.

[11] C. C. Lin, L. C. Kuo, and H. R. Chuang, "A Horizontally Polarized Omnidirectional Printed Antenna for WLAN Applications," **IEEE Transactions on Antennas and Propagation**, vol. 54, no. 11, 2006, pp. 3551–3556.

[12] R.-L. Li, V. F. Fusco, and H. Nakano, "Circularly Polarized Open-Loop Antenna," **IEEE Transactions on Antennas and Propagation**, vol. 51, no. 9, 2003, pp. 2475–2477.

[13] R. Li, G. DeJean, J. Laskar, and M.M. Tentzeris, "Investigation of Circularly Polarized Loop Antennas with a Parasitic Element for Bandwidth Enhancement," **IEEE Transactions on Antennas and Propagation**, vol. 53, no. 12, 2005, pp. 3930–3939.

[14] X. Yang, Y. Z. Yin, W. Hu, and S. L. Zuo, "Low-Profile, Small Circularly Polarized Inverted-L Antenna with Double-Folded Arms," **IEEE Antennas and Wireless Propagation Letters**, vol. 9, 2010, pp. 767–770.

[15] Y. Zhang and T. Fukusako, "Design of Circularly Polarized Low-Profile and Slender Antenna with a Helical Element," **IEEE Antennas and Wireless Propagation Letters**, vol. 11, 2012, pp. 523–526.

[16] Y. Saito and T. Fukusako, "Low-Profile and Electrically Small Meander-Line Antenna using a Capacitive Feed Structure," **IEEE Antennas and Wireless Propagation Letters**, vol. 11, 2012, pp. 1281-1284.

[17] Y. Tanogashira and T. Fukusako, "Directional Radiation Pattern of Surface Wave Antenna using Dog Bone Structure**," IEICE Communication Express**, vol. 1, no. 2, 2012, pp.85–88.

[18] T. Wu, R.L. Li, and M. M. Tentzeris, "Mechanically Stable, Low Profile, Omni-Directional Solar-Cell Integrated Antenna for Outdoor Wireless Sensor Nodes," **Antennas and Propagation Society International Symposium (APSURSI 2009)**, Charleston, SC, June 2009, pp. 1-4.

[19] C. A. Balanis, Antenna Theory: **Analysis and Design, 3d ed.**, John Wiley & Sons Inc., New York, 2005.

[20] D. H. Lee, A. Chauraya, Y. Vardaxoglou and W. S. Park, "A Compact and Low-Profile Tunable Loop Antenna Integrated with Inductors," **IEEE Antennas and Wireless Propagation Letters**, vol. 7, 2008, pp. 621-624.

[21] M. Kim and H. Arai, "Low-Profile Loop-Shaped Inverted-F Wire Antenna with Dual-Mode Operation," **IEEE Antennas and Wireless Propagation Letters**, vol. 7, 2008, pp. 62-65.

[22] W. Hong and K. Sarabandi, "Low Profile Miniaturized Planar Antenna with Omnidirectional Vertically Polarized Radiation," **IEEE Transactions on Antennas and Propagation,** vol. 56, no. 6, June 2008, pp. 1533-1540.

[23] J. Oh and K. Sarabandi, "Low Profile, Miniaturized, Inductively Coupled Capacitively Loaded Monopole Antenna," **IEEE Transactions on Antennas and Propagation**, vol. 60, no. 3, March 2012, pp. 1206-1213.

[24] J. Oh and K. Sarabandi, "Low Profile Vertically Polarized Omnidirectional Wideband Antenna with Capacitively Coupled Parasitic Elements," **IEEE Transactions on Antennas and Propagation**, vol. 62, no. 2, February 2014, pp. 977-982.

[25] A. Alford and A. G. Kandoian, "Ultra-High Frequency Loop Antenna," **Transaction on the American Institute of Electrical Engineers (AIEE)**, vol. 59, 1940, pp. 843-848.

[26] C.-C. Lin, L.-C. Kuo, and H.-R. Chuang, "A Horizontally Polarized Omnidirectional Printed Antenna for WLAN Applications," **IEEE Transactions on Antennas and Propagation**, vol. 54, no. 11, November 2006, pp. 3551-3556.

[27] C. H. Ahn, S. W. Oh, and K. Chang, "A Dual-Frequency Omnidirectional Antenna for Polarization Diversity of MIMO and Wireless Communication Applications," **IEEE Antennas Wireless Propagation Letters**, vol. 8, 2009, pp. 966-970.

[28] Y. Yu, F. Jolani, and Z. Chen, "A Wideband Omnidirectional Horizontally Polarized Antenna for 4G LTE Applications," **IEEE Antennas and Wireless Propagation Letters**, vol. 12, 2013, pp. 686-689.

[29] K. Wei, Z. Zhang, Z. Feng, and M. F. Iskander, "A MNG-TL Loop Antenna Array with Horizontally Polarized Omnidirectional Patterns**," IEEE Transactions on Antennas and Propagation**, vol. 60, no. 6, June 2012, pp. 2702-2710.

[30] H. A. Wheeler, "A Helical Antenna for Circular Polarization," **Proceeding of the IRE**, vol. 35, no. 12, December 1947, pp. 1484–1488.

[31] J. D. Kraus, "The Helical Antenna," **Proceeding of the IRE**, 1949, pp. 263–272.

[32] B. Li and Q. Xue, “Polarization-Reconfigurable Omnidirectional Antenna Combining Dipole and Loop Radiators,” **IEEE Antennas and Wireless Propagation Letters**, vol. 12, 2013, pp. 1102–1105.

[33] Y. Yu, Z. Shen, and S. He, “Compact Omnidirectional Antenna of Circular Polarization,” **IEEE Antennas and Wireless Propagation Letters**, vol. 11, 2012, pp. 1466–1469.

[34] B. C. Park and J. H. Lee, “Omnidirectional Circularly Polarized Antenna Utilizing Zeroth-Order Resonance of Epsilon Negative Transmission Line,” **IEEE Transactions on Antennas and Propagation**, vol. 59, no. 7, 2011, pp. 2717–2720.

[35] B. C. Park and J. H. Lee, “Dual-Band Omnidirectional Circularly Polarized Antenna using Zeroth- and First-order Modes,” **IEEE Antennas Wireless Propagation Letters**, vol. 11, 2012, pp. 407–410.

[36] W. W. Li and K. W. Leung, “Omnidirectional Circular Polarized Dielectric Resonator Antenna with Top-load Alford Loop for Pattern Diversity Design,” **IEEE Transactions on Antennas and Propagation**, vol. 61, no. 8, August 2013.

[37] F. R. Hsiao and K. L. Wong, “Low-Profile Omnidirectional Circularly Polarized Antenna for WLAN Access Points,” **Microwave Optical Technology Letters**, vol. 46, no. 3, August 2005, pp. 227–231.

[38] Y. M. Pan and K. W. Leung, “Wideband Circularly Polarized Dielectric Bird-Nest Antenna with Conical Radiation Pattern,” **IEEE Transactions on Antennas and Propagation**, vol. 61, no. 2, February 2013.

[39] J. S. McLean, “A Re-Examination of the Fundamental Limits on the Radiation Q of Electrically Small Antenna,” **IEEE Transactions Antennas Propagation**, vol. 44, no. 5, May 1996, pp. 672–675.

[40] G. Breed, “Basic Principles of Electrically Small Antennas,” **Journal of High Frequency Electronics**, 2007, pp. 50-53.

[41] H. Maema and T. Fukusako, "Radiation Efficiency Improvement for Electrically Small and Low-Profile Antenna by Stacked Elements", **IEEE Antennas & Wireless Propagation Letters**, vol. 12, February 2014, pp.305-308.

[42] M.-C. Tang and R. W. Ziolkowski, "A Study of Low-Profile, Broadside Radiation, Efficient, Electrically Small Antennas Based on Complementary Split Ring Resonators," **IEEE Transactions on Antennas and Propagation**, vol. 61, no. 9, September 2013.

[43] S. Zhu, D. G. Holtby, K. L. Ford, A. Tennant, and R. J. Langley, "Compact Low Frequency Varactor Loaded Tunable SRR Antenna," **IEEE Transactions on Antennas and Propagation**, vol. 61, no. 4, 2013.

[44] L. Wang, M. Q. Yuan, and Q. H. Liu, "A Dual-Band Printed Electrically Small Antenna Covered by Two Capacitive Split-Ring Resonators," **IEEE Antennas and Wireless Propagation Letters**, vol. 10, 2011, pp. 824–826.

[45] S. Zhu, K. L. Ford, A. Tennant and R. J. Langley, "Small Antenna over AMC Surface with/out Vias," **European Conference on Antennas and Propagation (EUCAP)**, Prague, March 2012, pp. 2712-2715.

[46] O. S. Kim, "Electrically Small Circularly Polarized Spherical Antenna with Air Core," **7th European Conference on Antennas and propagation (EUCAP 2013)**, Gothenburg, Sweden, 2013, pp. 233–236.

[47] K. Lertsakwimarn, R. Suwalak and C. Phongcharoenpanich, "A Compact Loop Antenna with Parasitic Split Ring for UHF RFID Application," **Progress In Electromagnetics Research Symposium Proceedings (PIER2013)**, Taipei, March.2013.

[48] X. Quan and R. Li, "A Broadband Dual-Polarized Omnidirectional Antenna for Base Station," **IEEE Transactions on Antennas and Propagation**, vol. 61, no. 2, February 2013, pp. 943-947.

[49] S. R. Best, "A Discussion on the Properties of Electrically Small Self-resonant Wire Antennas," **IEEE Antennas and Propagation Magazine**, vol. 46, no. 6, 2004, pp. 9–22.

[50] R. F. Harrington, "Effect of Antenna Size on Gain, Bandwidth, and Efficiency," **J. Research NBS**, vol. 64D, no. 1, January 1960, pp. 1–12.

[51] A. R. Lopez, "Fundamental Limitation of Small Antennas: Validation of Wheeler's Formulas", **IEEE Antennas and Propagation Magazines**, vol. 48.4, August 2006, pp.28-36.

[52] G. Vandenbosch, "Reactive Energies, Impedance, and *Q* Factor of Radiating Structures" **IEEE Transactions. Antennas and Propagation**, vol. 58, 4, April 2010, pp.1112-1127.

[53] R. Suwalak, C. Phongcharoenpanich, D. Torrungrueng, and M. Krairiksh, "Determination of Dielectric Property of Construction Material Products using a Novel RFID Sensor," **Progress in Electromagnetics Research**, vol. 130, 2012, pp. 601–617.

[54] F. Yang, Q. Qiao, and A. Z. Elsherbeni, "Reconfigurable Sensing Antennas: Concept, Design, and Applications," **Antennas and Propagation in Wireless Communication (APWC2013)**, Torino, Italy, September 2013, pp. 748-752.

RELATED PUBLICATIONS

Journal Papers

[1] **K. Lertsakwimarn**, C. Phongcharoenpanich and T. Fukusako, "Circularly Polarized Low-Profile Antenna for Radiating Parallel to Ground Plane for RFID Reader Applications," International Journal of Antennas and Propagation, Article ID 349817, pp.1-10, vol. 2013, 2013.

[2] **K. Lertsakwimarn**, C. Phongcharoenpanich and T. Fukusako, "Design of Circularly Polarized and Electrically Small Antenna with Omnidirectional Radiation Pattern," IEICE Trans. Communication, pp.2739-2746, vol. E97-B, no. 12, December 2014.

[3] **K. Lertsakwimarn**, C. Phongcharoenpanich and T. Fukusako, "A Low-Profile and Compact Split-Ring Antenna with Horizontally Polarized Omnidirectional Radiation," International Journal of Antennas and Propagation, pp.1-11, (in press)

Conference Papers

[1] **K. Lertsakwimarn** and C. Phongcharoenpanich, "Metallic Tag Antenna with Defected Ground Plane for UHF-RFID System," Proceedings of the 1st International Symposium on Technology for Sustainability (ISTS 2011), Bangkok, pp.289-292, Jan.2012.

[2] R. Suwalak, **K. Lertsakwimarn** and C. Phongcharoenpanich, "A Circularly Polarized Patch Antenna with Rectangular Slot on Defected Ground Plane for RFID Reader," Proceedings of the 1st International Symposium on Technology for Sustainability (ISTS 2011), Bangkok, pp.293-296, Jan.2012.

[3] **K. Lertsakwimarn**, R. Suwalak and C. Phongcharoenpanich, "A Compact Loop Antenna with Parasitic Split Ring for UHF RFID Application," Progress In Electromagnetics Research Symposium Proceedings (PIER2013), pp.219-222, Taipei, Taiwan, March.2013.

[4] **K. Lertsakwimarn**, C. Phongcharoenpanich and T. Fukusako, "A Low Profile Circularly Polarized Antenna with Double U-shaped Arms for UHF RFID Applications," JCEEE conference, International session co-operated with IEEE APS Fukuoka Chapter, Number 03-1A-03, Kumamoto, Japan, September 2013.

[5] **K. Lertsakwimarn**, C. Phongcharoenpanich and T. Fukusako, "Design of Circularly Polarized and Electrically Small Antenna with Omnidirectional Radiation Pattern," IEICE technical report, pp.53-58, vol. 113, 384, Kagoshima, Japan, January 2014.

[6] **K. Lertsakwimarn**, C. Phongcharoenpanich and T. Fukusako, "Design of Circularly Polarized Low-Profile Antenna for Radiating Parallel to Ground Plane," ITE technical report, pp.61-64, vol. 38, 5, Nagasaki, Japan, January 2014.

[7] **K. Lertsakwimarn**, C. Phongcharoenpanich and T. Fukusako, "A horizontally polarized, low-profile and compact antenna for radiating parallel to ground plane," 2014 IEEE International Workshop on Electromagnetics; Applications and Student Innovation (iWEM), pp.12-13, Sapporo, Japan, August 2014.

[8] **K. Lertsakwimarn**, C. Phongcharoenpanich and T. Fukusako, "Electrically Small Antenna with Circularly Polarized and Omnidirectional Radiation Pattern," 2014 IEEE International Conference on Antennas and Applications (CAMA 2014), Number APP2.4, Antibes Juan-les-Pins, France, November 2014.

[9] **K. Lertsakwimarn**, C. Phongcharoenpanich and T. Fukusako, "A horizontally polarized, low-profile and compact antenna for radiating parallel to ground plane," 2014 Thailand-Japan Microwave (TJMW2014), Number P.32, Bangkok, Thailand, November 2014.

Hindawi Publishing Corporation
International Journal of Antennas and Propagation
Volume 2013, Article ID 349817, 10 pages
http://dx.doi.org/10.1155/2013/349817

Hindawi

Research Article

Circularly Polarized Low-Profile Antenna for Radiating Parallel to Ground Plane for RFID Reader Applications

Kittima Lertsakwimarn,[1] Chuwong Phongcharoenpanich,[1] and Takeshi Fukusako[2]

[1] *Faculty of Engineering, King Mongkut's Institute of Technology Ladkrabang, Chalongkrung Road, Ladkrabang, Bangkok 10520, Thailand*
[2] *Graduate School of Science and Technology, Kumamoto University, 2-39-1 Kurokami, Chuo-ku, Kumamoto 860-8555, Japan*

Correspondence should be addressed to Kittima Lertsakwimarn; wimand.mai@gmail.com

Received 4 September 2013; Revised 4 October 2013; Accepted 5 October 2013

Academic Editor: Z. N. Chen

This paper presents a low-profile printed antenna with double U-shaped arms radiating circular polarization for the UHF RFID readers. The proposed antenna consists of double U-shaped strip structures and a capacitive feeding line to generate circular polarization. A part of the U-shaped arms is bent by 90° to direct the main beam parallel to the ground plane. From the results, −10 dB $|S_{11}|$ and 3 dB axial ratio of the antenna cover a typical UHF RFID band from 920 MHz to 925 MHz. The bidirectional beam is obtained with the maximum gain of 1.8 dBic in the parallel direction to the ground plane at the 925 MHz. The overall size of the proposed antenna including ground plane is 107 mm × 57 mm × 12.8 mm ($0.33\lambda_0 \times 0.17\lambda_0 \times 0.04\lambda_0$).

1. Introduction

Radio frequency identification (RFID) systems in the ultra-high-frequency (UHF) band are getting a standard in widely used for many applications such as supply chain management, logistics, and tracking [1]. Different frequency ranges for the UHF RFID band have been allocated depending on countries and regions such as 865–868 MHz in Europe, 902–928 MHz in North and South Americas, 950–956 MHz in Japan, and 920–925 MHz in some Asian countries. Many linearly polarized reader antennas have been designed with small size and sufficient bandwidth and used for RFID systems; however, a problem of missing tag detection may take place due to a polarization mismatch. For avoiding this problem, the use of antennas radiating circular polarization (CP) can be a good option [2, 3].

On the other hand, portable RFID readers in addition to fixed type of readers have been actively used in recent years. Considering this situation, antennas for handheld RFID readers have been required to have a low-profile and a small size structure with light weight [4–9]. In fact, since 5-6 years ago, wearable RFID readers on a hand have appeared on the fields of health care and inspection services, so that they can use their both hands at their working places freely without holding their reader. For achieving such situation, a low-profile CP reader antenna is required for wearable devices with a compact design, and directing its main beam parallel to the ground plane can make the maximum use of the advantages of the low-profile design [10].

Recently, low-profile and small CP antennas have still received a lot of research attention, although other types of UHF RFID reader antennas with meandered, microstrip, and helical element have been published in the literature [4–9]. In [4], an antenna with four meandered monopole elements fed by a series feeding network has been reported, and another antenna with arrayed two bent elements is presented in [5]. In [6], double-sided, crossed-dipole antenna for CP radiation loaded with two metal strips for phase delay is published. A compact circularly polarized microstrip antenna has been presented in [7]. Furthermore, some microstrip antennas for typical commercial handheld readers are linearly or circularly polarized. However, such antennas based on microstrip antennas limit the size and the bandwidth, and the main beam of those is directed to the normal direction to the ground [8]. Some study groups have reported horizontally polarized printed loop antennas in [11, 12], and some groups

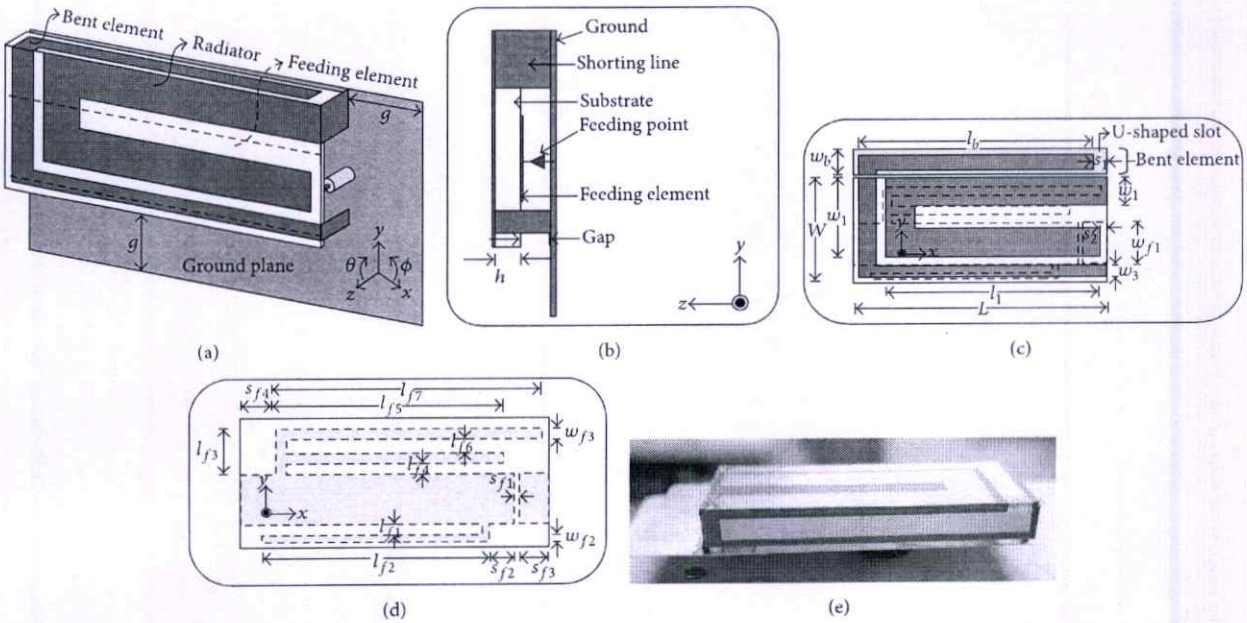

FIGURE 1: Geometry of the proposed antenna. (a) Perspective view, (b) side view, (c) radiating element, (d) feeding element, and (e) photograph of the fabricated antenna.

have studied on open-loop antennas generating CP [13, 14]. Moreover, an inverted-L CP antenna and a slender CP antenna have been reported in [15, 16], respectively. However, the main beam direction is not parallel to the ground, and the bandwidth is not sufficient. A study group involving one of the authors has recently reported a low-profile antenna with high radiation efficiency in [17, 18], but the polarization is linear. For now, as far as the authors know, almost no one has reported on circularly polarized and low-profile antennas radiating parallel to the ground plane.

In this paper, a compact and low-profile antenna for radiating CP parallel to the ground plane is proposed for RFID readers at UHF band (from 920 MHz to 925 MHz). In Section 2, the antenna design and characteristics of the proposed antennas are discussed. The principle to generate CP in this antenna is also discussed in Section 3. In Section 4, the design process is presented. Finally, the discussions in this paper are concluded in Section 5.

2. Antenna Design

In this section, the antenna design is presented. The antenna is designed using the CST MW Studio [19]. Figure 1 shows the proposed antenna structure consisting of double U-shaped strips and a capacitive feeding structure of both sides of Arlon Diclad522 ($\varepsilon_r = 2.6$) with a thickness of $h = 0.8$ mm. The dimension is $L = 87$ mm $(0.27\lambda_0) \times W = 37$ mm $(0.11\lambda_0)$ in length and width. The air gap between radiating element and ground plane is chosen as 11.8 mm $(0.036\lambda_0)$ as shown in Figure 1(b). The length and width of double U-shape are optimized because these dimensions affect the resonance frequency at which the length of U-shape is $\lambda_0/4$ as shown in Figure 1(c). One of the arms of the U-shape (bent element) is bent by 90° in the x-y plane from the radiating element. This forms a U-shaped slot with the ground plane on the bent element in the z-x plane. Figure 1(d) shows the capacitive feeding structure which is installed underneath the radiator (double U-shaped elements) and includes an L-shaped stub and an F-shaped stub with a capacitive gap for matching. A photograph of the fabricated antenna is shown in Figure 1(e). The ground plane size is chosen so as to minimize the axial ratio (AR) in the y-direction and not to allow the leakage current on the coaxial cable. The ground plane size is extended in the $+x$- and $-y$-directions with the same size by $g = 20$ mm, respectively from the substrate dimension. This effect will be discussed in Section 4.

The double U-shaped radiator determines the resonant frequency. Considering the principle to generate CP discussed later, the structure should have a half-cut structure of the split-ring resonator antenna [20] with the same resonant frequency as shown in Figure 2. For making a low-profile structure on the ground plane, the feeding structure shown in Figure 1(d) should be used so as to keep sufficient impedance characteristics as discussed later. Furthermore, a part of the arms should be bent by 90° in the x-y plane, so that the main beam can be directed in the y-direction. Table 1 shows the optimized structural parameters of the proposed antenna.

Figure 3 shows simulated and measured $|S_{11}|$ characteristics. The simulated and measured $|S_{11}|$ bandwidth at −10 dB are found from 916 MHz to 934 MHz (1.8%) and 916 MHz to 930 MHz (1.4%), respectively, covering a typical UHF RFID band (920 to 925 MHz; Thailand). The simulated and measured radiation patterns of left-hand CP (LHCP) and right-hand CP (RHCP) at 925 MHz are shown in Figure 4 in x-y

Table 1: The optimized structural parameters.

Parameter	Size in mm	Parameter	Size in mm	Parameter	Size in mm	Parameter	Size in mm
W	87.0	w_b	9.0	s_{f1}	1.5	l_{f4}	3.0
L	37.0	l_b	80.5	s_{f2}	7.0	l_{f5}	61.0
h	0.8	s_1	10.0	s_{f3}	8.5	l_{f6}	4.0
w_1	28.0	s_2	5.0	s_{f4}	10.0	l_{f7}	75.0
w_2	10.0	w_{f1}	14.5	l_{f1}	3.0	g	20.0
w_3	4.0	w_{f2}	2.0	l_{f2}	64.0	Gap	11.8
l_1	73.5	w_{f3}	3.0	l_{f3}	13.0		

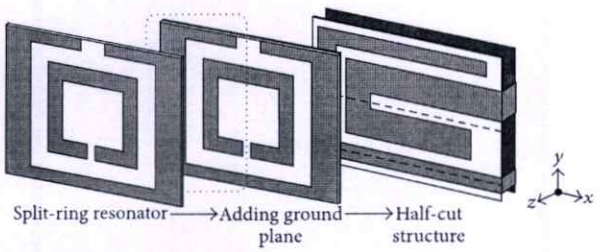

Figure 2: The antenna evolution.

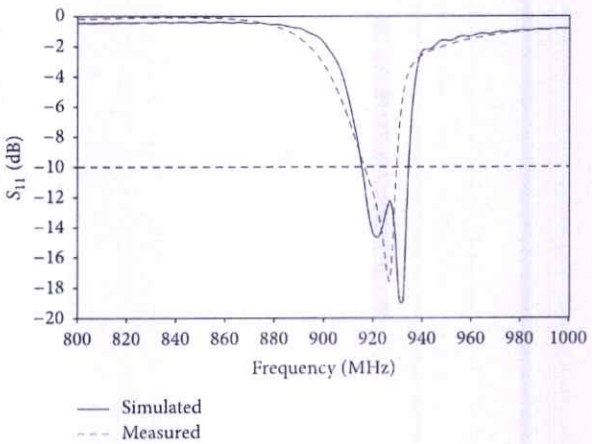

Figure 3: Simulated and measured $|S_{11}|$.

plane and y-z plane. The simulated and measured half-power beamwidth (HPBW) of RHCP are 105° and 110°, respectively, in y-z plane where the main beam (RHCP) direction is declined only by 20° from the y-direction (parallel to the ground plane). However, the obtained gain in the y-direction is slightly lower by only 0.6 dB than that in the main beam direction. The simulated and measured gains are 1.8 dBic and 2.8 dBic, respectively, in y-direction. The radiation patterns of RHCP and LHCP have been normalized by the simulated and measured peak gain of RHCP (copolarization), respectively. Therefore, we can understand that, in the y-direction, the cross-polarization of LHCP is more than 15 dB lower than RHCP. This indicates that the AR in the y-direction is less than 3 dB. Furthermore, considering the discussion below, it can be said that the measured results in the radiation patterns show reasonable agreements with the simulated results. As shown in Figure 5(a), the AR in y-z plane is less than 3 dB in the θ angle range from 70° to 95° and 70° to 90° for simulated and measured results, respectively. In the boresight direction at $\theta = 90°$, the measured AR is higher by approximately 1 dB than the simulated AR, although the measured AR is at around 3 dB. Considering the results of radiation performances discussed above with Figures 4 and 5, we can find small differences between the simulated and measured results, although they show reasonable agreements. The small differences are mainly due to fabrication errors, especially those are related to our hand-made fabrications of U-shaped slot. As shown in Figure 5(b), the 3 dB AR in the y-direction can also be observed in the UHF band. As a result, we can understand that the proposed antenna can radiate CP in the y-direction covering the UHF RFID band.

3. Principle of Generating Circular Polarization

The generation mechanism of CP is discussed in this section. The antenna elements have two metallic layers sandwiching the dielectric substrate to equip the radiator and the feeding structure with the L-shaped and F-shaped stubs. The radiator and the feeding structure have been overlapped as shown in Figure 1(c). The e-field (electric field) distributions at different phases are shown in Figure 6. At phase = 0°, the strongest field of Z-component is found mainly around the U-shaped slot on the bent element as shown in Figure 6(a). As shown in Figure 6(b), e-field directed to $+z$ with high density can be found; however, the e-field to $-z$ shows low density. This asymmetrical distribution is due to the difference in the presence of the radiator and ground plane. At phase = 90°, strong field directed in x- and $\pm z$- directions can be found on the U-shaped slot as shown in Figure 6(c); however, the components in $\pm z$ directions finally are canceled out by each other in the far field. Since the length between the feeding point (around $x = 0$ mm) on the feeding line and the bent part of the U-shaped slot is about half wavelength, the voltage at the feeding line gets lower at 90° phase than that at the bent point in the U-shaped slot. Therefore e-field is pulled into the feeding line as shown in Figure 6(d) resulting in having a symmetrical distribution between $\pm z$-directions. As

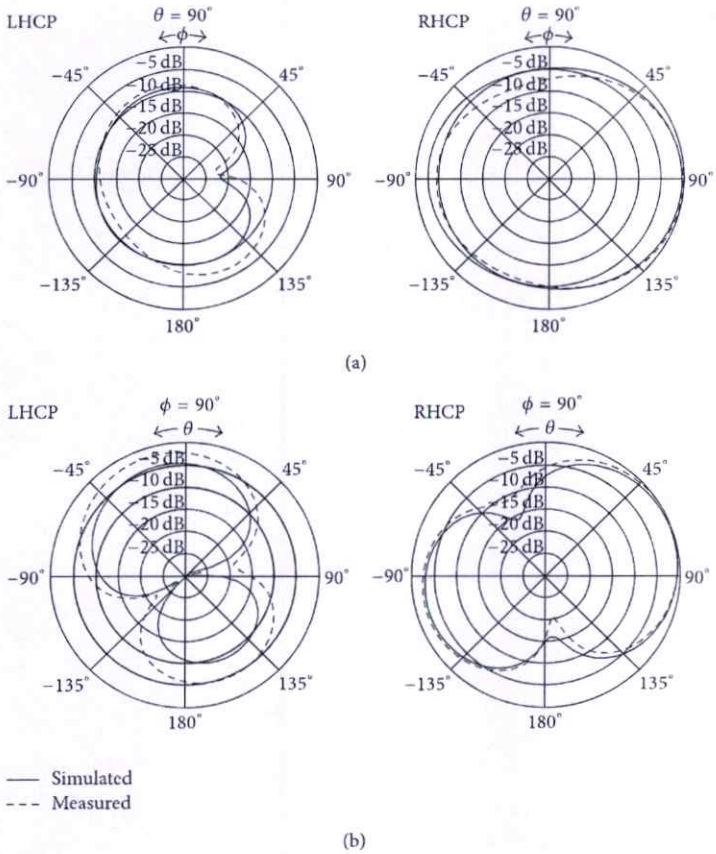

FIGURE 4: Radiation patterns at 925 MHz. (a) x-y plane and (b) y-z plane.

a result, at phase = 90°, only the X-component at the bent part of the U-shaped slot contributes to radiate. With the same analogy, the e-field generates CP with 90°-phase difference of orthogonal e-field components at phase = 180° and 270°, respectively.

On the other hand, this antenna radiates the same sense of CP, although the 3 dB AR can be obtained at $\theta = -120°$. This radiation is explained by the e-field behavior around the feeding point outside of the radiating element. At phase = 0°, the normal e-field can be observed by the same principle of the U-shaped slot mentioned above. At phase = 90°, the e-field is pulled into the feeding point following the same principle of the above explanation. Therefore, the e-field rotates in the clockwise direction with respect to the $-y$-direction.

4. Effects of Structural Parameters

The proposed antenna is a low profile and can radiate CP in the y-direction with respect to the ground plane. This section discussed the effects of structural parameters on the AR and antenna gain.

4.1. Effects of the Bent Element. One of interests in this antenna is a fact that CP is radiated in the y-direction with $\theta = 90°$, even though the structure is low profile. Bending a part of U-shaped elements with a bent angle α (from 0° to 90°), as shown in Figure 7, contributes to increase the θ angle of main beam direction in the y-z plane ($\phi = 90°$). The input impedance characteristics can be kept the same, as shown in Figure 8(a), in this range of α. When $\alpha = 0°$, the peak gain can be observed in the z direction at 0° as shown in Figure 8(b). With an increase in α from 30° to 90°, the main beam direction θ is shifted from 0° to 70° in the y-z plane. For $\alpha = 90°$, the 3 dB AR can be observed at $\theta = 90°$ in the y-z plane as shown in Figure 8(c).

4.2. Effects of L-Shaped and the Capacitive Gap Feeding Structure. Effects of the stubs in the feeding structure are discussed. The use of a coupled feeding line with the radiator element is one of the techniques for designing low-profile antennas [17] to cancel the inductivity at a frequency range with around 50 Ω impedance. Figure 9 shows the evolution of feeding structure that starts from a simple rectangular strip to the proposed structure with adding the capacitive gap, the L-shaped stub on a lower edge of the line, the short stub, the long stub, and the F-shaped stub on an upper edge.

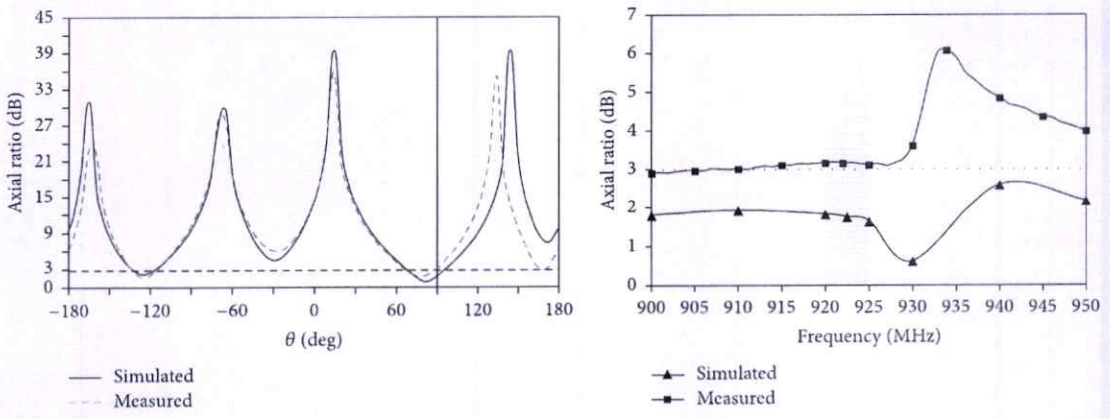

FIGURE 5: Simulated and measured AR pattern of the proposed antenna in y-z plane ($\phi = 90^{\circ}$) at 925 MHz (a) as a function of θ and (b) as a function of the frequency at $\theta = 90^{\circ}$.

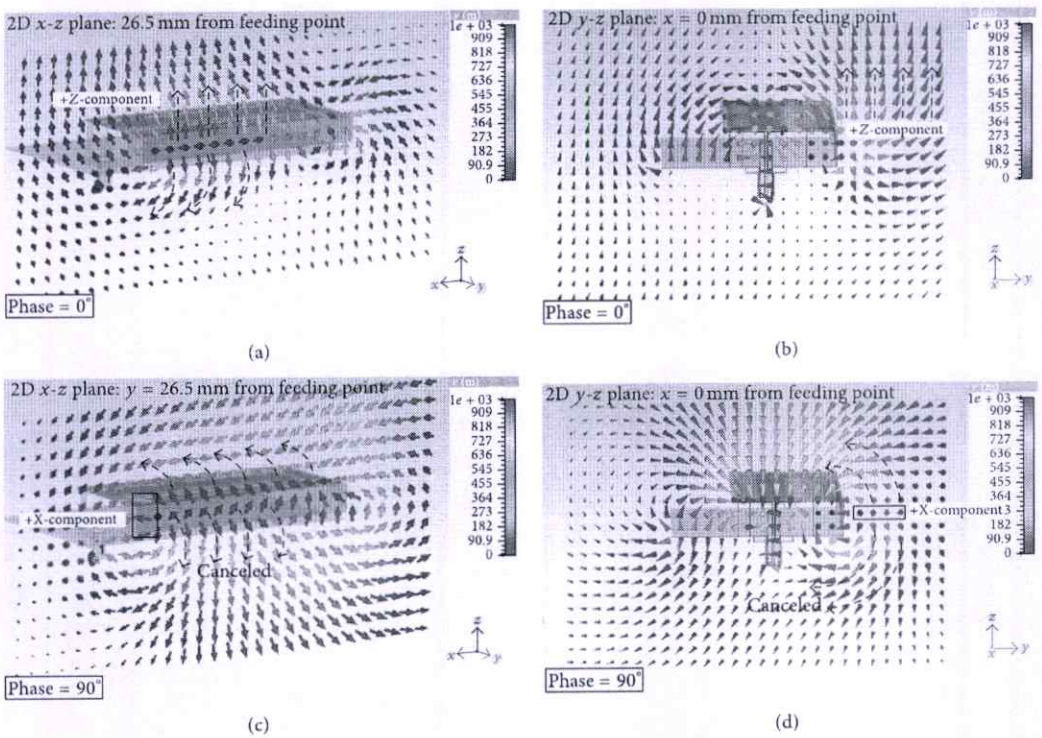

FIGURE 6: Electric field distributions in different phases at 920 MHz (a) in the x-z plane at phase = 0°, (b) in the y-z plane at phase = 0°, (c) in the x-z plane at phase = 90°, and (d) in the y-z plane at phase = 90°.

For matching to 50 Ω with a sufficient bandwidth, the capacitive gap and the L-shaped stub are installed resulting in the shift of the characteristics as shown in Figure 10. With the simple rectangular feeding structure, the input impedance characteristic shows a small kink (with a dotted line) at the right side of the Smith chart centering the horizontal axis. When only the capacitive gap is installed, the kink is shifted to a different place (the kink shown with a dashed line) along the circle of a real axis counterclockwisely. After this, when the L-shaped stub having a parallel capacitance is installed, the kink, shown with a solid line, is magnified passing the center showing a narrow bandwidth since the kink size is still bigger than the circle of VSWR = 2.

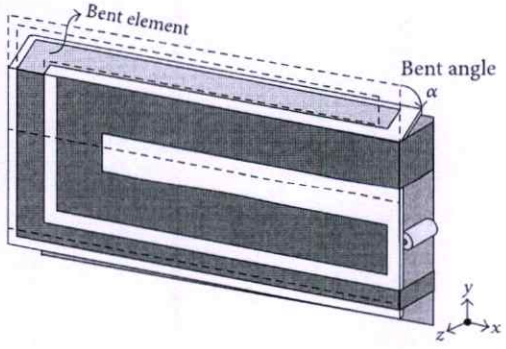

FIGURE 7: Direction of bending angle α on the element.

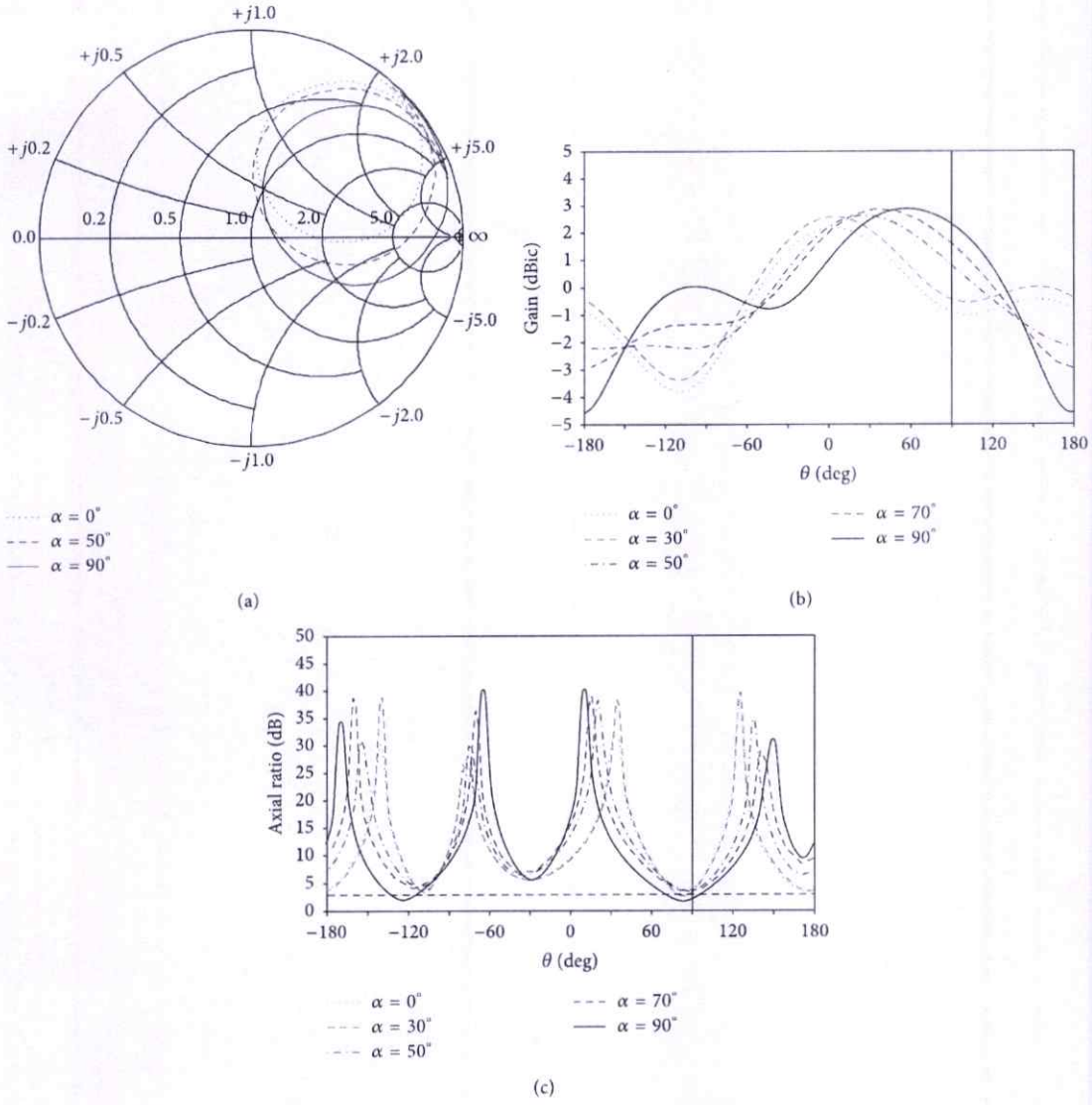

FIGURE 8: Simulated results of (a) input impedance characteristics with α, (b) antenna gain pattern, and (c) AR pattern of the proposed antenna in y-z plane at 925 MHz as a function of the bending angle α ($\phi = 90°$).

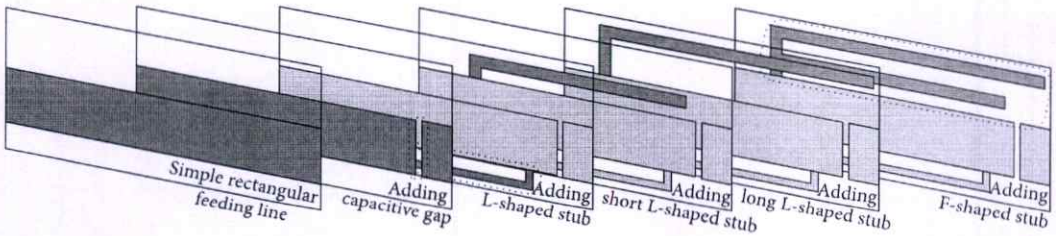

FIGURE 9: Feeding structure evolution.

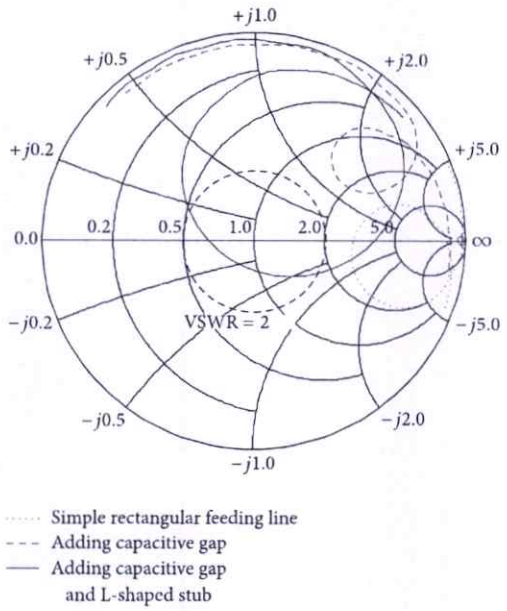

FIGURE 10: Simulated input impedance characteristics when the gap and L-shaped stub are installed.

4.3. Effects of F-Shaped Stub Feeding Structure. As the final step, the F-shaped stub is installed for enhancing the bandwidth. The F-shaped stub is a combination of short and long L-shaped stubs. Figure 11(a) shows the effect of installing the short and long L-shaped stubs on input impedance characteristics. When the short stub is installed, the impedance can be matched well to 50 Ω with a sufficient bandwidth; however, as shown in Figure 11(b), the main beam direction is around 60°. On the other hand, when the long stub is installed, the main beam direction is shifted closer to $\theta = 90^\circ$ as shown in Figure 11(b); however, the impedance bandwidth is narrow as shown in Figure 11(a) with a larger kink.

The F-shaped stub has the both functions of the short and long stubs; that is, the short stub is required for matching, and the long stub is for radiating CP in the direction at $\theta = 90^\circ$. Similarly, the F-shaped stub makes a small kink inside the circle of VSWR = 2 in the Smith chart and also makes the main beam direction closer to $\theta = 90^\circ$ resulting in 3 dB AR in $+y$-direction as shown in Figures 11(b) and 11(c). With the metallic arm along the $+y$-direction of the long or F-shaped stub, the e-field inside the radiator can be perpendicular to the ground plane and the stub element nearby the U-shaped slot. This behavior leads to direct the main beam closer to $\theta = 90^\circ$. As a result, in the final structure, the simulated and measured impedance can be matched to 50 Ω as shown in Figure 11(a) with the simulated bandwidth of 18 MHz, and the main beam direction is at $\theta = 70^\circ$ as shown in Figure 4. In the direction at $\theta = 90^\circ$, AR can be kept less than 3 dB with a sufficient simulated gain of 1.8 dBic.

4.4. Effects of Ground Plane Size. Figure 12(a) shows the variation in AR pattern with the ground plane size. Comparing the size (default) which is the same as the radiator in x-y plane, the ground plane is extended by $g = 20$ mm in $+x$- and $-x$-, $+x$- and $-y$-, $-x$- and $-y$-, and $\pm x$- and y-directions at the same time. When the ground is extended in $+x$ and $-y$-directions, the AR is minimized at around $\theta = 90^\circ$. This extension in the $+x$ direction contributes to have the e-field, near the open end of radiator, directed in x- or z direction in wider area of x-z plane at phase = 0° or 90°, respectively. In this case, the HPBW is about 105° covering the $\theta = 90^\circ$ direction as shown in Figure 12(b).

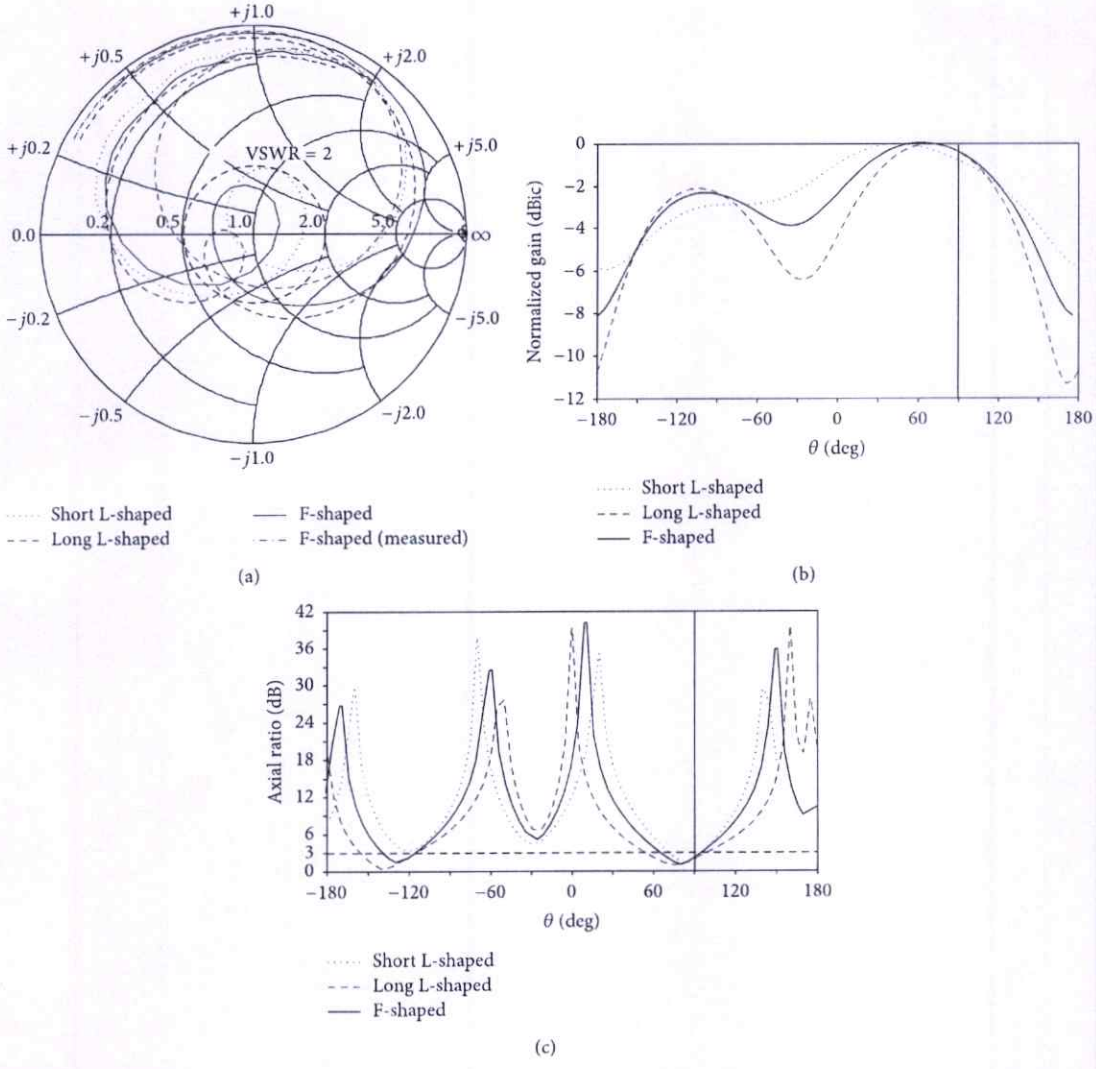

FIGURE 11: Simulated results of (a) input impedance characteristics, (b) antenna gain, and (c) AR pattern with θ. $\phi = 90^\circ$ in y-z plane at 925 MHz when the short, long, and F-shaped stubs are installed.

For the extension in the $+x$ and $-y$-directions, the main beam direction in which the minimum AR can be obtained gets closer to $\theta = 90^\circ$ with an increase in g from 5 to 25 mm as shown in Figure 13(a). For $g = 25$ mm, the angle for the minimum AR is the closest to $\theta = 90^\circ$; however, the antenna gain at $\theta = 90^\circ$ is smaller than that for $g = 20$ mm as shown in Figure 13(b). Therefore, the parameter g should be chosen as 20 mm for this design. Choosing $g = 20$ mm with the extension in the $+x$ and $-y$-directions, we have confirmed that the ground plane size has a sufficient area enough to suppress the leakage current on the coaxial cable.

5. Conclusion

This paper has proposed a low-profile and circularly polarized antenna with double U-shaped arms considering an application for handheld RFID readers at 920 MHz to 925 MHz band. The structure consists of a modified double U-shaped radiator and ground plane. A part of the arms of the radiator has been bent by 90° in the x-y plane for directing CP radiation parallel to the ground plane ($\theta = 90^\circ$). For keeping the sufficient impedance bandwidth for the RFID band, some matching stubs and a capacitive gap have been installed on the feeding structure, and the design process has been discussed. In addition to them, effects of the ground plane size on the CP direction have been discussed, and a sufficient antenna gain has been also confirmed in this direction. The measured results show good agreements with the simulated results. Furthermore, the principle for generating CP has been analyzed taking notice of the e-field distributions. Based on this principle, the U-shaped slot can contribute to achieve a low-profile antenna for radiating CP parallel to the ground.

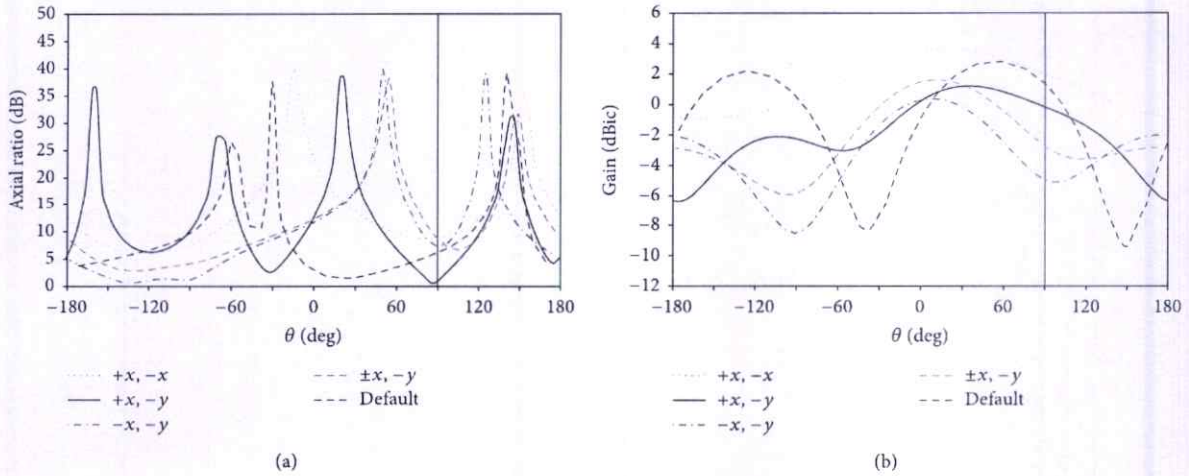

FIGURE 12: Simulated results of (a) AR pattern and (b) antenna gain in y-z plane at 925 MHz as a function of the ground plane size by g = 20 mm ($\phi = 90^\circ$).

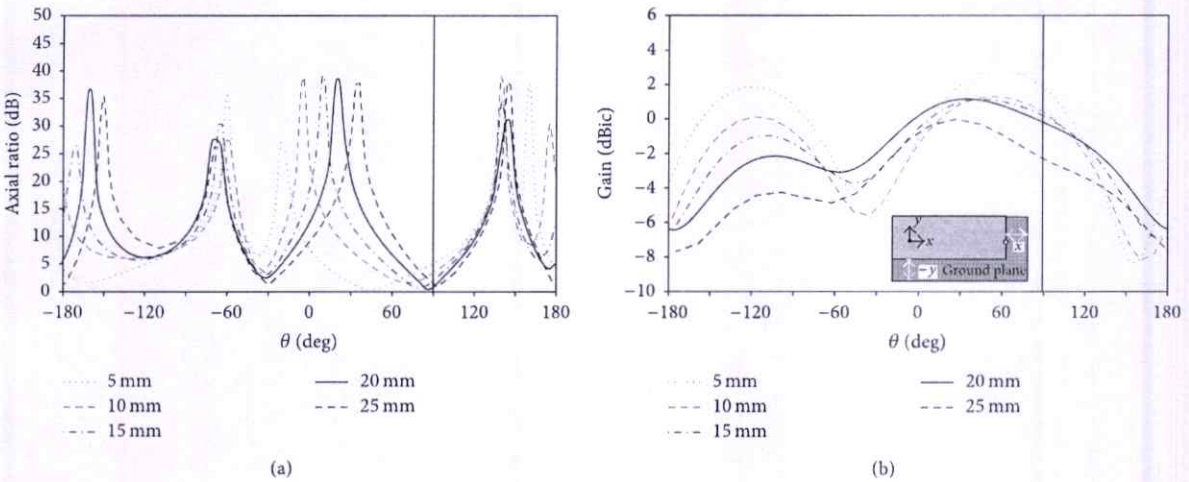

FIGURE 13: Simulated results of (a) AR pattern and (b) antenna gain in y-z plane at 925 MHz as a function of the extension in $+x$- and $-y$-direction g ($\phi = 90^\circ$).

Acknowledgment

This work is supported by the Thailand Research Fund (TRF) through the Royal Golden Jubilee Ph.D. Program under Grant no. PHD/0324/2552.

References

[1] K. Finkenzeller, *RFID Handbook*, Wiley, New York, NY, USA, 2nd edition, 2004.

[2] X. Chen, G. Fu, S.-X. Gong, Y.-L. Yan, and W. Zhao, "Circularly polarized stacked annular-ring microstrip antenna with integrated feeding network for UHF RFID readers," *IEEE Antennas and Wireless Propagation Letters*, vol. 9, pp. 542–545, 2010.

[3] W.-G. Lim, W.-I. Son, K.-S. Oh, W.-K. Kim, and J.-W. Yu, "Compact integrated antenna with circulator for UHF RFID system," *IEEE Antennas and Wireless Propagation Letters*, vol. 7, pp. 673–675, 2008.

[4] J.-H. Bang, C. B. Ochir, H.-S. Koh, E.-J. Cha, and B.-C. Ahn, "A small and lightweight antenna for handheld RFID reader applications," *IEEE Antennas and Wireless Propagation Letters*, vol. 11, pp. 1076–1079, 2012.

[5] J. J. Yu and S. Lim, "Design of an electrically small, circularly polarized, parasitic array antenna for an active 433.92 MHz RFID handheld reader," *IEEE Transactions on Antennas and Propagation*, vol. 60, no. 5, pp. 2549–2554, 2012.

[6] Y.-F. Lin, Y.-K. Wang, H.-M. Chen, and Z.-Z. Yang, "Circularly polarized crossed dipole antenna with phase delay lines for RFID handheld reader," *IEEE Transactions on Antennas and Propagation*, vol. 60, no. 3, pp. 1221–1227, 2012.

[7] N. Nasimuddin, Z. N. Chen, and X. Qing, "Asymmetric-circular shaped slotted microstrip antennas for circular polarization

and RFID applications," *IEEE Transactions on Antennas and Propagation*, vol. 58, no. 12, pp. 3821–3828, 2010.

[8] P. V. Nikitin and K. V. S. Rao, "Helical antenna for handheld UHF RFID reader," in *Proceedings of the 4th Annual IEEE International Conference on RFID (RFID '10)*, pp. 166–173, Orlando, Fla, USA, April 2010.

[9] W.-I. Son, M.-Q. Lee, and J.-W. Yu, "Module integrated antenna with circular polarization for mobile UHF RFID reader," *IEEE Transactions on Microwave Theory and Techniques*, vol. 59, no. 4, pp. 1157–1165, 2011.

[10] S.-H. Chang and W.-J. Liao, "A novel dual band circularly polarized GNSS antenna for handheld devices," *IEEE Transactions on Antennas and Propagation*, vol. 61, no. 2, pp. 555–562, 2013.

[11] K. Wei, Z. Zhang, and Z. Feng, "Design of a wideband horizontally polarized omnidirectional printed loop antenna," *IEEE Antennas and Wireless Propagation Letters*, vol. 11, pp. 49–52, 2012.

[12] C. C. Lin, L. C. Kuo, and H. R. Chuang, "A horizontally polarized omnidirectional printed antenna for WLAN applications," *IEEE Transactions on Antennas and Propagation*, vol. 54, no. 11, pp. 3551–3556, 2006.

[13] R.-L. Li, V. F. Fusco, and H. Nakano, "Circularly polarized open-loop antenna," *IEEE Transactions on Antennas and Propagation*, vol. 51, no. 9, pp. 2475–2477, 2003.

[14] R. Li, G. DeJean, J. Laskar, and M. M. Tentzeris, "Investigation of circularly polarized loop antennas with a parasitic element for bandwidth enhancement," *IEEE Transactions on Antennas and Propagation*, vol. 53, no. 12, pp. 3930–3939, 2005.

[15] X. Yang, Y. Z. Yin, W. Hu, and S. L. Zuo, "Low-profile, small circularly polarized inverted-L antenna with double-folded arms," *IEEE Antennas and Wireless Propagation Letters*, vol. 9, pp. 767–770, 2010.

[16] Y. Zhang and T. Fukusako, "Design of circularly polarized low-profile and slender antenna with a helical element," *IEEE Antennas and Wireless Propagation Letters*, vol. 11, pp. 523–526, 2012.

[17] Y. Saito and T. Fukusako, "Low-profile and electrically small meander-line antenna using a capacitive feed structure," *IEEE Antennas and Wireless Propagation Letters*, vol. 11, pp. 1281–1284, 2012.

[18] Y. Tanogashira and T. Fukusako, "Directional radiation pattern of surface wave antenna using dogbone structure," *IEICE Communication Express*, vol. 1, no. 2, pp. 85–88, 2012.

[19] CST-Microwave Studio and User's Manual CST-Microwave Studio, Framingham, Mass, USA, 2006.

[20] K. Lertsakwimarn, R. Suwalak, and C. Phongcharoenpanich, "A compact loop antenna with parasitic split ring for UHF RFID application," in *Progress in Electromagnetics Research Symposium (PIERS '13)*, pp. 219–222, Taipei, Taiwan, 2013.

1st International Symposium on Technology for Sustainability (ISTS2011)

26-29 January 2012, KMITL, Bangkok Thailand

Co-organized by:
Institute of National Colleges of Technology, Japan
and
King Mongkut's Institute of Technology Ladkrabang, Thailand

CIT018 *"Application of Ontology to Hydroponics"*
Areeworn Phutthisathian, Nakulrad Pantasen, Noppadol Maneerat, Ruttikorn Varakulsiripunth, Kaoru Takahashi, Yasushi Kato

CIT019 *"Off-line Signature Verification Using Gray Level Co-orcurence Matrix Texture Analysis"*
Nguyen thi Minh Nguyet, Pittak Thumwarin, Takenobu Matsuura

Communication Technology (COT)

COT001 *"A Hybrid Mobility Model for MANET Simulation in an Earthquake Scenario"*
Anurat Kamhangharn, Chanboon Sathitwiriyawong

COT002 *"The Analysis of Symmetrical PRUS (Paired Repeated Unequally Spaced) Channels Allocation for FDM Lightwave System"*
Ashira Jumpates, Suthichai Noppanakeepong, Nainapas Injoungjirakit

COT003 *"A Novel Dual-Band Helical Antenna for Radio Beacon Receiver"*
Rassamitut Pansomboon, Supakit Kawdungta, Ravipat Phudpong, Chuwong Phongcharoenpanich

COT004 "*Folded Arm H-Slot Antenna with Matching Rectangular Slot for UHF RFID Tag"*
Nattaset Mhudtongon, Kittisak Phaebua, Chuwong Phongcharoenpanich

COT005 *"A Dual-Band RFID-Reader Antenna using Truncated Bowen Knot Structure"*
Putuch Charoenchue, Chuwong Phongcharoenpanich, Kraison Aunchaleevarapan

COT006 *"Improvement of Unidirectional Antenna Using a Hemispherical Monopole with Circular Reflector for IEEE 802.11 a/b/g/n"*
Kanawat Nuangwongsa, Chuwong Phongcharoenpanich, Sompol Kosulvit

COT007 *"Metallic Tag Antenna with Defected Ground Plane for UHF-RFID System"*
Kittima Lertsakwimarn, Chuwong Phongcharoenpanich

COT008 *"A Circularly Polarized Patch Antenna with Rectangular Slot on Defected Ground Plane for RFID Reader"*
Rattapong Suwalak, Kittama Lertsakwimarn, Chuwong Phongcharoenpanich

COT009 *"Modal Characteristics of a Circular Microstrip Antenna on Circular Ground Plane for SDARS Applications"*
Sanchai Eardprab, Chuwong Phongcharoenpanich

COT010 *"Performance Enhancement of Single Loop Antenna with Arbitrary Structure using Evolution Strategies Optimization for LF-RFID Applications"*
Sarayoot Todnatee, Chuwong Phongcharoenpanich

COT011 *"Pulse Distortion and Time Delay in UWB Propagation Channel with Human Body Shadowing"*
Sathaporn Promwong, Sanit Teawchim, Musleemin Noitubtim, Chalermpan Fongsamut, Tanabath Laohawat

Metallic Tag Antenna with Defected Ground Plane for UHF-RFID System

Kittima Lertsakwimarn and Chuwong Phongcharoenpanich

Faculty of Engineering, King Mongkut's Institute of Technology Ladkrabang (KMITL), Bangkok 10520, Thailand

Abstract— **In this paper, the passive ultra high frequency (UHF) radio frequency identification (RFID) tag is presented for the applications to distinguish metallic from non-metallic. Typically, UHF RFID tag antennas have some limitation for using with metallic material. Therefore, it is desirable to design UHF RFID tag antennas that can be worked well with metallic products. The proposed antenna structure consists of defected ground plane, T-structure including longitudinal strip and rectangular strip with shorting-pin connected to the ground plane. The parametric study is described. It is found that the antenna with defected ground plane can increase difference maximum read range of tag antenna between on metallic plate and in free space. The proposed UHF RFID tag antenna can adjust the resistance and the reactance by charging the longitudinal strip of T-structure. A compact tag prototype is fabricated with area of only 90×20×3 mm^3. The experimental results of maximum read range on the metallic plate and in free space are 83 mm and 24 mm, respectively. The simulation and measurement results of the proposed RFID tag antenna are also presented.**

Index Terms— **Radio frequency identification (RFID), tag, T-structure, metallic object.**

I. Introduction

Radio frequency identification (RFID) is a technology used for object identification. There are numerous applications of RFID technologies such as retail, transportation, manufacturing and supply chain systems. Its applications are constantly being announced in very wide areas [1] because it is superior to bar codes and infrared technologies. Various bands in RFID systems such as low frequency (LF), high frequency (HF), ultra high frequency (UHF), and microwave frequency, UHF-RFID systems are very popular because the operating range is further than the LF- and HF-RFID systems. The LF- and HF-RFID systems use the near-field coupling techniques whereas the UHF-RFID utilizes the far-field radiation technique. The typical system operation consists of tag, reader and information management system. The reader uses an antenna to transmit radio energy to interrogate a transponder or tag that is attached to the item to be identified.

Generally, the types of tag can be classified into three different categories: active, semi-active and passive tags. The active and semi-active tags are necessary to operate with battery and it will limit the life time. The passive tag has no problem about the energy restrictions that makes the passive RFID systems will be used in many high-volume applications, such as warehousing and retail store applications [2-4] The passive tag consists of the antenna used to receive the RF energy and the tag chip that is used to convert RF to DC energies. The system requires novel solutions for tag antennas to be used with different objects. The communication in these systems is based on backscattering of modulated electromagnetic wave. The materials of object affects the performance of tag antennas, and therefore considering the material of mounted the object in tag antenna design is crucial for achieving reliable identification with passive RFID technology [1]. There are several products made from different materials such as wood, plastic and metal in logistics system. The metallic objects make strong reflection of the electromagnetic waves in RFID communication. The performance of most RFID tags will be degraded when it is mounted with metallic object. One of the most challenges in the design of RFID tag is to reduce the effects of interference from the metallic surface, which is achieved for instance by inserting the tag in a high permittivity substrate or embedding it with ground plane [2]. In literature, there are many researches about the design of metal RFID tag antenna in recent years such as the invert-F antenna (IFA), planar invert-F antenna (PIFA), and patch-type antenna [5-7].

This paper proposes the RFID tag antenna for the applications to distinguish metallic from non-metallic objects. The allocated UHF band in Thailand is 920 – 925 MHz. In Section II, we show antenna configuration. The design and simulation of results the proposed antennas are given in Section III. Section IV presents our experimental. Finally, conclusion is given in Section V.

II. Antenna Configuration

In this section, the antenna configuration will be addressed. The design antenna consists of a radiator with T-structure strip on one side of a dielectric substrate and defected ground plane on the other side. The advantages of the designed structure includes low profile, light weight, ease of fabrication, and low fabrication costs.

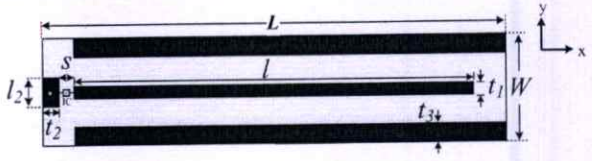

(a) Front view

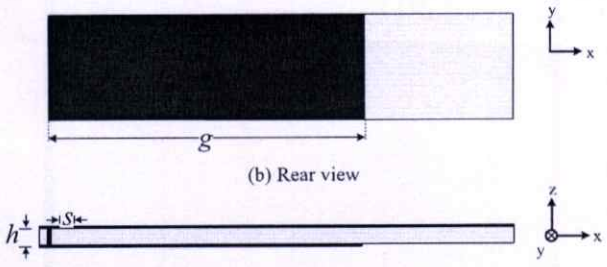

Figure 1. The propose antenna configuration

Figure 1 illustrates the antenna configuration. The proposed antenna consists of T-structure including longitudinal strip and rectangular strip with shorting-pin connected to the ground plane. The ground plane was defected to only 50 mm to make work well on metallic object. The overall size of tag antenna ($L\times W\times h$) in this paper is $90\times20\times3$ mm^3. The width (W) and length (L) of tag antenna are suitable for implementation, which is convenient to mount and remove tag antenna with mountable objects. The antenna is designed on FR4 substrates with the thickness h of 3 mm, relative permittivity of 4.3 and loss tangent of 0.02. The width of rectangular strip contained shorting-pin t_2 is fixed about $\lambda/50$ (3.12 mm) which is very short comparing with wavelength. The length of strip that is connected to the IC chip l_2 is first fixed at 20 mm and last length fixed at 4 mm. The width of the gap to attach IC chip s is 2 mm. The thickness of T-structure strip t_1 is 2 mm that is identical to the length of IC chip. The width of parasitic parallel line t_3 is 5.5 mm. The simple to design and easy for fabrication are described.

III. Antenna Design And Simulation

In this section, the antenna design and the simulation results will be addressed. The antenna was designed using the CST MW Studio[8] and the antenna evolution is initialized with T-structure to study the impedance characteristic variations. Next, the second will be added to parasitic parallel line. Both length of T-structure and width of parasitic parallel can be used for adjusting the resistance and the reactance of antenna to meet the required specifications. And the last step will be defected of ground plane to make maximum percentage of difference read range of tag antenna between attach on metallic and in free space.

A. T-Structure and parasitic parallel antenna

Most of tag antennas are designed based on conjugate match with the chip impedance for maximum power transfer. To improve performance, gain, efficiency and polarization of tag antenna are enhanced. In this paper, metal tag antenna is designed for UCODE G2XL chip [9], whose input impedance is about 21.65-j191.70 Ω at 922.5 MHz.

1a. T-Structure antenna

The antenna evolution is initialized with longitudinal strip length of $\lambda/2$ of T-structure show in figure 2 to study the variations of the impedance characteristics. This can be used for adjusting the resistance and the reactance of antenna to meet the required specifications.

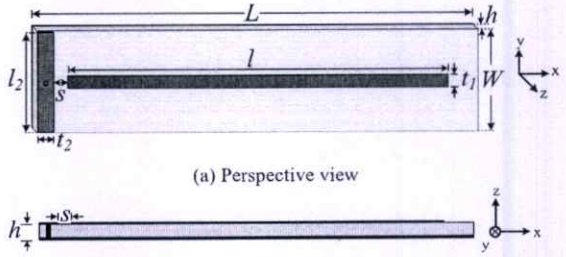

Figure 2. T-structure antenna configuration

The impedance of these parameter variations at the operating frequency of 922.5 MHz are shown in figure 3. The increased parameter l (length of longitudinal strip) is also studied. The simulation results of the reactance and the resistance are changed to shift the operating frequency. Therefore, the parameter l can be control the impedance of the RFID tag antenna. From those described in the above. Matching impedance of antenna found that the adjustment length of longitudinal strip of T-structure antenna, resistance is mismatching impedance. To adjust the length of longitudinal strip of T-structure antenna is not appropriate to adjust the RFID tag antenna to matching impedance. The next step will add a parasitic parallel line. By placing parallel with a longitudinal strip line which will be discussed in the next section

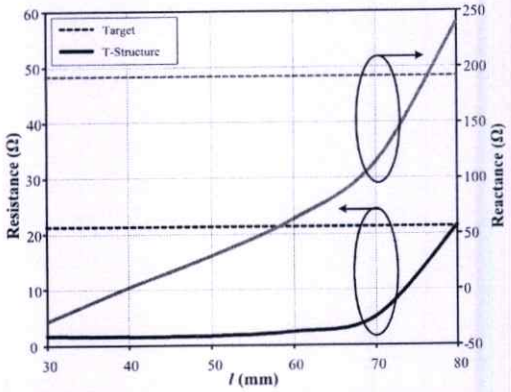

Figure 3. Simulated impedance versus l at the operating frequency on metallic plate

1b. T-Structure and parasitic parallel antenna

Figure 1a shows the structure of the RFID tag antenna with a T-structure and parasitic parallel. The parameters parasitic parallel line is placed parallel to the longitudinal strip line which is the length of the parameters parasitic parallel line will start at the same location as length of longitudinal strip line. But the line long to the edge of the antenna with the aim to ease of design. Then, we studied characterization of the impedance of the RFID tag antenna when changing the width of the parasitic line parameters (t_3) increments from the bottom of the RFID tag antenna.

Results of the impedance of the RFID tag antenna from the model when changes in line widths parasitic line

parameters display shown in Figure 4, it can seen that when the width of parasitic parallel lines increased at the operating frequency of 922.5 MHz, results that the reactance and the resistance are changed to shift the operating frequency. Therefore, in adjusting impedance of the RFID tag antenna this match conjugate by adjust the longitudinal strip length and width of the line parasitic parallel will make the appropriate value.

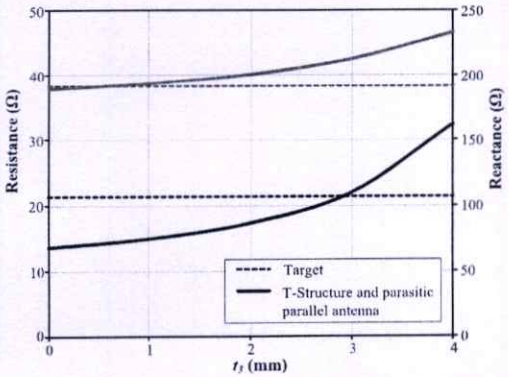

Figure 4. Simulated impedance versus t_3 at the operating frequency on metallic plate

2. T-Structure and parasitic parallel antenna with defected ground plane

The objective of the antenna is designed to work well with metallic objects. In other words that has meaning, does not work when not mounted on a metallic placed such as in the air, etc. So, after studying the various parameters, the T-structure and parasitic parallel antenna has matching impedance when attached to the metallic plate. Next, change material of the simulated antenna is placed in a free space. When calculating the percentage of transmission coefficient, it is changed from 96.8% when mounted on a metallic plate is 42.2% when placed in a free space. Then calculates the maximum read range from the Friis free space transmission equation .The percentage difference of the maximum read range of the antenna was mounted on a metallic plate and placed in the free space is equal to 50% which is less than desirable. Thus, further studies to defect the ground plane of the antenna when mounted on a metallic plate and placed in the free space. Consider the performance from maximum read range tags.

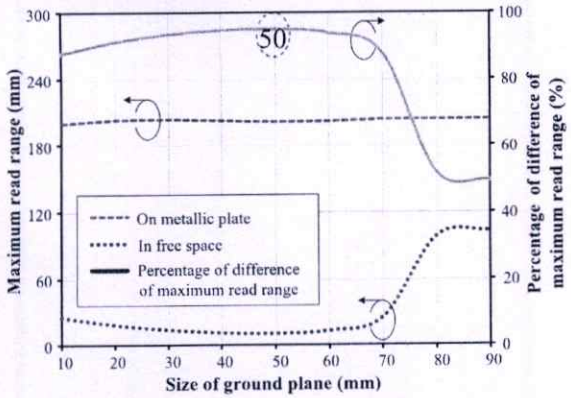

Figure 5. Calculated result of read range antenna when in free space and on metallic plate with vary size ground plane

Figure 5 shows the maximum read range of T-structure and parasitic parallel antenna when in free space and on metallic plate with vary size ground plane. From the graph, the maximum read range of the antenna when mounted on metallic plate is relatively stable, and when placed in a free space has changed. Therefore, reducing the ground plane will affect the reading range of the antenna when placed in free space. In the graph of percentage difference of maximum read range between mounted on metallic plate and in free space, found that defected ground plane only of 50 mm will be the maximum percentage difference between the maximum read range of the antenna when mounted on a metallic plate and in free space are equal to 95%.

The optimum parameters of the propose antenna on metallic object show in Table 1. The size of metallic object is $1.5\lambda \times 1.5\lambda$ mm^2. These parameters can achieve the impedance at the operating frequency (922.5 MHz) are 22.46+j197.14 Ω and 3.6+j93.54Ω, respectively.

TABLE I. PHYSICAL DIMENSION OF THE ANTENNA PARAMETERS

Parameters	L	W	l	l_2	t_1	t_2	t_3	s	g
Size in mm	90	20	75.4	4	2	3.14	5.5	2	50

The simulated result of radiation pattern in XZ-plane and YZ-plane are shown in figure 6 and 7. In figure 6, it can seen that the direction of the antenna main beam does not vary with the size of the metallic plate, and its directivity is increased as the of metallic plate increases. The simulated result of radiation pattern of antenna on $1.5\lambda \times 1.5\lambda$ metallic plate and in free space at the operating frequency are shown in figure 7.The half-power beamwidth in XZ-plane and YZ-plane are about 63.8 and 70.4 degrees respectively. The front to back ratio is 12.7 dB.

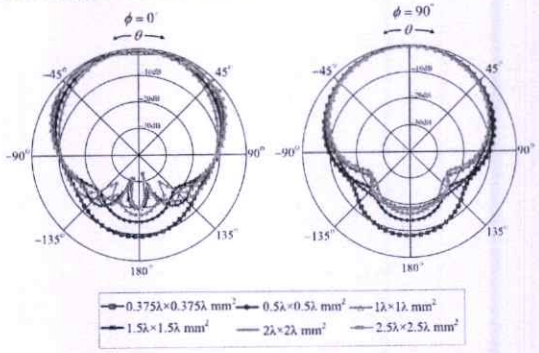

Figure 6. Simulated radiation patterns with different sizes of metallic plate

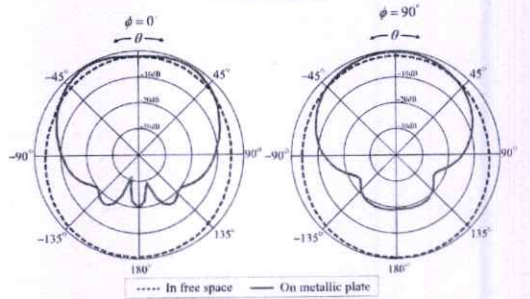

Figure 7. Simulated radiation pattern in free space and on metallic material

The actual tag antenna performance is the assessed communication distance. Therefore, the loss power transfer between chip and the proposed antenna is significant. The power reflection coefficient is given by

$$\Gamma = \frac{Z_a + Z_c^*}{Z_a + Z_c}. \qquad (1)$$

The R_a and R_c are the resistance of the antenna and IC chip, respectively. In the same fashion, the impedance of the antenna and IC chip are Z_a and Z_c. The $|S_{11}|$ expressed in decibels

$$RL(\text{dB}) = -20\log_{10}|S_{11}| \qquad (2)$$

is illustrated in Fig. 8. The $|S_{11}|$ of the proposed antenna on metallic object is less than -3 dB that cover the operating frequency of 914-926. It is noted that this frequency range can cover the operating frequency of UHF RFID in Thailand (920-925MHz).

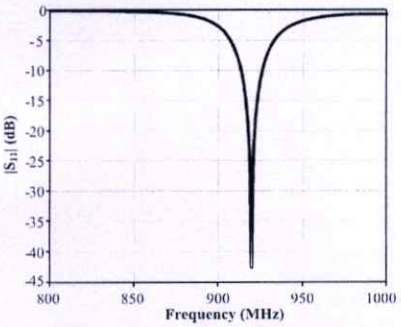

Figure 8. Simulated $|S_{11}|$ of tag antenna on metallic object

IV. Experimental Result

In the measurement, a Motorola RFID Reader model is XR450 [10] whereas the standard dipole antenna of reader model is MP651B. The linearly polarized reader antenna with the gain of 2.15 dBi[11] were used in the measurements. A photograph of the proposed tag antenna is depicted in figure 9. The tag antenna was first measured in free space and later attached to a 1.5λ×1.5λ aluminum metallic plate. The maximum read range of tag antenna in free space and on metallic plate are 24 mm and 83 mm, respectively.

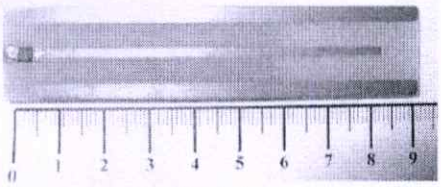

(a) Front view

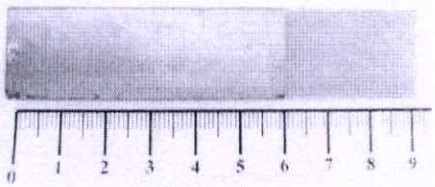

(b) Rear view

Figure 9. Photograph of the prototype antenna

V. Conclusion

This paper proposes UHF RFID tag antenna design for the applications to distinguish metallic from non-metallic, which it is design tag antennas that can be worked well with metallic products. In the design, the defected ground plane make to given maximum percentage of maximum difference read range of tag antenna between on metallic plate and in free space. It mean that tag is work well in metallic plate and bad work in free space. The resistance and the reactance of the proposed antenna can be adjusted by changing longitudinal strip of T-structure and width of parasitic parallel line. The simulation results illustrated the performance of proposed antenna in terms of $|S_{11}|$, and the advantage of proposed antenna is suitable for fabrication. The experimental result shows that the maximum read range of tag antenna in free space and on metallic object with size of 1.5λ×1.5λ aluminium metallic plate are 24 mm and 83 mm, respectively. The distance reading that is based on the performance of readers and antennas to send data and make it longer by adding the reader will send the data and the gain of the antenna however, must be sent under the standard constraints of the country are issued by the National Telecommunications Commission. It is therefore concluded that the proposed antenna can reduce the impact of metals on the efficiency of the RFID tag antenna.

VI. References

[1] S.L. Chen, S.K. Kuo and C.T. Lin, "A metallic RFID tag design steel bar and wire-rod management application in the steel industry," *Progress In Electromagnetics Research, PIER 91*, pp.195–212, 2009.

[2] L. Sydanheimon, L. Ukkonen, and M. Kivikoski, "Effects of size and shape of metallic objects on performance of passive radio frequency identification," *Int J Adv Manuf Technol (2006)*, vol. 30, pp. 897-905, October 2006.

[3] K. Finkenzeller, RFID Handbook, 2nd ed. Wiley, New York, 2003.

[4] N Raza, V Bradshaw, M Hague, "Application of RFID technology," *IEE Colloquium on RFID Technology*, no. 123, pp. 1/1-1/5, 1999.

[5] K. H. Kim, J. G. Song, D. H. Kim, H. S. Hu, and J. H. Park, "Fork-shaped RFID tag antenna mountable on metallic surfaces," *Electronics Letters*, vol. 43, no. 25, pp. 1400–1402, 2007.

[6] H Kwon and B. Lee, "Compact slotted planar inverted-F RFID tag mountable on metallic objects," *Electronics Letters*, vol. 41, no. 24, pp. 1308–1310, 2005.

[7] B. Yu, S. J. Kim, B. Jung, F. J. Harackiewicz, and B. Lee, "RFID tag antenna using two-shorted microstrip patches mountable on metallic objects," *Microwave and. Optical Technology Letters*, vol. 49, no. 2, pp. 414–416, 2007.

[8] CST-Microwave Studio, User's Manual, 2006.

[9] NXP, Ultrahigh frequency smart label ICs [online] Available URL:http://www.nxp.com/acrobat_download/literature/9397/75016225.pdf.

[10] Available URL:http://www.motorola.com/Business/US-EN/Business+Product+and+Services/RFID/RFID+Readers/XR450+Fixed+RFID+Reader_US-En

[11] Available URL:http://www.testmart.com/sp.cfm/ANT/ANRI/MP651B.html

PIERS 2013 Taipei

Progress In Electromagnetics Research Symposium

Program

March 25–28, 2013
TAIPEI

www.emacademy.org
www.piers.org

15:00 A Wideband Circularly Polarized Magneto-electric Dipole Antenna
Kwai Man Luk (City University of Hong Kong, China); Mingjian Li (City University of Hong Kong, China);

15:20 **Coffee Break**

Session 1P5b
Small Size and Low-profile Antennas

Monday PM, March 25, 2013
Room E
Organized by Takeshi Fukusako
Chaired by Takeshi Fukusako

15:40 Use of Transparent Dielectric Resonator Antenna as a Light Cover
Xiao Sheng Fang (City University of Hong Kong, China); Kwok Wa Leung (City University of Hong Kong, China);

16:00 A Consideration of Grounded Helical Antenna for Coupled-resonant Wireless Power Transfer
Hiroshi Hirayama (Nagoya Institute of Technology, Japan); Tomohiro Amano (Nagoya Institute of Technology, Japan); Nobuyoshi Kikuma (Nagoya Institute of Technology, Japan); Kunio Sakakibara (Nagoya Institute of Technology, Japan);

16:20 A Compact Loop Antenna with Parasitic Split Ring for UHF RFID Application
Kittima Lertsakwimarn (King Mongkut's Institute of Technology Ladkrabang, Thailand); Rattapong Suwalak (King Mongkut's Institute of Technology, Thailand); Chuwong Phongcharoenpanich (King Mongkut's Institute of Technology, Thailand);

16:40 Compact Size Antenna for Car FM Radio
Dau-Chyrh Chang (Oriental Institute of Technology, Taiwan, R.O.C.); Fong-Yi Lin (Oriental Institute of Technology, Taiwan); Bing-Hao Zeng (Lorom Industrial Co. Ltd, Taiwan); Jay Chen (Lorom Industrial Co. Ltd, Taiwan);

17:00 Triple-band Circularly Polarized Small Microstrip Antenna with Crank Slits
Takafumi Fujimoto (Nagasaki University, Japan); Akinori Tanaka (Nagasaki University, Japan);

17:20 Gain Enhancement of Circularly Polarized Slender Antenna Using a Wider Helical Element
Ye Zhang (Kumamoto University, Japan); Takeshi Fukusako (Kumamoto University, Japan);

17:40 A New Method of Antenna Miniaturization
Li-Yuan Cheng (National Chiao Tung University, Taiwan); Fu-Chiarng Chen (National Chiao Tung University, Taiwan);

Session 2A1
Manipulating Wave with Metamaterials and Photonic Crystal 1

Tuesday AM, March 26, 2013
Room A
Organized by Che Ting Chan, Zhi Hong Hang
Chaired by Zhi Hong Hang

08:40 Transformation Bending Device Emulated by Graded-index Waveguide
Y. Wang (Nanjing University, China); C. Sheng (Nanjing University, China); Hui Liu (Nanjing University, China); Y. J. Zheng (Nanjing University, China); Cong Zhu (Nanjing University, China); S. M. Wang (Nanjing University, China); S. N. Zhu (Nanjing University, China);

09:00 Resonantly Confined Modes in Optical Fibers with Circularly Aligned High-index Rods
Yasuo Ohtera (Tohoku University, Japan); Haruka Hirose (Tohoku University, Japan); Hirohito Yamada (Tohoku University, Japan);

09:20 Manipulating Electromagnetic Waves in Subwavelength Dimensions by Meta-atoms
Bo Hou (Soochow University, China); Sucheng Li (Soochow University, China);

09:40 Terahertz Metamaterial Absorbers for Sensing and Imaging
Patrick Kung (The University of Alabama, USA); Seongsin Margaret Kim (The University of Alabama, USA);

10:00 Anisotropic Guidance Correction on the Analytical Design Approach of Thin-film Photonic Lüneburg Lens
Hanhong Gao (Massachusetts Institute of Technology, USA); Baile Zhang (Nanyang Technological University, Singapore); George Barbastathis (Massachusetts Institute of Technology, USA);

10:20 **Coffee Break**

10:40 Operational Slow Line Underpinned by a 1D Metamaterial
Darell Dowlet (UPMC Univ Paris 06, France); Thierry Ditchi (UPMC Univ. Paris 6, ESPCI-Paris Tech, France); Emmanuel Geron (ESPCI-Paris Tech, France); Jerome Lucas (ESPCI-Paris Tech, France);

Progress In Electromagnetics Research Symposium Proceedings, Taipei, March 25–28, 2013 219

A Compact Loop Antenna with Parasitic Split Ring for UHF RFID Application

Kittima Lertsakwimarn, Rattapong Suwalak, and Chuwong Phongcharoenpanich
Faculty of Engineering, King Mongkut's Institute of Technology Ladkrabang
Bangkok 10520, Thailand

Abstract— This paper presents a compact loop antenna with parasitic split ring for the reader of the UHF RFID application. The proposed antenna is made up of the rectangular loop structure (feeding element) and the parasitic split ring to reduce the overall antenna dimension. It is found that the size can be decreased by 50% of the typical single loop antenna. The simulation is carried out by using CST Microwave Studio program based on the Finite Integral Technique (FIT). Furthermore, the antenna parameters are optimized using the Quasi Newton method. The effect of the antenna parameters on the impedance bandwidth are investigated in this paper. The comparison between the simulation and experimental results are also discussed. From the results, the antenna has the $|S_{11}|$ less than -10 dB along the bandwidth of 12 MHz (1.6%). It can be operated in UHF RFID system in Thailand with the frequency band from 920 MHz to 925 MHz. The omnidirectional beam is obtained with the maximum gain of 1.5 dBi at the center frequency of 922.5 MHz. The antenna is designed on FR4-substrate. The overall size of the proposed antenna is 51 mm $\times$ 38 mm $\times$ 0.8 mm ($0.15\lambda\times$ $0.11\lambda\times$ 0.02λ). It is easily embedded inside handheld reader. Moreover, the proposed antenna is simple structure, low profile and easy fabrication. Therefore, the compact loop antenna with parasitic split ring can be employed with a handheld UHF RFID reader.

1. INTRODUCTION

Radio frequency identification (RFID) is a technology used for object identification. The RFID technology has been used for many applications such as retail, transportation, manufacturing and goods flow systems [1]. There are various frequency bands of RFID systems such as low frequency (LF), high frequency (HF), ultra high frequency (UHF), and microwave frequency. The UHF-RFID systems are very popular because the operating range is further than the LF- and HF-RFID systems. The LF- and HF-RFID systems use the near-field coupling techniques whereas the UHF-RFID utilizes the far-field radiation technique. The typical system operation consists of tag, reader and information management system. The reader uses an antenna to transmit radio energy to interrogate a transponder or tag that is attached to the item to be identified.

Generally, the RFID reader can be classified into two different categories: stationary and handheld readers. The advantage of handheld reader is used to read the data from the tags attached on goods or materials that are not convenient to move. For this reason, the handheld reader is suitable to use for crawl items in a retail store or warehouse management, including gathered information about pallets of goods. The special considerations in the design of handheld reader antenna are compact size, light weight, strong structure, durable use and convenient movement [2].

In recent years, there are many types of studied antennas for handheld RFID reader such as a printed dipole antenna [3], three-element printed Yagi antenna [4], helical antenna [2] and four non-meandered printed inverted-F antenna [5], that mainly focus on the design of the compact size antenna. By using the same fashion as the printed dipole antenna in [3], the proposed antenna design utilizes the printed loop antenna with parasitic split ring on FR4-substrate.

This paper proposes the compact loop antenna and parasitic split ring on FR4-substrate for the reader of RFID applications. The allocated UHF band in Thailand is 920–925 MHz. In Section 2, antenna design is shown. The simulation and experimental results of the proposed antennas are given in Section 3. Finally, conclusion is given in Section 4.

2. ANTENNA DESIGN

In this section, the antenna design and the simulation results will be addressed. The antenna is simulated using the CST Microwave Studio [6], and the antenna evolution is initialized with rectangular loop structure with total length of perimeter of one wavelength to study various characteristics. Next, two parasitic parallel lines of the same size will be added which are placed above and below of the rectangular loop. It is noted that the width of the loop and length of the parasitic

parallel lines have identical size. The last step is to add the parasitic split ring in place of parasitic parallel lines. The width and the length of the rectangular loop and parasitic split ring can be adjusted to meet the required characteristics.

2.1. Rectangular Loop Antenna with Parasitic Parallel Lines

The simulation of the antenna evolution is initialized with the rectangular loop antenna with perimeter of one wavelength on FR4-substrate as shown in Fig. 1(a). The antenna is designed to operate at 922.5 MHz where it is the center frequency of UHF RFID band in Thailand. It is found that the rectangular loop antenna can be operated at 922.5 MHz with omnidirectional pattern in vertical plane. According to the principle of loop antenna when the circumference is about the wavelength, the maximum radiation will be perpendicular to the plane of the loop. When the loop size is smaller than one wavelength, the radiation is gradually changed from an omnidirectional pattern in vertical plane to an omnidirectional pattern in horizontal plane [7]. Therefore, the requirement of the antenna design is to radiate in horizontal plane of the loop. Then, parasitic parallel lines will be add with the same size which are placed above and below the loop, in order to reduce the size of loop antenna. Fig. 1(b) illustrates the rectangular loop antenna with parasitic parallel lines configuration.

From the result of $|S_{11}|$ at the operating frequency of 922.5 MHz as shown in Fig. 2, it can be seen that when add parasitic parallel lines, the $|S_{11}|$ is decreased. However, with the added parasitic parallel lines of the loop antenna, the total size of the antenna cannot be sufficiently reduced. The next step is to add the parasitic split ring structure in place of the parasitic parallel lines which will be discussed in the next section.

2.2. Rectangular Loop Antenna with Parasitic Split Ring

In order to apply the antenna for handheld reader application in horizontal plane, the size of the antenna and radiation pattern must be suitable for implementation with handheld RFID reader. Fig. 3 shows the structure of the rectangular loop antenna and parasitic split ring. This structure can be further reduced the overall size of the antenna. The proposed antenna parameters must be optimized.

3. SIMULATION AND EXPERIMENTAL RESULTS

All simulations were performed by using CST Microwave Studio. The optimum antenna parameters are tabulated in Table 1. The $|S_{11}|$ versus frequency of the proposed antenna is shown in Fig. 4. This antenna can be operated along the UHF RFID band. It is found that the $|S_{11}|$ is lower than -10 dB from 915 MHz to 930 MHz or 1.6% bandwidth of UHF band. For the measurement, a photograph of the proposed prototype tag antenna is depicted in Fig. 5. The measurement of $|S_{11}|$

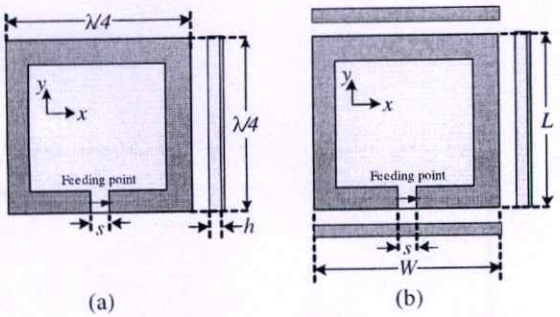

Figure 1: The antenna structure. (a) The single rectangular loop antenna structure. (b) The rectangular loop antenna with parasitic parallel lines structure.

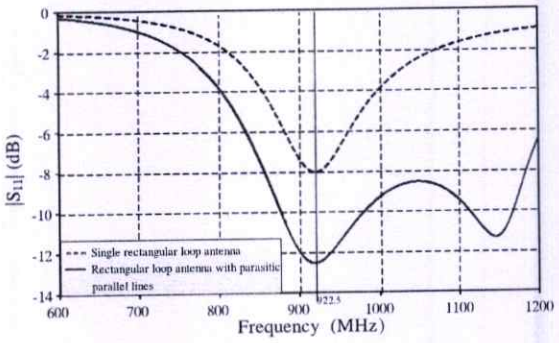

Figure 2: The simulation result of the $|S_{11}|$ of the single rectangular loop antenna and rectangular loop antenna with parasitic parallel lines structure.

Table 1: The optimum antenna parameters.

Parameters	W	L	w_1	l_1	t_1	t_2	t_3	s_1	s_2	h
Size in mm	51	38	26.5	23.5	4	7	3	2	7	0.8

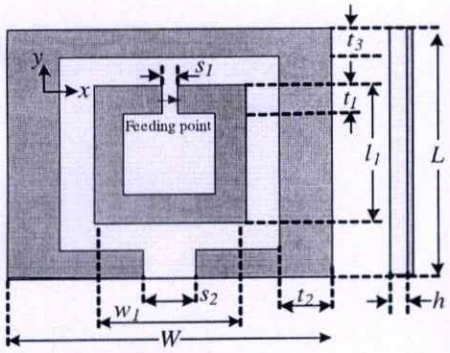

Figure 3: The proposed antenna configuration.

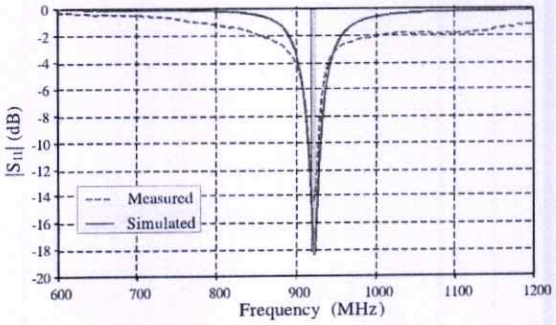

Figure 4: Simulated and measured $|S_{11}|$ versus frequency.

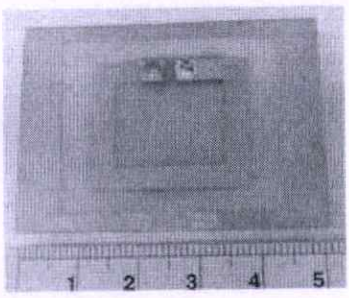

Figure 5: Photograph of the proposed prototype antenna.

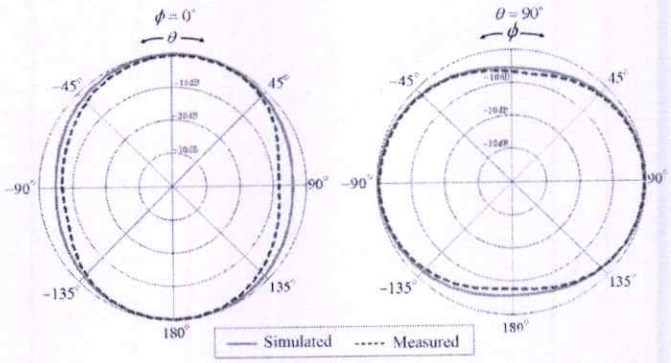

(a) xz-plane (b) xy-plane

Figure 6: Simulated and measured radiation patterns at 922.5 MHz.

and radiation pattern was carried out using the Agilent E5230A vector network analyzer (VNA), which agree fairly well with the simulation result, as shown in Fig. 4 and Fig. 6. The measurement of $|S_{11}|$ is lower than -10 dB from 916 MHz to 928 MHz (1.2% bandwidth).

4. CONCLUSIONS

A compact loop antenna with parasitic split ring is proposed in this paper. The proposed antenna can be operated from 920 MHz to 925 MHz for the reader of the UHF RFID application. The proposed antenna is achieved by using the rectangular loop structure (feeding element) together with the parasitic split ring to reduce the overall antenna dimension. It is found that the size can be decreased by 50% of the typical single loop antenna. The overall size of the proposed antenna is 51 mm $\times$ 38 mm $\times$ 0.8 mm ($0.15\lambda \times 0.11\lambda \times 0.02\lambda$). The antenna radiates the omnidirectional beam. The directivity is 1.7 dBi at 922.5 MHz. The prototype was fabricated and measured to verify the simulations. The measurement results show good agreement with the simulations ones. Therefore, the characteristics of the proposed compact loop antenna with parasitic split ring can achieve the requirement of the UHF RFID application.

ACKNOWLEDGMENT

This work is supported by the Thailand Research Fund (TRF) through the Royal Golden Jubilee Ph.D. Program under Grant No. PHD/0324/2552.

REFERENCES

1. Finkenzeller, K., *RFID Handbook*, 2nd Edition, Wiley, New York, 2003.
2. Nikitin, P. V. and K. V. Rao, "Helical antenna for handheld UHF RFID reader," *Proc. IEEE Int. Conf. RFID*, 166–173, Apr. 14–16, 2010.

3. Hua, R. C. and T. G. Ma, "A printed dipole antenna for ultra high frequency (UHF) radio frequency identification (RFID) handheld reader," *IEEE Transactions on Antennas and Propagation*, Vol. 55, No. 12, 3742–3745, 2007.
4. Nikitin, P. V. and K. V. S. Rao, "Compact printed Yagi antenna for handheld UHF RFID reader," *Proc. IEEE Antennas and Propagation Society International Symposium (APSURSI)*, 1–4, Jul. 11–17, 2010.
5. Xie, Z. M., X. Z. Lai, and R. J. Hu, "Compact UHF RFID reader antenna using bended fold dipole structure for mobile RFID system," *Proceedings of the 2011 International Conference on Machine Learning and Cybernetics*, 414–417, Jul. 10–13, 2011.
6. CST-Microwave Studio, *User's Manual*, 2006.
7. Huang, Y. and K. Boyle, *Antennas from Theory to Practice*, John Wiley & Sons, 2008.

AUTHOR BIOGRAPHY

Name	Kittima Lertsakwimarn
Birthday Date	August 29, 1987 in Prachinburi, Thailand.
Address	241, M.1, Thatoom District, Srimahaplo Amphur, Prachinburi Province, 25140
Educational Background	
2005 - 2008	B. Eng. in Electrical Engineering from Burapha University, Chonburi, Thailand
2009 - 2010	M. Eng. in Telecommunication Engineering from King Mongkut's Institute of Technology Ladkrabang (KMITL), Bangkok, Thailand,
2011 - Now	Ph.D. student, in Electrical Engineering, King Mongkut's Institute of Technology Ladkrabang, Bangkok, Thailand, supported by a scholarship from the Thailand Research Fund through in the Royal Golden Jubilee (RGJ) program.
April 2013 - March 2014	Visiting researcher at the Department of Computer Science and Electrical Engineering, Kumamoto University, Kumamoto, Japan under the support from RGJ.
Research interests	Antenna designs for telecommunication, RFID and sensor applications.